DYRK1A-RELATED TRABECULAR DEFECTS IN MALE TS65DN MICE EMERGE DURING A CRITICAL DEVELOPMENTAL WINDOW

by

Jonathan M. LaCombe

A Dissertation

Submitted to the Faculty of Purdue University

In Partial Fulfillment of the Requirements for the degree of

Doctor of Philosophy

Department of Biology at IUPUI

Indianapolis, Indiana

August 2021

THE PURDUE UNIVERSITY GRADUATE SCHOOL
STATEMENT OF COMMITTEE APPROVAL

Dr. Randall Roper, Chair

Department of Biology

Dr. Charles Goodlett

Department of Psychology

Dr. Joseph Wallace

Department of Biomedical Engineering

Dr. Jiliang Li

Department of Biology

Dr. Jason Meyer

Department of Biology

Approved by:

Dr. Theodore Cummins

I dedicate this work to those who have the will to take their destiny into their own hands.

This dissertation and my journey serve as evidence
that we hold the power to turn our dreams into reality.

ACKNOWLEDGMENTS

When I began my pursuit of science in 2010, I was a bored barista with an insatiable curiosity for science. Fortunately for me, Dr. Martin Vaughan indulged my curiosity and presented opportunities that would change my life. Dr. Kathy Marrs and Dr. Greg Anderson were hugely influential in developing my career as a young scientist through our close work with Dr. Martin O'Donnell, Dr. Bill Scott, and Dr. Geno Samaritoni. In the lab of Dr. Anderson, I received what would be the foundation of my benchtop laboratory training by Barbara Coffey. Rick Frey was a teacher and a mentor to me throughout my time at IUPUI; our conversations were always interesting and I always came away with more knowledge than I had. Other faculty and staff including Anje Longfellow, Shari O'Dowell, Suzanne Merrell, and Dawn Bauman were always there to help. These people collectively prepared me for the most difficult journey of my life: graduate school.

I was again fortunate in finding a fantastic graduate advisor. Dr. Randall Roper was a primary influence on my development into a professional scientist. Dr. Charles Goodlett was also hugely influential in my development. Dr. Jiliang Li, Dr. Joseph Wallace, and Dr. Jason Meyer were amazing teachers and committee members, each never hesitating to help or share knowledge.

An often-neglected subject in relation to graduate school is the relationships you develop with your peers, who become like family. While moving on from grad-life is indeed glorious, I'm left missing those who I've learned so much from, respected, and looked forward to seeing every day. Thank you Jared Thomas and Laura Hawley; you were amazing partners and I look forward to calling you "Dr." someday. Thank you Kourtney Sloan, and Kelsey Cave; I would have never been able to produce the tremendous amount of data for this dissertation without you. Thank you Matthew Blackwell and Avery Deaton; you two were amazing students and it was a ride to watch you develop into scientists. Thank you Imaani Washington; teaching K101 lab was never the same after you started.

To end this already long-winded acknowledgement, I want to again thank a handful of people who took a chance on me. Thank you Dr. Martin Vaughan, Dr. Kathy Marrs, Dr. Greg Anderson, and Dr. Randall Roper. You all saw something in me that I'm not even sure I see yet, but thank you for helping me get to where I am now.

TABLE OF CONTENTS

LIST OF TABLES

LIST OF FIGURES

ABSTRACT

Down syndrome (DS) is a complex genetic disorder caused by the triplication of human chromosome 21 (Hsa21). The presence of an extra copy of an entire chromosome greatly disrupts the copy number and expression of over 350 protein coding genes. This gene dosage imbalance has far-reaching effects on normal development and aging, leading to cognitive and skeletal defects that emerge earlier in life than the general population.

The present study begins by characterizing skeletal development in young male Ts65Dn mice to test the hypothesis that skeletal defects in male Ts65Dn mice are developmental in nature.Femurs from young mice ranging from postnatal day 12- to 42-days of age (P12-42) were measured and analyzed by microcomputed tomography (μCT). Cortical defects were present generally throughout development, but trabecular defects emerged at P30 and persisted until P42.

The gene *Dual-specificity tyrosine-regulated kinase 1a* (*Dyrk1a*) is triplicated in both DS and in Ts65Dn mice and has been implicated as a putative cause of both cognitive and skeletal defects. To test the hypothesis that trisomic *Dyrk1a* is related to the emergence of trabecular defects at P30, expression of *Dyrk1a* in the femurs of male Ts65Dn mice was quantified by qPCR. Expression was shown to fluctuate throughout development and overexpression generally aligned with the emergence of trabecular defects at P30.

The growth rate in trabecular measures between male Ts65Dn and euploid littermates was similar between P30 and P42, suggesting a closer look into cellular mechanisms at P42. Assessment of proliferation of BMSCs, differentiation and activity of osteoblasts showed no significant differences between Ts65Dn and euploid cellular activity, suggesting that the cellular microenvironment has a greater influence on cellular activity than genetic background.

These data led to the hypothesis that reduction of *Dyrk1a* gene expression and pharmacological inhibition of DYRK1A could be executed during a critical period to prevent the emergence of trabecular defects at P30. To tests this hypothesis, doxycycline-induced cre-lox recombination to reduce *Dyrk1a* gene copy number or the DYRK1A inhibitor CX-4945 began at P21. The results of both genetic and pharmacological interventions suggest that trisomic *Dyrk1a* does not influence the emergence of trabecular defects up to P30. Instead, data suggest that the critical window for the rescue of trabecular defects lies between P30 and P42.

CHAPTER 1. INTRODUCTION

1.1 Down syndrome

Down syndrome (DS) results from trisomy of human chromosome 21 (T21), is the most viable human trisomy, and occurs in about 1 in 800 live births(de Graaf, Buckley, & Skotko, 2015). The cause of DS is correlated with advanced maternal age and hypotheses that seek to explain this correlation suggest loss in maternal regulation of oocyte recombination events(Middlebrooks et al., 2014; Stewart et al., 1988). Maternal nondisjunction during meiosis I accounts for 70-80% of live DS births, while nondisjunction during meiosis II accounts for only 20-30% (Allen et al., 2009; Ghosh, Feingold, & Dey, 2009; Stewart et al., 1988). Hypotheses also exist suggesting that all nondisjunction events originate during meiosis I and resolve during either meiotic stage(Lamb et al., 1997). While the "old egg hypothesis" was widely accepted based on the correlation between increased incidence of DS with maternal age, comprehensive studies concede that the source of nondisjunction is multifactorial, suggesting both age-dependent and age-independent factors(Oliver et al., 2008). Mosaicism of T21 was initially attributed to mitotic nondisjunction, but was later determined that mosaicism more often originates from an initial nondisjunction event in either meiosis I or meiosis II, followed by a rescue event whereby a copy of Hsa21 is lost during cell division(Papavassiliou, Charalsawadi, Rafferty, & Jackson-Cook, 2015). Robertsonian translocation events also produce DS phenotypes, contributing to between 3.3% and 4.6% of individuals with DS in the U.S. and China, respectively(Shin, Siffel, & Correa, 2010; Zhao et al., 2015). While the origins of DS seem conserved globally, other factors including socioeconomic status and preconceptive folate supplementation have been associated with DS originating from errors in meiosis II(Allen et al., 2009; Bean et al., 2011; Ghosh et al., 2009; Hollis et al., 2013; Hunter et al., 2013). Considering the many origins of DS phenotypes, it is not surprising that DS presents with a wide variability of phenotypes and a wide variability in terms of individual functionality(Papavassiliou et al., 2009). Due to the genetic origins of DS, the phenotypes classified as hallmarks of DS emerge as a result of dysregulation of gene expression and molecular signaling during development.

The advent of prenatal screening and diagnosis of DS in conjunction with corrective surgery has greatly increased the lifespan of those with DS to over 60 years of age(Bittles &

Glasson, 2004; Esbensen, Johnson, Amaral, Tan, & Macks, 2016). Speech, physical, and occupational therapy have also contributed to the overall health, well-being, and quality of life for those affected by DS(Agarwal Gupta & Kabra, 2014). Current research is aimed at evaluating the genotype-phenotype relationship to understand the contribution of trisomic genes on specific phenotypes towards developing therapeutics that improve the lives of individuals with DS. Single gene triplications alone cause chaos at a molecular, cellular, and organismal level. Indeed, Charcot-Marie-Tooth, a genetic disease causing neuropathy, originates from increased dosage of *peripheral myelin protein 22 PMP22*(Rice & McLysaght, 2017). Similarly, duplication and triplication of *α-synuclein* (*SNCA*) is associated with early-onset Parkinson's disease(Rice & McLysaght, 2017). These studies exemplify the consequences of increased dosage of a single gene – phenotypes in DS are the result of increased dosage of over 350 genes(Roper & Reeves, 2006). The connection between increased gene dosage and abnormal phenotypes has been supported by experiments that improve phenotypes by correcting gene dosage of trisomic genes in otherwise trisomic mice(Blazek, Abeysekera, Li, & Roper, 2015; Chakrabarti et al., 2010; Kleschevnikov et al., 2017; Lana-Elola, Watson-Scales, Fisher, & Tybulewicz, 2011). These reports suggest therapeutic potential in targeting molecular pathways affected by increased gene dosage of Hsa21 genes in an effort to treat or prevent the emergence of DS phenotypes.

1.2 DYRK1A

Initially identified as a gene that, when disrupted in *Drosophila melanogaster*, caused defects in brain volume and cell number by Heidenreich in 1982, then again by Fischbach and Heisenberg in 1984, *minibrain* would soon be the prime focus of DS investigators. Studies would go on to sequence the gene and characterize the protein as a serine-threonine kinase conserved in mice and humans as dual specificity tyrosine-regulated kinase 1A (*DYRK1A*), and similar to reports from *Drosophila* studies contributes to neuronal phenotypes and reduced cell number in mice (Song et al., 1996; Tejedor et al., 1995). *DYRK1A* was mapped to Hsa21 at 21q22.2 and shown to be capable of producing learning defects similar to DS phenotypes when at increased gene dosage, such as in T21 (Becker & Joost, 1999; Smith et al., 1997; Song et al., 1996). Guimera et al. demonstrated that *DYRK1A* and the murine homolog *Dyrk1a* was indeed overexpressed in individuals with DS and in the Ts65Dn mouse model of DS(Guimera, Casas, Estivill, & Pritchard, 1999).

In humans, *DYRK1A* has been demonstrated to be a dosage-sensitive gene critical for development. Microdeletions and truncation of a *DYRK1A* allele causes intellectual disability and microcephaly(Moller et al., 2008; B. W. van Bon et al., 2011). Further characterized as autosomal dominant mental retardation 7 (MRD7) or *DYRK1A*-related intellectual disability syndrome (OMIM 614104), disruption of *DYRK1A* has wide-reaching consequences resembling DS phenotypes including autism spectrum disorder, craniofacial defects, feeding difficulty, hypotonia, irregular gait, and foot deformities(Meissner et al., 2020; B. W. van Bon et al., 2016; B. W. M. van Bon, Coe, de Vries, & Eichler, 1993). Other defects found in significant fractions of those affected include seizures and skeletal abnormalities(B. W. M. van Bon et al., 1993). The effects of overexpression of *DYRK1A* were characterized in a young boy mosaic in 80% of mucosal cells and 40% of lymphocytes for a duplication of a 2.56Mb segment of HSA21 encompassing *DYRK1A*. The boy presented with developmental delay, mild intellectual disability, aberrant craniofacial features, hyperopia, astigmatism, and hypotonia, similar to phenotypes observed in DS(Schnabel et al., 2018). Taken together, these case studies provided further evidence for *DYRK1A* as a target for understanding the genotype-phenotype relationship of triplicated genes in DS.

Transgenic mice overexpressing *Dyrk1a* displayed cognitive defects similar to those observed in DS(Altafaj et al., 2001). In 2002 another mouse model was introduced that had an impaired allele of *Dyrk1a*; Fotaki et al. demonstrated that haploinsufficiency of the gene resulted in growth delays and deficits in brain development(Fotaki et al., 2002). Subsequent experiments identified the role of *Dyrk1a* in the central nervous system, motor function, and cognitive function(Benavides-Piccione et al., 2005; Fotaki, Martinez De Lagran, Estivill, Arbones, & Dierssen, 2004; Marti et al., 2003). Those experiments demonstrated that a gene dosage threshold must be met for proper development(Fotaki et al., 2002). The first attempt to decipher how trisomic *Dyrk1a* dysregulates molecular signaling was described by Arron et al. in 2006. They were able to show that 1.5x overexpression of *Dyrk1a* and *Dscr1* (*Rcan1*) disrupts the Nfatc molecular pathway, which the authors describe as a putative origin of heart defects in DS and hypothesize that other tissues are affected in a time- and tissue-dependent manner(Arron et al., 2006; Lee et al., 2009). The effect of trisomic *Dyrk1a* on the appendicular skeleton was explored at embryonic day 17.5 (E17.5) and six weeks (P42) in Ts65Dn mice, demonstrating that reduction in *Dyrk1a* gene dosage was time-dependent. Normalization of the gene in otherwise trisomic male mice had no effect on bone defects at E17.5, but improved the skeletal phenotype significantly at P42(Blazek,

Abeysekera, et al., 2015; Blazek, Malik, et al., 2015). Together, these experiments demonstrate the value in characterizing the genotype-phenotype relationship of trisomic *Dyrk1a* in Ts65Dn mice.

1.3 Pharmacological Targeting of DYRK1A

The first molecule described to inhibit DYRK1A *in vitro* at micromolar concentrations (0.33μM) was epigallocatechin-3-gallate (EGCG), a polyphenol found in green tea(Bain, McLauchlan, Elliott, & Cohen, 2003). Molecules like EGCG are termed epicatechins due to their epimerized catechin base, which can change based on environmental stimuli including temperature, pH, and time(Seto, Nakamura, Nanjo, & Hara, 1997). Enzymatic analyses described a relative specificity toward DYRK1A over other kinases, leading to deeper investigations concerning the effect of EGCG at the cellular and organismal level(Bain et al., 2003). After determining the mechanism of EGCG inhibition, *in vivo* studies followed to report no effect on cognitive deficits at multiple doses, but improvement of bone defects when provided *ad libitum* at a concentration of 0.124mg/mL (~9mg/kg/day) (Adayev, Chen-Hwang, Murakami, Wegiel, & Hwang, 2006; Blazek, Abeysekera, et al., 2015; Goodlett et al., 2020; Stringer, Abeysekera, Dria, Roper, & Goodlett, 2015; Stringer et al., 2017). Improved bone phenotypes at low doses and lack of cognitive improvement at all doses suggests a potential therapeutic benefit in bone health when consumed at low doses such as that found in green tea.

Similar results were observed in serum EGCG concentrations between humans consuming a green tea beverage containing 1.66mg/mL green tea catechins (0.31mg/mL EGCG) and mice administered EGCG with a maximal serum concentration observed at about one hour after consumption that quickly and exponentially reduces(Masukawa et al., 2006; Ramachandran, Jayavelu, Murhekar, & Rajkumar, 2016). These studies suggest that the bioavailability of EGCG is poor and may not provide lasting inhibitory activity. The stability of EGCG was also brought into question due to the molecule's tendency to change conformation and precipitate in response to changes in the environment including pH, temperature, time, and protein interactions(Seto et al., 1997). A notable phenomenon that may provide some insight into EGCG bioavailability is observed when hot tea infusions cool and produce "tea cream," a precipitate formation caused by the binding of catechins with caffeine and/or protein(Penders, Jones, Needham, & Pelan, 1998;

Siebert, Troukhanova, & Lynn, 1996). Together, these results suggest that the bioavailability of EGCG may limit its therapeutic potential for DYRK1A inhibition.

Green tea extracts (GTE) were shown to improve cognitive phenotypes associated with DS in mice and humans, adding confusion to the field(De la Torre et al., 2014). A key difference in the methodology was the use of a GTE instead of pure EGCG. Also present in green tea and GTE mixtures are caffeine and other polyphenols including catechins epicatechin-3-gallate (ECG), epigallocatechin (EGC), and epicatechin (EC)(Musial, Kuban-Jankowska, & Gorska-Ponikowska, 2020). Reports describing improvements in DS phenotypes as a result of GTE administration credit EGCG and inhibition of DYRK1A, but in another study ECG showed inhibitory activity against DYRK1A, suggesting that other polyphenols in GTE may have unforeseen consequences(De la Torre et al., 2014; Gu et al., 2020). The presence of caffeine in GTE may also affect the outcome in these experiments, demonstrated by a study that reported a synergistic effect between catechins and caffeine in reducing degranulation of mast cells(Yashima, Sato, & Kazama, 2021). A group recently reported the use of EGCG as a method of generating a mouse model for liver failure(Wang et al., 2019). This and a report pointing to EGCG as the cause of liver failure in a young man raise concern over the unregulated use of EGCG and polyphenols as therapeutic solutions(Patel, Beer, Kearney, Phillips, & Carter, 2013).

Harmine, a beta carboline compound used by shamen in the Amazon and as a drug to treat Parkinson's disease in 1929 was later identified as a potent DYRK1A inhibitor with an IC_{50} of 0.08μM(Bain et al., 2007). Due to the inhibitory activity on monoamine oxidase (MAO) and hallucinogenic effects, the pharmaceutical value of harmine was limited to *in vitro* studies. Synthetic compounds inhibiting the ATP binding site of DYRK1A at nanomolar concentrations were later identified. INDY and the prodrug proINDY were described to have an IC_{50} of 0.24μM and X-ray crystallography of the DYRK1A/INDY complex revealed binding of the drug to the ATP binding pocket of DYRK1A(Ogawa et al., 2010). Modifications to INDY resulted in other potent DYRK1A inhibitors such as BINDY and FINDY in 2015 and 2016, respectively(Kii et al., 2016; Masaki et al., 2015). While attractive, these inhibitors have not yet been validated or safety tested in mouse models of DS since their initial description which replaces any therapeutic promise with doubt.

In 2016, a group in Korea repurposed an anti-cancer drug that had passed clinical trials as a DYRK1A inhibitor. CX-4945 displayed a much higher affinity to DYRK1A than harmine and

INDY with an IC_{50} of 6.8nM(H. Kim et al., 2016). The drug was shown to be effective against hematological cancers and reducing osteoclast activity while increasing osteoblast activity, suggesting an overall inhibitory effect on the hematopoietic progenitor lineage and a stimulatory effect on the mesenchymal lineage (Chon, Bae, Lee, & Kim, 2015; Son, Moon, & Kim, 2013). Together, these reports suggest a potential therapeutic application of CX-4945 for inhibiting DYRK1A to improve cognitive and skeletal defects.

1.4 Cellular Components of Skeletal Development

Increased gene dosage from T21 and the molecular signaling dysregulation that results disrupts cellular processes(Chiang, Jiang, Newburger, & Lawrence, 2018; Czerminski & Lawrence, 2020). To understand skeletal phenotypes associated with DS, it is important to first understand the cells that contribute to those phenotypes. The basic multicellular unit (BMU) is responsible for building, maintaining, and remodeling bone during development and throughout life. The BMU is comprised of osteoblasts and osteoclasts which deposit bone and degrade bone, respectively. The tandem action and tight regulation of these cells is necessary for proper bone development and bone health.

Osteoclasts originate from hematopoietic stem cells in the bone marrow. Hematopoietic stem cells are capable of differentiating into all the blood cells in the body such as red blood cells, platelets, and lymphocytes. Hematopoietic stem cells in the bone marrow compartment give rise to common myeloid progenitors (CMP) when stimulated by stem cell factor (SCF), interleukin-3 (IL-3) and interleukin-6 (IL-6). CMPs exposed to granulocyte/macrophage colony stimulating factor (GM-CSF) differentiate into granulocyte monocyte progenitors (GMPs). GMPs stimulated by monocyte/macrophage colony stimulating factor (M-CSF) and receptor activation of NF-κB ligand (RANKL) commit to monocytes, which are considered osteoblast precursors when expressing Mac-1, c-Fms, and RANK, but not c-Kit(Feng & Teitelbaum, 2013). Osteoclast precursors fuse to form multinucleated osteoclasts. Osteoclasts are considered mature after multiple fusions, resulting in multiple nuclei. Although multiple nuclei are required for mature osteoclast functionality, not all nuclei are active and osteoclasts with more nuclei have diminished activity(Burr & Allen, 2013).

Osteoclast precursors are recruited to the bone surface by signaling factors secreted by osteoblasts, osteocytes, and damaged bone. There, the precursors fuse into mature multinucleated

cells. The cells polarize and attach to the bone to form a sealing zone along the periphery of the membrane contacting the surface. The inner area of the membrane in contact with the bone surface then ruffles, increasing total surface area to maximize the secretion of hydrolytic enzymes and internalization of degraded matrix. As bone matrix is degraded, the osteoclast migrates and repeats the process. Osteoclasts undergo apoptosis at the conclusion of the remodeling process through a mechanism that is not completely understood(Burr & Allen, 2013).

Mesenchymal progenitors differentiate into the cells that compose the body's major organs such as neurons in the brain, cells in smooth and cardiac muscles, adipocytes that store fat, chondrocytes responsible for cartilaginous joints, and osteoblasts which build bone. Osteoblast progenitors mature as specific transcription factors are expressed. The primary transcription factor *RUNX2* is required for the entire osteoblast lineage and *Runx2* null mice are not viable. Following expression of *RUNX2*, the cells must express *SP7*/*OSTERIX* to mature. Similar to *RUNX2*, *SP7*/*OSTERIX* is required for development and knockouts result in perinatal lethality. Mature osteoblasts polarize, adopt a cuboidal shape, and undergo an internal rearrangement of organelles that optimizes secretion of collagen and minerals before binding to the bone surface (or cartilaginous matrix). The cells secrete and deposit type I collagen and other proteins to form osteoid, an unmineralized collagen matrix. Osteoid mineralization occurs in two distinct phases: primary and secondary mineralization. Primary mineralization is characterized as the initial incorporation of the inorganic calcium-phosphate mineral that constitutes the skeleton known as hydroxyapatite. The initial mineralization composes over 70% of the mineral content in the skeleton and occurs over a period of 2-3 weeks. The minerals are deposited as small crystals that grow when more are added by osteoblasts through the nucleation process. Secondary mineralization occurs over a much longer period, usually about a year, and results in the complete mineralization of spaces within the mineralized collagen matrix(Burr & Allen, 2013)

Following the completion of collagen and mineral deposition, osteoblasts undergo apoptosis, transition into lining cells, or become embedded in the bone to become osteocytes. It is estimated that 60-80% of osteoblasts undergo apoptosis, which can begin as early as the osteoblast progenitor phase. It is important to make the point that this has been studied *in vitro* and may occur through different mechanisms and at different rates *in vivo*. When osteoblasts transition to lining cells, they lose their functionality, but some studies have shown that they can still produce matrix in response to parathyroid hormone (PTH). Lining cells serve as an intermediary between the

extracellular space and the bone matrix, allowing exchange of osteocyte-derived signaling molecules, minerals, and metabolites. While still under investigation, it is hypothesized that during remodeling, lining cells retract and cover the BMU, forming a canopy that isolates the bone-degrading enzymes and signaling molecules to that particular site. The canopy is also thought to form capillaries that supply the cells required for remodeling(Burr & Allen, 2013).

Osteoblasts that are embedded in the bone become osteocytes, which serve as sensory cells that are instructive to other cells in the bone microenvironment. Osteocytes comprise over 90% of the cells in bone matrix and on bone surfaces. Growing evidence suggests that osteocytes instruct cells of the bone microenvironment through hormones and signaling molecules that regulate the proliferation, maturation, activity, and survival of osteoblasts and osteoclasts. Osteocytes reside in concentric rings of bone matrix called lacunae. Dendritic processes extend from the cell body through canals in the bone, called canaliculi, which extend to the periosteal and endosteal surfaces of cortical bone. The dendritic processes have been shown to have mechanosensory functions as well as the ability to respond to circulating ion and hormone signals. In response to microdamage, osteocytes secrete factors that signal remodeling processes.

1.5 Osteogenesis

Bone formation during early development is accomplished through one of two processes depending on the site of bone formation. Intramembranous ossification occurs primarily in the skull, while endochondral ossification occurs in the appendicular skeleton. Intramembranous ossification and endochondral ossification differ in both the location of ossification and whether or not it occurs with a cartilage template. Intramembranous ossification occurs in mesenchyme with no template or foundation, while endochondral ossification begins with construction of a cartilage foundation in which to build upon. Intramembranous ossification occurs primarily during development and during bone healing. Most of the skull, clavicle, and scapulae are formed through intramembranous ossification. Another key difference between intramembranous ossification and endochondral ossification is the presence of a marrow cavity. The exception to this is the mandible, which grows so thick that embedded osteocytes become hypoxic and release growth factors that promote blood vessel development to maintain osteocyte survival, resulting in a marrow cavity. Intramembranous ossification begins when cells in mesenchyme condense into a blastema. The cells within the blastema begin to express *RUNX2*, the osteoblast fate transcription factor.

Osteoblasts begin producing a collagen extracellular matrix that forms a foundation for other osteoblasts to build upon, termed the ossification center. These primary ossification centers are comprised of woven bone, a hastily and haphazardly produced unorganized collagen structure. As more osteoblasts are recruited, ossification centers fuse together and a more organized lamellar bone is produced(Burr & Allen, 2013).

Excluding the skull, clavicle, and scapulae, the skeleton is constructed by a process termed endochondral ossification. Similar to intermembranous ossification, mesenchymal cells cluster to form a blastema. In endochondral ossification, however, the blastemal cells express *SOX9* and differentiate into chondroblasts. The cells begin producing a cartilage matrix that eventually envelops neighboring cells. Enveloped chondroblasts differentiate into chondrocytes and begin forming the perichondrium, a fibrous cartilage template that serves as a structural foundation or scaffold for the bone. Mesenchymal cells surrounding the perichondrium express *RUNX2* and differentiate into osteoblasts, which ossify the perichondrium by depositing a collagen matrix and hydroxyapatite.

1.6 Skeletal Abnormalities in DS

Down syndrome presents with hallmark skeletal abnormalities in all individuals such as atypical craniofacial structure and short stature as a result of disproportionately shorter arms and legs(Baptista, Varela, & Sardinha, 2005; Barden, 1983; Richtsmeier, Baxter, & Reeves, 2000). Craniofacial morphology is influenced by neural crest cell migration and *sonic hedgehog* (*Shh*) signaling which has been shown to be defective in the Ts65Dn mouse model(Roper, VanHorn, Cain, & Reeves, 2009). Both skeletal phenotypes can be observed as early as the second trimester and remain throughout life(Bromley, Lieberman, Shipp, & Benacerraf, 2002a, 2002b; Longo, DeFigueiredo, Cicero, Sacchini, & Nicolaides, 2004). Growth velocity is reduced in children with DS and the skeletal age is delayed compared to chronological age(de Moraes, Tanaka, de Moraes, Filho, & de Melo Castilho, 2008; Myrelid, Gustafsson, Ollars, & Anneren, 2002). Maximal height is reached around age 15, precocious compared to the general population who continue experience skeletal growth as late as age 20(Angelopoulou, Souftas, Sakadamis, & Mandroukas, 1999; de Moraes et al., 2008).

All individuals with DS have reduced bone mineral density (BMD) and reduced bone strength compared to the general population(Baptista et al., 2005). Peak bone mass is attained

nearly a decade before the general population, contributing to the early onset of osteoporotic phenotypes and a steeper decline in BMD over time as compared to normal individuals(Carfi et al., 2017; Costa et al., 2018; McKelvey et al., 2013). Compromised bone quality and strength are hypothesized to predispose those with DS to fragility fractures(Angelopoulou et al., 1999; Baptista et al., 2005; de Moraes et al., 2008). Indeed, 12% of respondents of a survey conducted by DS Connect® reported skeletal abnormalities. Of the 39 respondents reporting broken bones, 31 were long bone fractures. The majority of fractures (~64%) seem to occur between one and 15 years of age(LaCombe & Roper, 2020). While these data may not accurately represent the population, the data seem to fit considering both the increased activity of children with DS compared to sedentary adults with DS and the reduced BMD and bone strength characteristic of DS.

Males begin losing bone mass earlier than females with DS, suggesting a protective effect of female biological sex in maintaining BMD(Carfi et al., 2017; Costa et al., 2017; Costa et al., 2018; Tang et al., 2019). The aforementioned phenotypes lead to early onset osteoporosis and an increased risk of fractures(Angelopoulou et al., 1999; Baptista et al., 2005). While it is attractive to attribute accelerated loss of bone mass in males to reduced testosterone, it may not be entirely accurate. Indeed, hypogonadism is a common phenotype in males with DS, but reduction in testosterone is not observed (Hasen, Boyar, & Shapiro, 1980; Hsiang, Berkovitz, Bland, Migeon, & Warren, 1987; Pueschel, Orson, Boylan, & Pezzullo, 1985). Contrary to common knowledge, estrogens have been shown to be important in maintaining bone health and reducing fracture risk in both men and women(Ohlsson & Vandenput, 2009; Vandenput & Ohlsson, 2009). Surprisingly, the limited studies that exist assessing estradiol in males with DS report that estradiol is elevated(Hestnes et al., 1991). Taken together, there is insufficient evidence to support any hypotheses suggesting that deficits in sex hormones as a result of hypogonadism cause bone defects in individuals with DS(LaCombe & Roper, 2020).

Particular cellular sources of skeletal abnormalities in DS remain unknown, although many clues suggest an impairment in both bone formation and resorption by osteoblasts and osteoclasts, respectively(LaCombe & Roper, 2020). The foundation of the hypothesis that reduced osteoclast activity is sufficient in and of itself to produce compromised skeletal phenotypes rests on one report of a histological sample obtained post mortem from a middle aged man with DS(Grimwood, Kumar, Bickerstaff, & Suvarna, 2000). The next-best approach available to determine the cellular contribution to skeletal phenotypes is serum biomarkers Procollagen 1 Intact N-Terminal

Propeptide (P1NP) for bone formation and Carboxy Terminal Telopeptide (Ctx) for bone resorption. Available literature agrees that serum P1NP is significantly decreased in people with DS. Serum Ctx is also decreased, but not to a significant degree(Garcia-Cerro, Rueda, Vidal, Lantigua, & Martinez-Cue, 2017; McKelvey et al., 2013). A major critique of current studies is the wide age range from which samples were collected. This and pooling sexes prohibit accurate assessment of bone health, but identify a potential problem nonetheless. Increased sample sizes in future studies will allow separation of sexes and age groups to determine sex- and time-specific effects of trisomy on the cellular source of skeletal phenotypes in DS(LaCombe & Roper, 2020).

1.7 Mouse Models of the DS Skeleton

Mouse models serve as a powerful tool for the study of human disease, including DS. As with any model, whether it be a cellular or organismal model, all existing mouse models have significant caveats to consider. Studies seeking to utilize mice for the study of skeletal dynamics, for example, must consider that the growth plate never closes despite reaching skeletal maturity within four to six months. The result is continued longitudinal growth throughout life. Another major difference between human and mouse bone is the absence of osteons in the cortical bone of mice(Jilka, 2013; LaCombe & Roper, 2020). A major challenge in investigating DS phenotypes in a mouse model is that genes homologous to Hsa21 are distributed across mouse chromosome 10 (Mmu10), Mmu16, and Mmu17. This challenge has been met by the development of several models that duplicate segments of the aforementioned chromosomes or are transchromosomic for Hsa21(Gardiner, Fortna, Bechtel, & Davisson, 2003; Gupta, Dhanasekaran, & Gardiner, 2016; Kazuki et al., 2020; O'Doherty et al., 2005).

The Ts(17^{16})65Dn mouse is the most well-studied mouse model of DS. Many DS-related phenotypes have been described in Ts65Dn, including skeletal defects(Blazek, Abeysekera, et al., 2015; Blazek, Gaddy, Meyer, Roper, & Li, 2011; Blazek, Malik, et al., 2015; Reeves et al., 1995). These phenotypes are attributed to the presence of a freely segregating chromosome composed of the centromeric region of mouse chromosome 17 (Mmu17) and the distal arm of Mmu16. In addition to increased gene dosage of about 100 genes homologous to Hsa21 genes, about 35 protein coding genes in the centromeric region of Mmu17 are also triplicated(Gardiner et al., 2003; Gupta et al., 2016). The genotype-phenotype relationship for extraneous Mmu17 genes in Ts65Dn have not yet been described. Most studies on Ts65Dn mice have been limited to males. This is primarily

due to the subfertile nature of males, which requires researchers to reserve females for both colony maintenance and generation of gene knockout models in otherwise trisomic mice(Moore et al., 2010; Roper, St John, Philip, Lawler, & Reeves, 2006). While these caveats seem prohibitive, studies have shown similarities in craniofacial and skeletal abnormalities between the Ts65Dn mouse model and males with DS(Blazek, Abeysekera, et al., 2015; Blazek et al., 2011; Blazek, Malik, et al., 2015; Fowler et al., 2012; Roper et al., 2006). Male Ts65Dn mice have decreased BMD and compromised architectural measures. Assessment of mechanical strength by three-point bending demonstrated reduced strength in Ts65Dn males, supporting the hypothesis of increased fracture risk in DS males(Angelopoulou et al., 1999; Blazek, Abeysekera, et al., 2015; de Moraes et al., 2008; LaCombe & Roper, 2020). Histology of trabecular bone showed a reduced bone formation rate (BFR), mineral apposition rate (MAR), and osteoblast number(Blazek, Abeysekera, et al., 2015). Contrary to the single report on osteoclast number in humans, more osteoclasts were found in Ts65Dn mice(Blazek, Abeysekera, et al., 2015; Grimwood et al., 2000). This discrepancy is likely caused by the poor statistical power of the report in humans. Biomarker analysis in Ts65Dn mice also echoed humans with DS, again with the exception of Ctx, a biomarker for osteoclast activity. Bone formation marker P1NP was decreased significantly in Ts65Dn mice and humans while the bone resorption marker was only slightly decreased in Ts65Dn mice(Fowler et al., 2012; McKelvey et al., 2013). Together, skeletal studies utilizing Ts65Dn have demonstrated similarities to phenotypes observed in DS presumably due to the increased gene dosage of about 100 homologous Hsa21 genes.

Gene knockout models utilizing Ts65Dn as a foundation to understand the contribution of individual genes on DS phenotypes have been immensely valuable. As discussed previously, gene dosage reduction of *Dyrk1a* in otherwise trisomic mice had no noticeable effect on appendicular skeletal abnormalities at E17.5, but significantly improved trabecular phenotypes at P42, suggesting a time-dependent effect of trisomic *Dyrk1a* in Ts65Dn and DS(Blazek, Abeysekera, et al., 2015; Blazek, Malik, et al., 2015). Similarly, gene dosage reduction of another triplicated gene in Ts65Dn, *Kcnj6*, provided insight to the triplicated gene's role in memory impairment observed in DS(Kleschevnikov et al., 2017). These studies have also provided evidence that the characteristic phenotypes of DS are the result of increased gene dosage of more than a single gene and suggest complex gene interactions that are not fully understood.

To uncover how groups of genes interact to produce DS phenotypes, segmental duplication models were developed. It was hypothesized that a specific region of Hsa21, termed the Down syndrome critical region (DSCR), was sufficient to produce phenotypes observed in DS. The development of a segmental tandem duplication of the homologous 33 gene segment of Mmu16 in the Ts1Rhr mouse model allowed a direct test to that hypothesis which was subsequently shown to be false. While disruptive, duplication of the DSCR was insufficient to cause craniofacial and skeletal phenotypes characteristic of DS phenotypes(Olson, Richtsmeier, Leszl, & Reeves, 2004; Olson et al., 2007). The Ms1Rhr model, which is haploinsufficient for the DSCR, was shown to have significant deleterious effects on skeletal measures(Olson et al., 2007). Crossing the Ms1Rhr with Ts65Dn produced a trisomic mouse missing the DSCR, which resulted in significant changes in craniofacial morphology distinct from both models(Olson et al., 2004).

The most comprehensive genetic approach to dissecting genotype-phenotypes relationships in a DS mouse model was designed by Cre/loxP recombination resulting in a tandem duplication of about 148 genes homologous to Hsa21. A subset of models with contiguous segmental duplications of that region were generated to dissect the genotype-phenotype relationship of regions of Mmu16 when in triplicate. A further subset was generated to investigate the contribution of smaller regions when triplicated for a total of seven separate models(Lana-Elola et al., 2016). Comparing the phenotypes between the different models provided insight to the contribution of genetic regions on specific heart and bone phenotypes(Lana-Elola et al., 2016; Thomas et al., 2020). Together, segmental duplications and trisomic mouse models have demonstrated that while single genes or even regions may be insufficient to cause all DS phenotypes, they have very specific phenotypic contributions that are dependent on both dosage and time.

1.8 Introduction of Specific Aims

Interestingly, genetic normalization of *Dyrk1a* in Ts65Dn mice, the most well-studied DS mouse model, has no effect on improving percent bone volume (%BV/TV) at embryonic day (E17.5), suggesting that the window for effectively targeting *Dyrk1a* overexpression by genetic normalization lies later on in development(Blazek, Malik, et al., 2015). Indeed, genetic normalization of *Dyrk1a* significantly improved several appendicular skeletal measures by postnatal day 42 (P42) including %BV/TV, trabecular number, thickness, separation, 2D cross-

sectional area, and strength(Blazek, Abeysekera, et al., 2015). Recent data has shown that *Dyrk1a* expression in the brain varies during early postnatal development and fluctuates from postnatal day 12 (P12) to P42, suggesting that the timing of genetic or pharmacological interventions should occur within this window to achieve maximal results. We hypothesize that overexpression of *Dyrk1a* during a critical developmental window in the femurs of Ts65Dn mice dysregulates molecular mechanisms that in turn disrupt osteogenic gene expression and cause aberrant skeletal phenotypes. Completion of the following specific aims will test this hypothesis:

Specific Aim 1 (SA1): Characterize the emergence of an aberrant skeletal phenotype in male Ts65Dn mice by μCT analysis at ages ranging from P12 to P42. *Dyrk1a* expression will be quantified by qPCR from RNA isolated from the femurs of trisomic and euploid Ts65Dn mice to determine if overexpression precedes the emergence of a phenotype. The DYRK1A inhibitor CX-4945 will be administered via oral gavage prior to the window of overexpression to demonstrate the efficacy of pharmacological intervention to prevent the emergence of skeletal abnormalities. An inducible knockdown model will be utilized to test the hypothesis that genetic normalization prior to *Dyrk1a* overexpression will prevent the emergence of aberrant skeletal defects. Analysis of Ts65Dn, *Dyrk1a*$^{+/-}$ mice at the age of the emergence of skeletal phenotypes will determine if genetic normalization from the point of conception prevents skeletal defects. μCT analysis will be used to verify the success of these treatments at the point of phenotype emergence.

Specific Aim 2 (SA2): Characterize the effect of trisomy on proliferative activity in bone marrow stem cells (BMSCs) and osteoblast activity. EdU will be used to assess proliferative activity on BMSCs isolated from femurs of male Ts65Dn and euploid littermates. Osteoblast activity will be assessed by an ALP assay and mineralization assay at 14 days and 28 days post differentiation, respectively. CX-4945 will be administered to test the hypothesis that inhibition of DYRK1A will improve proliferation of BMSCs and activity of osteoblasts.

Specific Aim 3 (SA3): Define the molecular mechanism by which trisomy contributes to femur deficits. The Wnt/β-catenin and FoxO1/β-catenin signaling pathways are modulated by DYRK1A. qPCR of RNA isolated from femurs in SA1 will assess expression of *Dyrk1a*, *Bglap* (*osteocalcin*), *Runx2*, *Rbl2* (*p130*), and *Alpl* to determine the effect of *Dyrk1a* overexpression on osteogenic gene expression.

CHAPTER 2. METHODOLOGY

2.1 Mouse Models and Genotyping

2.1.1 Ts65Dn

The Ts(17^{16})Dn (Ts65Dn) mouse was designed to model Down syndrome(Davisson et al., 1993). It does so with a freely segregating chromosome consisting of a small portion of the *q* arm of Mmu16 from *Mir155* to *Zfp295* and the centromeric region of Mmu17 from the centromere to *6530411M01RIK(Duchon et al., 2011)*. The centromeric portion of Mmu17 contains between 35 and 70 genes nonorthologous to Hsa21(Duchon et al., 2011; Reinholdt et al., 2011; Roper, Goodlett, Martinez de Lagran, & Dierssen, 2020). Matings to produce experimental mice require Ts65Dn females (Stock Number 001924) and B6C3F1 males (Stock Number 100010) due to the sub fertile nature of Ts65Dn males. This cross also maintains approximately 50% C57BL/6 50% C3H/HeJ allelic background present in Ts65Dn mice. New Ts65Dn females from the Jackson Laboratory were added to the colony every 6 months to reduce strain variability. Female Ts65Dn mice were reserved for production of genetic manipulation experiments including Ts65Dn, *Dyrk1a*$^{+/-}$ and Ts65Dn, *Dyrk1a*$^{+/fl}$ mice (described below). Male Ts65Dn mice were used in cell culture experiments. Male mice were group-housed after weaning on a 12:12 light:dark cycle with white light off from 1900 to 0700. Food and water were available *ad libitum*.

Ts65Dn mice were genotyped to determine the presence of a freely segregating chromosome by amplifying the Mmu16/Mmu17 breakpoint using primers GTGGCAAGAGACTCAAATTCAAC (0.5μM) and TGGCTTATTATTATCAGGGCATTT (0.5μM) with 5U/μL Bioline MyTaq DNA Polymerase and 5x MyTaq Buffer to produce a 275bp band when resolved on a 1.5% agarose gel with 0.01% Syber Safe stain (Invitrogen by Thermo Fisher Scientific SYBR Safe DNA gel stain S33102). The PCR program consisted of denaturation at 94°C for 2.5min followed by 30 cycles of 15s at 94°C, 15s at 58.5°C, and 10s at 72°, followed by a final extension step at 72°C for 1 minute and a cooling step at 4°C for 5 minutes(Reinholdt et al., 2011).

2.1.2 Ts65Dn, *Dyrk1a*$^{+/fl}$

The mice utilized for the characterization of the Ts65Dn skeleton, DYRK1A inhibition, and conditional gene dosage reduction of *Dyrk1a* experiments were obtained by a cross of Ts65Dn females and *Dyrk1a*$^{+/fl}$ mice obtained from John Crispino at Northwestern University. *Dyrk1a*$^{+/fl}$ mice carry a *Dyrk1a* allele that has a *loxP* site between exons 4 and 5 and between exons 6 and 7(Thompson et al., 2015). Upon *Cre* recombinase activation, the genomic DNA containing exons 5 and 6 is excised. Translation of the truncated transcript results in a non-functional DYRK1A protein. Generation of this model began with C57BL/6 RP23 BAC genomic DNA and was maintained on a C57BL/6 mouse background(Thompson et al., 2015). After receiving the mice, our lab crossed *Dyrk1a*$^{+/fl}$ mice with C3H/HeJ mice from the Jackson Laboratory (Stock Number 000659) to obtain progeny on a 50% B6, 50% C3H background. Progeny were intercrossed and F1 generation mating produced male *Dyrk1a*$^{fl/fl}$ mice on a B6/C3H background that were then crossed with female Ts65Dn mice to produce euploid mice with a mutant *Dyrk1a* allele (WT, *Dyrk1a*$^{+/fl}$) and trisomic mice with a mutant *Dyrk1a* allele (Ts65Dn, *Dyrk1a*$^{+/fl}$). Transmission of the mutant *Dyrk1a* allele was verified with PCR amplification of either a 132bp amplicon or 232bp amplicon from an intronic region preceding exon 5 on *Dyrk1a* in WT or transgenic mice, respectively. The mutant *Dyrk1a* allele results from insertion of *loxP* sites flanking exon 5 and 6, thus providing an effective tool capable of reducing the functional copy number of *Dyrk1a* in various tissues from conception when bred to a mouse line expressing *Cre* or inducible with drug administration when bred to a mouse line that expresses a *Cre* driver activated upon exposure to a specific molecule. Male Ts65Dn, *Dyrk1a*$^{+/fl}$ mice were used for *in vivo* experiments such as inducible modulation of *Dyrk1a* to prevent the emergence of an aberrant phenotype and inhibition of DYRK1A with CX-4945.

Ts65Dn, *Dyrk1a*$^{+/fl}$ mice were genotyped by PCR as described by The Jackson Laboratory protocol using primers 25066: TACCTGGAGAAGAGGGCAAG (0.5μM) and 25067: GGCATAACTTGCATACAGTGG (0.5μM) with 5U/μL Bioline MyTaq DNA Polymerase and 5x MyTaq Buffer to produce a 132bp band for the WT allele and 232bp for the flox allele when resolved on a 1.5% agarose gel with 0.01% Syber Safe stain (Invitrogen by Thermo Fisher Scientific SYBR Safe DNA gel stain S33102). The PCR program consisted of denaturation at 95°C for 3min followed by 35 cycles of 20s at 95°C, 15s at 61°C, and 15s at 72°, followed by a final extension step at 72°C for 1 minute and a cooling step at 4°C for 5 minutes.

2.1.3 *rtTA* and *tetOcre*

Similar to preliminary breeding schemes, B6N.FVB(Cg)-Tg(CAG-rtTA3)4288Slowe/J (Jackson Laboratory Stock Number 016532) reverse tetracycline transactivator (rtTA) mice and B6.Cg-Tg(tetO-cre)1Jaw/J (Jackson Laboratory Stock Number 006234) mice were first intercrossed with C3H/HeJ mice to produce founder strains on a 50% B6 and 50% C3H background similar to Ts65Dn. F1 generation mating was repeated and the rtTa and tetO-cre progeny were crossed. Male progeny from that cross that were rtTA and Cre positive were mated to Ts65Dn, *Dyrk1a*$^{+/fl}$ females to generate test mice that would experience the loss of a floxed *Dyrk1a* allele after treatment with doxycycline, inducing activation of the tetracycline-responsive promotor element and excision of one copy of exon 5-6 of *Dyrk1a* by Cre.

Presence of the rtTA allele in test mice was determined by PCR using primers SApA For 1 CTGCTGTCCATTCCTTATTC (0.2μM), Ch8Rev2 CGAAACTCTGGTTGACATG (0.2μM), and Ch8For1 TGCCTATCATGTTGTCAAA (0.4μM) with 5U/μL Bioline MyTaq DNA Polymerase and 5x MyTaq Buffer to produce the carrier 330bp band and 363bp WT band when resolved on a 2% agarose gel with 0.01% Syber Safe stain (Invitrogen by Thermo Fisher Scientific SYBR Safe DNA gel stain S33102). The PCR program consisted of denaturation at 95°C for 2min followed by 35 cycles of 30s at 95°C, 30s at 56°C, and 45s at 72°, followed by a final extension step at 72°C for 5 minute and a cooling step at 4°C for 5 minutes.

Presence of the tetO-cre allele in test mice was determined by PCR using primers Wnt1CreF ATTCTCCCACCGTCAGTACG (0.5μM), Wnt1CreR CGTTTTCTGAGCATACCTGGA (0.5μM), TcdF CAAATGTTGCTTGTCTGGTG (0.5μM), and TcdR GTCAGTCGAGTGCACAGTTT (0.5μM) with 5U/μL Bioline MyTaq DNA Polymerase and 5x MyTaq Buffer to produce the carrier 475bp band and 200bp WT band when resolved on a 1.5% agarose gel with 0.01% Syber Safe stain (Invitrogen by Thermo Fisher Scientific SYBR Safe DNA gel stain S33102). The PCR program consisted of denaturation at 94°C for 3min followed by 35 cycles of 30s at 94°C, 1min at 55°C, and 1min 30s at 72°, followed by a final extension step at 72°C for 5 minute and a cooling step at 4°C for 5 minutes.

2.1.4 Cre Activation

Doxycycline was administered in chow (ENVIGO, Teklad Custom Diet TD.120769, 998.975g/kg 2018 Teklad Global 18% Protein Rodent Diet, 0.625g/kg Doxycycline hyclate, 0.4g/kg Blue Food Color), delivering an average daily dose of 2-3mg doxycycline per 4-5g chow consumed per day. Doxycycline chow was introduced at the time of weaning, postnatal day 21 (P21). Truncation of *Dyrk1a* was verified at P30 by PCR using tail DNA. Excision of the floxed region spanning exons 5 and 6 on one allele of *Dyrk1a* in Ts65Dn, *Dyrk1a*$^{+/fl}$, TetO-Cre^{+}, rtTA$^{+/-}$ mice that had received doxycycline feed was verified with PCR using novel primers ACCTGGAGAAGAGGGCAAGA (0.5μM) and GCCACTGTGTGAGGAGTCTT (0.5μM) with 5U/μL Bioline MyTaq DNA Polymerase and 5x MyTaq Buffer to produce a 214bp band for the truncated allele when resolved on a 1.5% agarose gel with 0.01% Syber Safe stain (Invitrogen by Thermo Fisher Scientific SYBR Safe DNA gel stain S33102). The PCR program consisted of denaturation at 95°C for 3min followed by touchdown for 35 cycles of 20s at 95°C, 20s at 60-55°C, and 30s at 72°, followed by a final cycle at 95°C for 20s, 20s at 55°C, 30s at 72°C, the final elongation at 72°C for 1 minute and a cooling step at 4°C for 5 minutes.

2.1.5 Ts65Dn, *Dyrk1a*$^{+/-}$ mice

Analysis of gene dosage reduction from conception utilized *Dyrk1a*$^{+/-}$ mice, generously donated by Dr. Mariona Arbones (Institut de Recerca Oncologica, Barcelona, Spain). (Fotaki et al., 2002). As described by Blazek et al., mice were backcrossed to B6C3HF1 mice for at least seven generations before crossing *Dyrk1a*$^{+/-}$ males with Ts65Dn females. Female Ts65Dn mice and male *Dyrk1a*$^{+/-}$ mice were bred to produce euploid, *Dyrk1a*$^{+/+}$ euploid, *Dyrk1a*$^{+/-}$, Ts65Dn, *Dyrk1a*$^{+/+}$and Ts65Dn, *Dyrk1a*$^{+/-}$ mice. When determining the effect of normalizing *Dyrk1a* expression in trisomic male mice from conception, male mice were aged 30 days before tissue collection.

Ts65Dn, *Dyrk1a*$^{+/-}$ mice were genotyped as first described by Fotaki et al. in 2002 to determine the presence of the PGKneo cassette in the homologous recombinant allele using a primer unique to the PGKneo cassette inserted into *Dyrk1a* exon 6 (referred to as exon 8 by Fotaki et al.) P1: ATTCGCAGCGCATCGCCTTCTATCGCC (0.5μM) and a primer for an intronic region just downstream of *Dyrk1a* exon 6 P3: CGTGATGAGCCCTTACCTATG (0.5μM) with

5U/μL Bioline MyTaq DNA Polymerase and 5x MyTaq Buffer to produce a 287bp band when resolved on a 1.5% agarose gel with 0.01% Syber Safe stain (Invitrogen by Thermo Fisher Scientific SYBR Safe DNA gel stain S33102). The PCR program consisted of denaturation at 94°C for 2min followed by 35 cycles of 15s at 94°C, 15s at 55°C, and 10s at 72°, followed by a final extension step at 72°C for 1 minute and a cooling step at 4°C for 5 minutes(Fotaki et al., 2002).

2.2 Microcomputed Tomography (μCT) Analysis

To determine when aberrant trabecular phenotypes emerge in Ts65Dn male mice, Ts65Dn, *Dyrk1a*$^{+/fl}$ male mice were aged 12, 15, 18, 24, 27, 30, and 42 days. Mice were euthanized with isoflurane and cervical dislocation. Femurs were collected, wrapped in gauze, placed in a 1.5mL microcentrifuge tube, and soaked in PBS. Femurs were stored at -80°C. For μCT analysis, right femurs were allowed to thaw prior to imaging with a high-resolution μCT system (SkyScan 1172, Bruker microCT Belgium). Analysis software was calibrated with two cylindrical hydroxyapatite phantoms (0.25 and 0.75g/cm^3 CaHA) each week of scanning. Samples were loaded into a modified 10mL tube fixed to the Bruker MicroCT instrument stage with sticky tack. Styrofoam was loaded with the sample to provide stability for the sample. The instrument was calibrated and flat field corrections were applied before scanning the HA phantoms or samples. Images were captured using 60kV with a 0.5mm aluminum filter at 12μm resolution. The entirety of samples from P12, P15, P18, P24, and P27 were scanned, but due to size constraints, samples from P30 and P42 were scanned from the distal condyle of the femur to at least the third trochanter. Image slices were reconstructed into 3D models with SkyScan NRECON and rotated to match vertical alignment with SkyScan ImageViewer. Trabecular geometry was analyzed by identifying a trabecular region of interest (ROI) based on the overall size of the bone and a distance of 10% of the total bone length beginning at the proximal end of the distal growth plate and extending distally using SkyScan CT analyzer (CTan) and a custom MatLab code to exclude the outer cortical bone as described in previous publications(Goodlett et al., 2020; Stringer et al., 2017; Thomas et al., 2020). The cortical ROI was defined as a region of seven transverse slices at 60% of the overall length of the bone from the proximal end of the growth plate and using MatLab, cortical geometry was measured as previously described(Goodlett et al., 2020; Stringer et al., 2017; Thomas et al.,

2020). Skeletal geometry measures are expressed as standardized nomenclature, symbols, and units for bone histomorphometry according to ASBMR guidelines (Dempster et al., 2013).

2.3 RNA isolation and cDNA synthesis

Femurs were removed from -80°C storage and allowed to thaw. Marrow was flushed by removal of the proximal and distal ends of the femur. Midshafts were placed into a P200 pipette tip (modified by cutting each end) that is inside a 1.5mL microcentrifuge tube. Tubes were centrifuged at 4°C for 10min at max speed. The mortar and pestle were prepared as follows: 1) ice bucket filled with ice, 2) mortar placed into the ice to pack the ice and form a mortar-shaped depression, 3) the mortar was removed 4) liquid nitrogen was poured into the ice bucket to keep the ice frozen and cool the mortar, 5) the mortar was placed into the indentation and filled with liquid nitrogen, 6) using personal protective equipment (PPE) like low temperature insulated gloves the mortar was gently rotated to prevent fusion with ice 7) the pestle was placed into the mortar filled halfway with liquid nitrogen to cool mortar and pestle 8) femur sample added. The midshaft was placed in a mortar with liquid nitrogen and ground to powder. Only a fine white powder remained after grinding. The bone powder was added to a 1.5mL microcentrifuge tube with 50µL of Trizol. The mortar and pestle were cleaned with a KimWipe in between samples. Bone powder was mixed with Trizol with a hand homogenizer for 1min. 150µL of Trizol was added and homogenized again. 300µL of Trizol was added, the sample was vortexed, and then centrifuged at 4°C for 10min at 10,000RPM. The supernatant was transferred to a second 1.5mL tube. The process was repeated by adding 50µL, 150µL, and 300µL of Trizol to the pellet after intermittent mixing with a hand homogenizer and vortexer when appropriate. The supernatant was incubated at RT for 5 min. Chloroform was added to the supernatant and shaken for 15s. The aqueous and organic layer were allowed to separate by incubation at RT for 5min. The samples were then centrifuged at 4°C for 10min at 10,000RPM. The aqueous layer (top) was carefully transferred to a third tube. RNA was precipitated by adding 800µL 100% isopropanol. Samples were not disturbed and incubated at RT for 5min. Samples were then centrifuged at 4°C for 15min at max speed (13,200RPM). Supernatant was carefully discarded by decanting into a waste container. 1mL of 75% EtOH was added to each sample and shaken for 15min. Samples were immediately centrifuged at 4°C for 15min at max speed. The supernatant was carefully discarded

by decanting into a waste container and centrifuged again at 4°C for 1min at max speed to consolidate the supernatant. The remaining supernatant was aspirated with a P200 using a fresh tip for each sample. Tubes were left open but covered with a KimWipe for 5min to evaporate the EtOH. RNA was resuspended with 20µL of HPLC grade water and the concentration was quantified by NanoDrop.

Synthesis of cDNA was conductedwith Applied Biosystems TaqMan Reverse Transcriptase Reagents (N8080234) using kit components and provided protocol. In detail, a master mix composed of the 10x buffer (1x Final), $MgCl_2$ (1.75mM), dNTP (2mM), hexamers (2.5mM), RNAse inhibitor (U/µL), and 2.5U/µL MultiScribe Reverse Transcriptase was combined with 1mg total RNA, and water to 40µL total volume per reaction. The PCR protocol provided by the Applied Biosystems was modified by doubling the time during the elongation step. The final protocol was as follows: 10min at 25°C, 60min at 37°C, 5min at 95°C, and a 4°C hold. Products were diluted 1:5 before final storage at -20°C and qPCR analysis.

2.4 Gene Expression Analysis by qPCR

Gene expression was assessed with qPCR by utilizing Applied Biosystems TaqMan Gene Expression Master Mix (4369016) and TaqMan probes for *Rn18s* (Mm03928990_g1), *Dyrk1a* exon 10-11 (Mm00432934_m1). 10µL of cDNA and 40µL of a reaction mix containing the aforementioned AB TaqMan Gene Expression Master Mix (25µL/rxn), the specified probe (2.5µL/rxn), and water (12.5µL/rxn) were loaded into a 96-well plate (Applied Biosystems N8010560) and briefly centrifuged before running on Applied Biosystems 7500 Real-Time PCR System (4351105). The PCR program was as follows: 2min at 50°C (holding stage), 10min at 95°C (holding stage), 15s at 95°C (cycling stage: step 1), 1min at 50°C (cycling stage: step 2), for 40 cycles. The ΔRn threshold was set at 0.1. $\Delta CT = CT_{Dyrk1a} - CT_{Rn18s}$. $\Delta\Delta CT = \Delta CT_{Ts65Dn} - \Delta CT_{WT}$. Fold change$=2^{-\Delta\Delta CT}$.

The normalized reporter (Rn) was defined as the difference between the reporter signal, FAM, and the quencher, ROX. The difference between the Rn of a given cycle and the Rn of the first cycle was defined as ΔRn. The cycle threshold (Ct) of 0.100 was chosen because it was a positive threshold that captured the exponential growth phase for all target genes. The difference between the gene of interest *Dyrk1a* and the housekeeping gene *Rn18s* in a given sample was

defined as ΔCt. Since *Rn18s* expression is conserved between genotypes, the ΔCt calculation produced a value that would be different between genotypes if *Dyrk1a* was overexpressed. The mean of euploid ΔCt values was subtracted from each trisomic ΔCt value to determine ΔΔCt, a value that represents the difference of *Dyrk1a* expression between genotypes. The ΔΔCt of the euploid samples as well as the average of the euploid ΔΔCt values should be close to 0. A negative ΔΔCt value would be produced if a gene was overexpressed; conversely, a positive ΔΔCt value would result if a gene was underexpressed compared to the WT. To make the data easier to interpret, the data was transformed to Fold Change with the calculation $2^{-\Delta\Delta Ct}$. The resulting values can only be positive; overexpression of a gene would be indicated by a value greater than 1, while underexpression of a gene would be indicated by a value between 0 and 1.

2.5 DYRK1A Inhibition in Ts65Dn, *Dyrk1a*$^{+/fl}$ mice

Trials were conducted with CX-4945 (Silmitasertib, purchased from SelleckChem, >99%, Catalog No.S2248) to assure safety of use in a nine-day treatment (P21-P29) and to verify efficacious delivery of the drug. Because CX-4945 was not soluble in PBS at the desired concentration of 75mg/kg/day, it was delivered in either a suspension of 10% DMSO and 90% PBS at 37°C or a suspension of 10% DMSO, 5% Kolliphor (Fisher Scientific, NC0917244), and 85% PBS. Subcutaneous injections were administered at the scruff of the neck and intraperitoneal injections were administered to the belly. These delivery methods resulted in precipitation of the drug beneath the skin, suggesting that dosing was not completely bioavailable using these methods (**Figure 19.**). An oral gavage trial with a 10mM suspension and a 25mM suspension was conducted followed by a subsequent necropsy which revealed no visual signs of precipitated drug in the digestive track. There were no differences in mouse weight during treatment between the groups receiving the 10mM and 25mM suspension. Given these factors, oral gavage with a 25mM suspension was determined to be the most efficacious way to deliver 75mg/kg/day CX-4945.

Ts65Dn, *Dyrk1a*$^{+/fl}$ male mice were treated with 75mg/kg/day CX-4945 as a 10% DMSO/90% PBS suspension delivered via oral gavage. CX-4945 was delivered as a neat yellow/orange powder. A 250mM solution was made with 24.5mg CX-4945 and 280μL DMSO, and gently heated by placing the solution in a 37°C water bath or heat block. The working suspension was made by diluting the stock 250mM DMSO solution to 25mM with PBS to make a suspension (10% total DMSO). The suspension was prepared fresh daily and kept in a 37°C heat

block until administered to experimental mice at 75mg/kg/day via oral gavage from weaning (perinatal day 21) to perinatal day 29. Control animals received a vehicle composed of 10% DMSO and 90% PBS.

2.6 Bone Marrow Stem Cell (BMSC) Isolation

Prior to bone marrow stem cell isolation, collection tubes were prepared as described by Dobson et al. 1999 and Amend et al. 2016: 1) the top of a 500µL microcentrifuge tube was removed with a razor blade so it fits inside a 1.5mL tube 2) a 23g syringe needle was used to make a hole in the bottom of the 500µL tube 3) the 500µL tube was placed inside the 1.5mL tube 4) a 1000µL pipette tip was modified by cutting 1-2mm of the tip with a razor blade 5) the top of the 1000µL tip was cut with a razor blade such that it fit inside the 500µL tube 6) the tubes were assembled and stored in 1000µL tip box modified so the 1.5µL microcentrifuge tubes fit in the holes 7) the tubes were then autoclaved(Amend, Valkenburg, & Pienta, 2016; Dobson, Reading, Haberey, Marine, & Scutt, 1999).

Ts65Dn and WT femurs and tibiae were collected inside a biosafety hood. The proximal and distal ends were removed with scissors to expose the marrow and the midshafts were placed into modified 1.5mL microcentrifuge tube prepared as described above. During the collection from multiple animals, tubes were incubated in a 37°C water bath until the next step. The midshafts were placed in a centrifuge preheated to 37°C and centrifuged at 10,000 RPM for 10 minutes. In a biosafety hood, the tubes were opened, midshafts were stored in separate tubes, and marrow pellets were resuspended with 500µL αMEM (10% FBS, L-glutamine, penicillin/streptomycin, and sodium carbonate). The cell suspension was transferred to a 50mL conical tube along with another 4.5mL αMEM. Cells were counted with a hemocytometer and plated in 1mL αMEM in a 24-well plate at a concentration of $1x10^5$ cells/mL (primary, 1°). The remaining cell suspension was plated on a 6-well plate in a total volume of 2mL/well. After 24 hours, primary cells on 24-well plates were washed with PBS and received fresh αMEM. Cells on the 6-well plates were washed with PBS and lifted with Trypsin. Cells were collected in a total or 2.5mL and counted with a hemocytometer. Cells were then plated in 1mL αMEM in a 24-well plate at a concentration of $1x10^5$ cells/mL (secondary, 2°).

2.7 EdU BMSC Proliferation Assay

BMSC proliferation was assessed by an EdU-based assay. Adherent primary cells were passed and 2° cells were plated the following day in 24-well plates at $1x10^5$ cells/mL with αMEM as described above. Cells were also treated with 10μM CX-4945 in DMSO or with the vehicle (DMSO). 48hrs later, cells were observed to verify growth before exchanging the media for a 1x EdU solution in αMEM and treatments were also administered. 24hrs later cells were fixed with 3.7% formaldehyde for 20 minutes, washed with 3% BSA in PBS, permeabilized with a 0.5% Triton X-100 solution, washed again with 3% BSA in PBS, and treated with the EdU Reaction Cocktail while protected from light for 30 minutes to label proliferating cells. The cells were washed with PBS and stained with a 1x solution of Hoechst stain while protected from light for 30 minutes to label the nuclei. Cells were washed again with PBS and inverted while covered from light for 5 minutes. Plates were wrapped in aluminum foil to protect from light and wrapped in plastic wrap to prevent humidity from forming ice inside the plates. Plates were then stored at -80°C until ready to image.

Cell nuclei stained with Hoechst were counted within a 500μm x 500μm area of proliferating cells in each well using a ZOE fluorescent cell imager (Product number 1450031) at 1x zoom using the blue light setting. Proliferating cells were visualized using the red light setting within the same area as the Hoechst-stained cells. A ratio of proliferating cells to non-proliferating cells was calculated to assess the effect of trisomy and CX-4945 treatment on proliferation of bone marrow stem cells (BMSCs).

2.8 ALP Osteoblast Lysate Assay

Primary cells isolated from femurs of 6-week-old male Ts65Dn and WT mice were seeded on 24-well plates at a concentration of $1x10^5$ cells/mL. Nonadherent cells were washed away with PBS 24 hours later. Cells along the top two rows of the plate received osteoblast differentiation media (αMEM supplemented with 15% FBS, L-glutamine, penicillin/streptomycin, sodium carbonate, dexamethasone, β-galactosidase, and ascorbic acid) only. The third row was additionally treated with 5μL of 2mM CX-4945 in DMSO (final concentration 10μM). The fourth row was additionally treated with 5μL DMSO. Media was replaced and treatments administered twice per week for 14 days. Osteoblast alkaline phosphatase (ALP) activity was assessed with the

abcam Alkaline Phosphatase Assay Kit (Colorimetric; ab83369). Due to limited stability of reagents, cell lysates were obtained by lifting cells from wells with Trypsin, lysing cells by centrifugation at 10,000 RPM followed by homogenization of pellet with tissue homogenizer and assay buffer supplied in kit, followed by centrifugation of sample, collection of the supernatant, and freezing of supernatant. As per the supplied protocol, the thawed supernatants were diluted by a factor of 10, 100, and 1000 before running on the assay. For each reaction, 80µL of the diluted sample and 50µL of 5mM pNPP substrate were added to each sample well on a 96-well flat-bottom plate and incubated for 60min at RT protected from light by aluminum foil. After incubation, 20µL of the kit-supplied stop buffer was added to the reaction. Absorbance values were obtained by a plate spectrophotometer set to measure the optical density (OD) at 405nm. ALP activity was calculated as: ALP = [B/(ΔT*V)*D], where B is the amount of pNP in sample calculated by the standard curve, ΔT is the reaction time (60min), V is the original sample volume (0.080mL), and D is the dilution factor (10, 100, or 1000). Units are defined as µmol/min/mL or U/mL. Cell lysate dilutions were plated in duplicate and averaged to give the ALP activity for each well of the 24-well plate.

2.9 Osteoblast Mineralization Assay

Osteoblast mineralization assessment was conducted based on the protocol described by Gregory CA et al(Gregory, Gunn, Peister, & Prockop, 2004). Briefly, primary cells isolated from femurs of 6-week-old male Ts65Dn and WT mice were seeded on 24-well plates at a concentration of $1x10^5$ cells/mL. Nonadherent cells were washed away with PBS 24 hours later. Cells along the top row of the plate received standard media (αMEM supplemented with 10% FBS, L-glutamine, penicillin/streptomycin, and sodium carbonate) and the remainder of the cells received osteoblast differentiation media (αMEM supplemented with 15% FBS, L-glutamine, penicillin/streptomycin, sodium carbonate, dexamethasone, β-galactosidase, and ascorbic acid). The third row was treated with 5µL of 2mM CX-4945 in DMSO (final concentration 10µM). The fourth row was treated with 5µL DMSO. Media was replaced and treatments administered every other day for 21 days. Cells were then washed 3x with PBS, fixed with 70% EtOH for 30 minutes on a platform shaker, and rinsed 3x with diH_2O. Plates inverted and allowed to dry for 15 minutes, then 1mL of 40mM Alizerin Red S was added to each well. Plates were incubated at RT for 30 minutes on a platform shaker. Alizerin Red S was aspirated from each well with a P1000 and each well was rinsed 5

times with diH_2O or until rinse was clear. Plates were inverted to dry for 15 minutes. Plates were photographed and stored at -20°C until quantification. Frozen plates were inverted and allowed to acclimate to RT before proceeding with quantification. 200µL 10% acetic acid was added to each well and placed on a shaker for 30 minutes at RT. A P1000 was used to scrape the contents of each well and transfer contents to a 1.5mL microcentrifuge tube. Tubes were vortexed for 30 seconds to homogenize the sample. 200µL mineral oil was added to each tube and placed on a heat block preheated to 85°C for 10 minutes. Tubes were then placed on ice for 5 minutes. Tubes were then centrifuged at max speed for 15 minutes. 200µL of the supernatant (beneath the oil layer) was transferred to a new 1.5mL microcentrifuge tube. In a chemical hood, 75µL 10% ammonium hydroxide was added to each tube, changing the color of the liquid to a purple shade. 150µL of the sample was then transferred to a well in a 96-well plate. The absorbance at 405nm was analyzed in a spectroscopic plate reader to quantify mineralization.

2.10 Gene Expression Analysis of Osteogenic Genes

The expression of a panel of osteogenic genes was assessed in RNA from femurs of euploid and trisomic Ts65Dn, *Dyrk1a*$^{+/fl}$ male mice aged to P30. RNA was isolated as described previously. cDNA was synthesized using TaqMan Reverse Transcription Kit as previously described. qPCR was performed with Applied Biosystems TaqMan Gene Expression Master Mix (4369016) and TaqMan probes for *Rn18s* (Mm03928990_g1), *Dyrk1a* exon 10-11 (Mm00432934_m1), *Bglap* (Mm03413826_mH), *Runx2* (Mm00501584_m1), *Rbl2* (Mm01242468_m1), and *Alpl* (Mm00475834_m1). 10µL of cDNA and 40µL of a reaction mix containing the aforementioned AB TaqMan Gene Expression Master Mix (25µL/rxn), the specified probe (2.5µL/rxn), and water (12.5µL/rxn) were loaded into a 96-well plate (Applied Biosystems, N8010560) and briefly centrifuged before running on Applied Biosystems 7500 Real-Time PCR System (4351105). The PCR program was as follows: 2min at 50°C (holding stage), 10min at 95°C (holding stage), 15s at 95°C (cycling stage: step 1), 1min at 50°C (cycling stage: step 2), for 40 cycles. The ΔRn threshold was set at 0.1. $\Delta CT = CT_{Dyrk1a} - CT_{Rn18s}$. $\Delta\Delta CT = \Delta CT_{Ts65Dn} - \Delta CT_{WT}$. Fold change=$2^{-\Delta\Delta CT}$.

2.11 Statistical Analyses

Statistical analyses were performed with GraphPad Prism 9.0.1. For the characterization of the Ts65Dn skeletal development experiment, a two-way ANOVA and Tukey's post hoc analysis was utilized to determine interactions between genotype and age. Differences were identified and individual measurements were then assessed at each age with a one-tailed t-test. A two-way ANOVA and Tukey's post hoc analysis was used for DYRK1A inhibition, conditional *Dyrk1a* gene dosage reduction, and congenital *Dyrk1a* gene dosage reduction experiments. Cell culture and osteogenic gene expression also utilized a two-way ANOVA and Tukey's post hoc analysis. Unpaired one-tailed t tests were used to determine the discrepancy observed in the P30 osteogenic gene analysis group assessing *Dyrk1a* expression. A subsequent cross-sectional analysis of %BV/TV at P30 across studies utilized a two-way ANOVA and Tukey's post hoc analysis.

CHAPTER 3. RESULTS

3.1 Characterizing the Emergence of an Aberrant Appendicular Skeletal Phenotype in Male Ts65Dn Mice

A major gap exists in the current knowledge base where skeletal development of male Ts65Dn mice is concerned. To date, skeletal defects have been identified in five ages: embryonic day 17.5 (E17.5)(Blazek, Malik, et al., 2015), postnatal day 42 (P42)(Blazek, Abeysekera, et al., 2015), three months (3M)(Fowler et al., 2012), 4M(Blazek et al., 2011), and 24M(Fowler et al., 2012). Trabecular defects were assessed and reported at P42, 3M, 4M and 24M, but the 3M and 24M study did not assess cortical bone geometry. The P42 study also reported rescue of trabecular defects and cortical cross-sectional area when *Dyrk1a* gene dosage was reduced in otherwise trisomic male Ts65Dn mice. Treatment with a DYRK1A inhibitor EGCG at 9mg/kg/day in drinking water also improved trabecular phenotypes but failed to affect cortical phenotypes(Blazek, Abeysekera, et al., 2015). To fill this gap in knowledge and characterize femur development in male Ts65Dn mice, euploid (Eu) and trisomic (Ts) male mice were aged to P12, P15, P18, P24, P27, P30, P42 (**Table 1**). At each age right femurs were analyzed by microcomputed tomography (μCT). Graphs of trabecular measures are reported in **Figure 1** and cortical measures are reported in **Figure 2**. Femurs collected at P6 were not used because the mineralized tissue did not meet minimal requirements for μCT analysis.

Characterization of Ts65Dn

Femur Development

Sample Size		
Age	**Euploid**	**Ts65Dn**
P12	11	8
P15	11	10
P18	11	8
P24	12	13
P27	10	9
P30	9	14
P42	10	10

Table 1. Sample sizes for each age of trabecular and cortical analysis in male Ts65Dn femurs

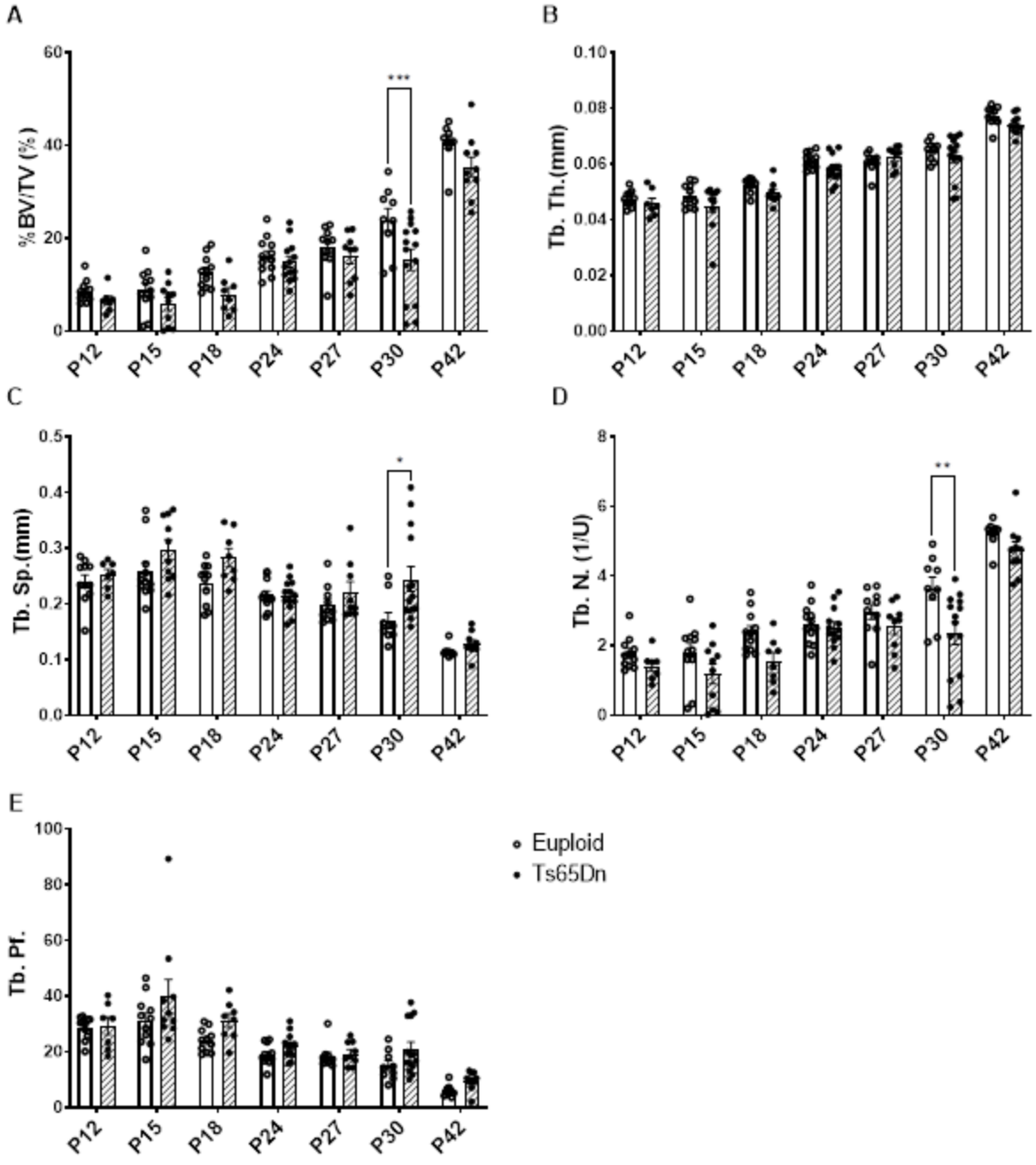

Figure 1. Male Ts65Dn femur trabecular measures during development. Bars are means, error bars are SEM. Two-way ANOVA. Tukey's post hoc *p≤0.01, **p≤0.001, ***p≤0.0001

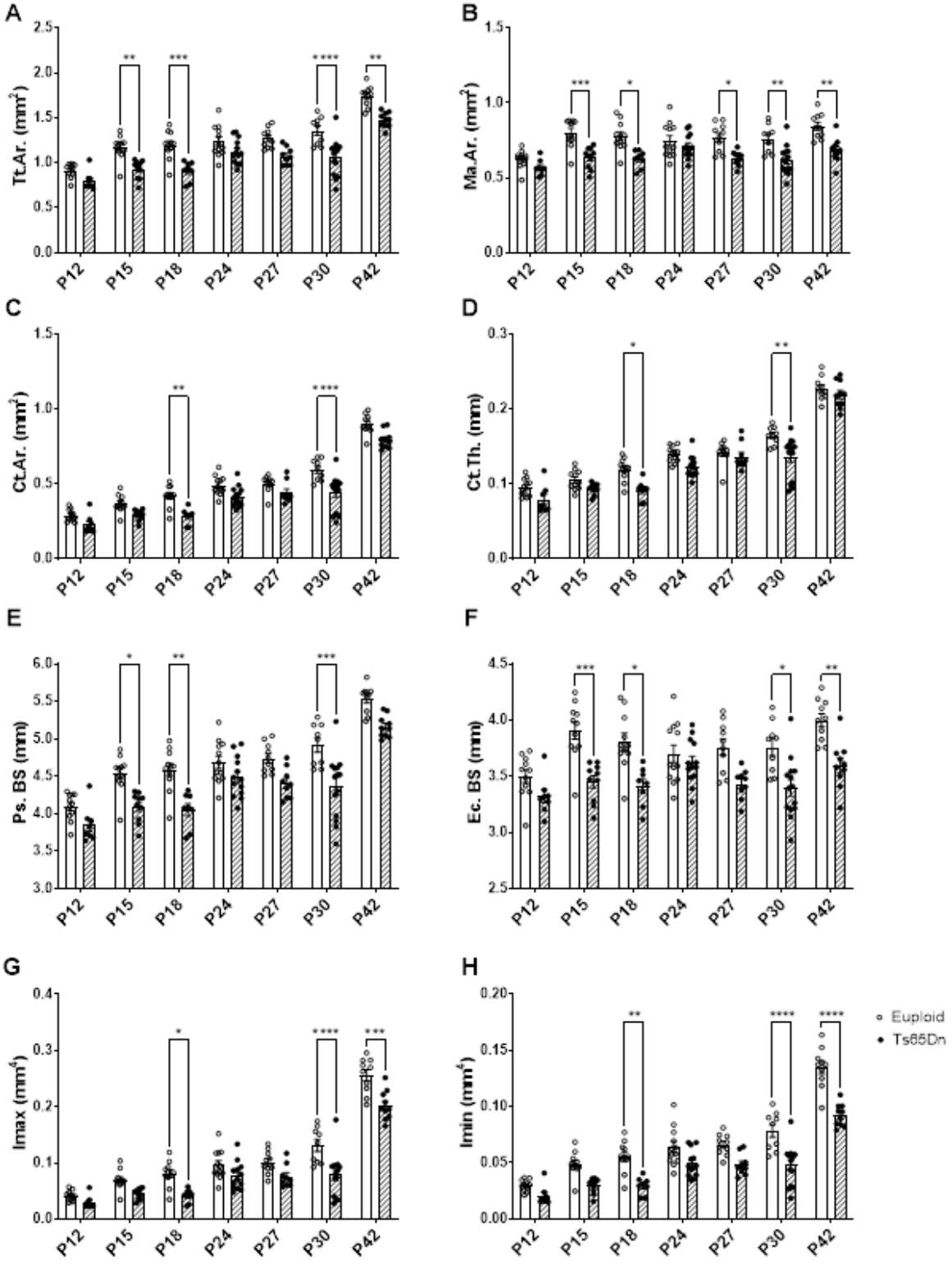

Figure 2. Male Ts65Dn femur cortical measures during development. Bars are means, error bars are SEM. Two-way ANOVA, Tukey's post hoc *p≤0.01, **p≤0.001, ***p≤0.0001

Figure 2. continued

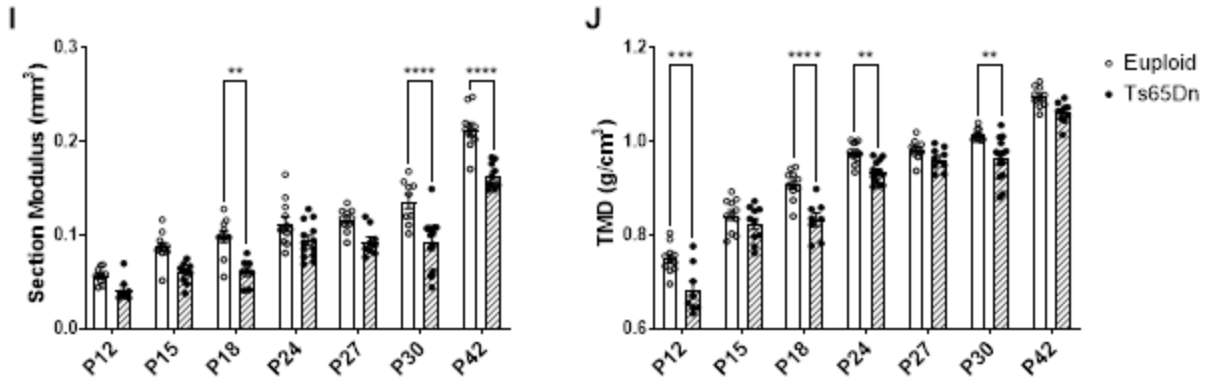

3.1.1 Grouped Femur Analysis

To determine main effects of genotype and age, two-way ANOVA and Tukey's post hoc multiple comparison tests were performed on trabecular and cortical femur geometry. Main effects of genotype and age were found for every measure (**Table 2.**). Interactive effects were found in Ma.Ar. ($p=0.0510$), Ec.BS ($p=0.0487$), Imax ($p=0.0322$), Imin ($p=0.0012$), Section Modulus ($p=0.0174$), and TMD ($p=0.0479$). These findings merited a detailed approach to analyze the genotype effects for each measure at each age.

Table 2. ANOVA results table for comparisons between Euploid and Ts65Dn trabecular and cortical geometry measures. [a] Main effect of genotype; [b] Main effect of age; [c] Interactive effect

Measure	Source of Variation		
	Genotype	Age	Interaction
%BV/TV [a b]	F (1, 131) = 19.64, p<0.0001	F (6, 131) = 84.69, p<0.0001	F (6, 131) = 1.358, p=0.2363
Tb.Th. [a b]	F (1, 131) = 7.439, p=0.0073	F (6, 131) = 96.54, p<0.0001	F (6, 131) = 0.7213, p=0.6331
Tb.Sp. [a b]	F (1, 131) = 15.52, p=0.0001	F (6, 131) = 26.01, p<0.0001	F (6, 131) = 1.757, p=0.1129
Tb.N. [a b]	F (1, 131) = 21.72, p<0.0001	F (6, 131) = 50.50, p<0.0001	F (6, 131) = 1.444, p=0.2025
Tb.Pf. [a b]	F (1, 131) = 11.45, p=0.0009	F (6, 131) = 29.51, p<0.0001	F (6, 131) = 0.8196, p=0.5566
Tt.Ar. [a b]	F (1, 132) = 94.13, p<0.0001	F (6, 132) = 58.17, p<0.0001	F (6, 132) = 1.745, p=0.1155
Ma.Ar. [a b]	F (1, 132) = 76.27, p<0.0001	F (6, 132) = 7.262, p<0.0001	F (6, 132) = 2.158, p=0.0510
Ct.Ar. [a b]	F (1, 132) = 69.71, p<0.0001	F (6, 132) = 156.3, p<0.0001	F (6, 132) = 1.513, p=0.1788
Ct.Th. [a b]	F (1, 132) = 37.91, p<0.0001	F (6, 132) = 161.0, p<0.0001	F (6, 132) = 1.636, p=0.1420
Ps.BS [a b]	F (1, 132) = 78.15, p<0.0001	F (6, 132) = 53.04, p<0.0001	F (6, 132) = 1.480, p=0.1897
Ec.BS [a b,c]	F (1, 132) = 73.44, p<0.0001	F (6, 132) = 5.617, p<0.0001	F (6, 132) = 2.181, p=0.0487
Imax[a b,c]	F (1, 132) = 65.65, p<0.0001	F (6, 132) = 140.5, p<0.0001	F (6, 132) = 2.383, p=0.0322
Imin [a b,c]	F (1, 132) = 115.0, p<0.0001	F (6, 132) = 96.64, p<0.0001	F (6, 132) = 3.938, p=0.0012
Section Modulus [a b,c]	F (1, 132) = 101.0, p<0.0001	F (6, 132) = 112.8, p<0.0001	F (6, 132) = 2.680, p=0.0174
TMD [a b,c]	F (1, 132) = 68.68, p<0.0001	F (6, 132) = 276.2, p<0.0001	F (6, 132) = 2.190, p=0.0479

3.1.2 P12 Skeletal Analysis

In P12 male Ts65Dn mice, unpaired one-tailed t-tests showed significant reductions in Total Cross-Sectional Area (Tt.Ar.) [t(17)=2.911, p=0.0049] (**Figure 4A**), Marrow Area (Ma.Ar) [t(17)=2.206, p=0.0207] (**Figure 4B**), Cortical Area (Ct.Ar) [t(17)=2.674, p=0.0080] (**Figure 4C**), Cortical Thickness (Ct.Th) [t(17)=2.359, p=0.0153] (**Figure 4D**), Periosteal Bone Surface (Ps.BS) [t(17)=2.584, p=0.0097] (**Figure 4E**), Endocortical Bone Surface (Ec.BS) [t(17)=2.088, p=0.0261] (**Figure 4F**), Maximum Polar Moment of Inertia (Imax) [t(17)=2.563, p=0.0101] (**Figure 4G**), Minimum Polar Moment of Inertia (Imin) [t(17)=2.884, p=0.0052] (**Figure 4H**), Section Modulus [t(17)=3.304, p=0.0021] (**Figure 4I**), and Tissue Mineral Density (TMD) [t(17)=3.450, p=0.0015] (**Figure 4J**) compared to Euploid male mice. Percent Bone Volume (%BV/TV) [t(16)=1.642, p=0.0600] (**Figure 3A**) and Trabecular Number (Tb.N) [t(16)=1.735, p=0.0510] (**Figure 3D**) were reduced in Ts65Dn compared to Euploid but did not reach statistical significance. No differences in Trabecular Thickness (Tb.Th) [t(16)=0.9191, p=0.1858] (**Figure 3B**), Trabecular Separation (Tb.Sp) [t(16)=0.7475, p=0.2328] (**Figure 3C**), and Trabecular Pattern Factor (Tb.Pf.) [t(16)=0.1349, p=0.4472] (**Figure 3E**). These results suggest that the skeletal defects characteristic of P42 male mice reported previously (reduced %BV/TV, Tb.Th, Tb.N and increased Tb.Sp)(Blazek, Abeysekera, et al., 2015) are present at P12, but not to the degree that was reported at P42. These data were the first to suggest that skeletal phenotypes get worse during development.

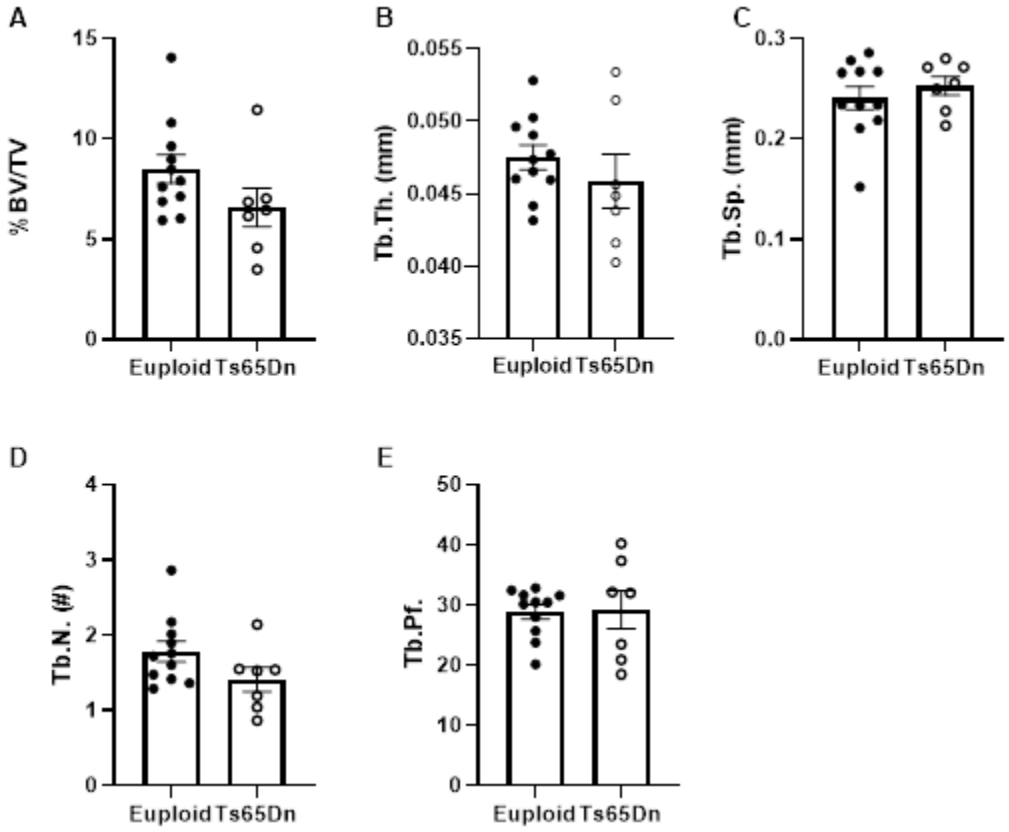

Figure 3. P12 trabecular geometry of Ts65Dn mice. Unpaired one-tailed t test *p≤0.01, **p≤0.001, ***p≤0.0001

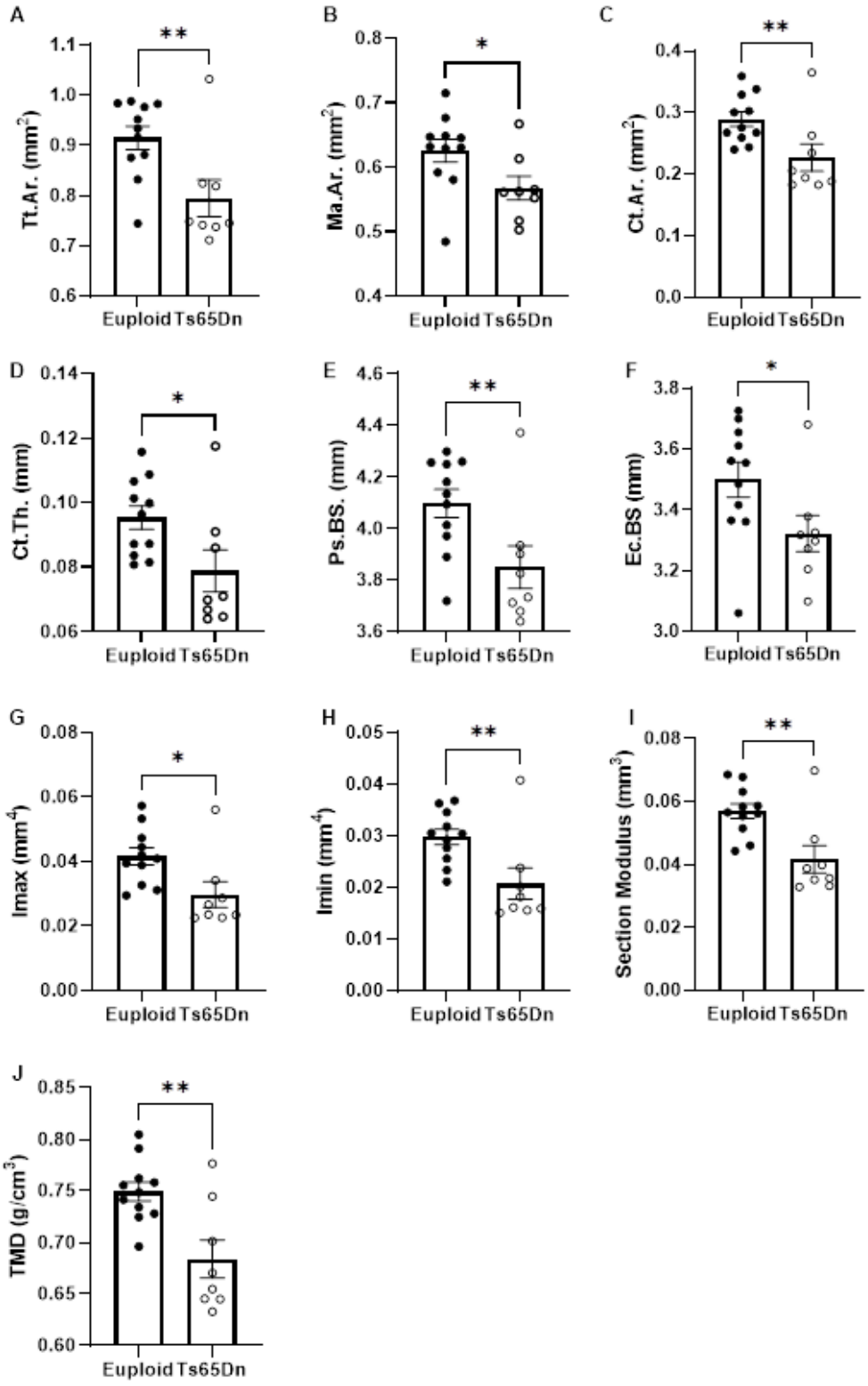

Figure 4. P12 cortical geometry of Ts65Dn mice. Unpaired one-tailed t test *p≤0.01, **p≤0.001, ***p≤0.0001

3.1.3 P15 Skeletal Analysis

Unpaired one-tailed t-tests showed significant reductions in the following measures in P15 male Ts65Dn mice: Tt.Ar. [t(19)=4.692, p<0.0001] (**Figure 6A**), Ma.Ar. [t(19)=4.621, p<0.0001] (**Figure 6B**), Ct.Ar. [t(19)=3.624, p=0.0009] (**Figure 6C**), Ct.Th. [t(19)=2.474, p=0.0115] (**Figure 6D**), Ps.BS. [t(19)=4.529, p=0.0001] (**Figure 6E**), Ec.BS [t(19)=4.770, p=0.0001] (**Figure 6F**), Imax [t(19)=3.993, p=0.0004] (**Figure 6G**), Imin [t(19)=4.853, p<0.0001] (**Figure 6H**), and Section Modulus [t(19)=4.656, p<0.0001] (**Figure 6I**). %BV/TV [t(19)=1.497, p=0.0755] (**Figure 5A**) and Tb.N. [t(19)=1.546, p=0.0693] (**Figure 5D**) were decreased but did not reach statistical significance. Tb.Sp. [t(19)=1.666, p=0.0560] (**Figure 5C**) was increased in Ts65Dn but also failed to reach statistical significance. There were no differences in Tb.Th. [t(19)=1.267, p=0.1102] (**Figure 5B**), Tb.Pf. [t(19)=1.348, p=0.0967] (**Figure 5E**), and TMD [t(19)=1.203, p=0.1219] (**Figure 6J**) in male Ts65Dn mice at 15 days of age. Like P12, these results suggest that the skeletal phenotype observed at P15 resembles the skeletal phenotype at P42, but not to the same degree. These data provide more evidence that skeletal phenotypes get worse during development.

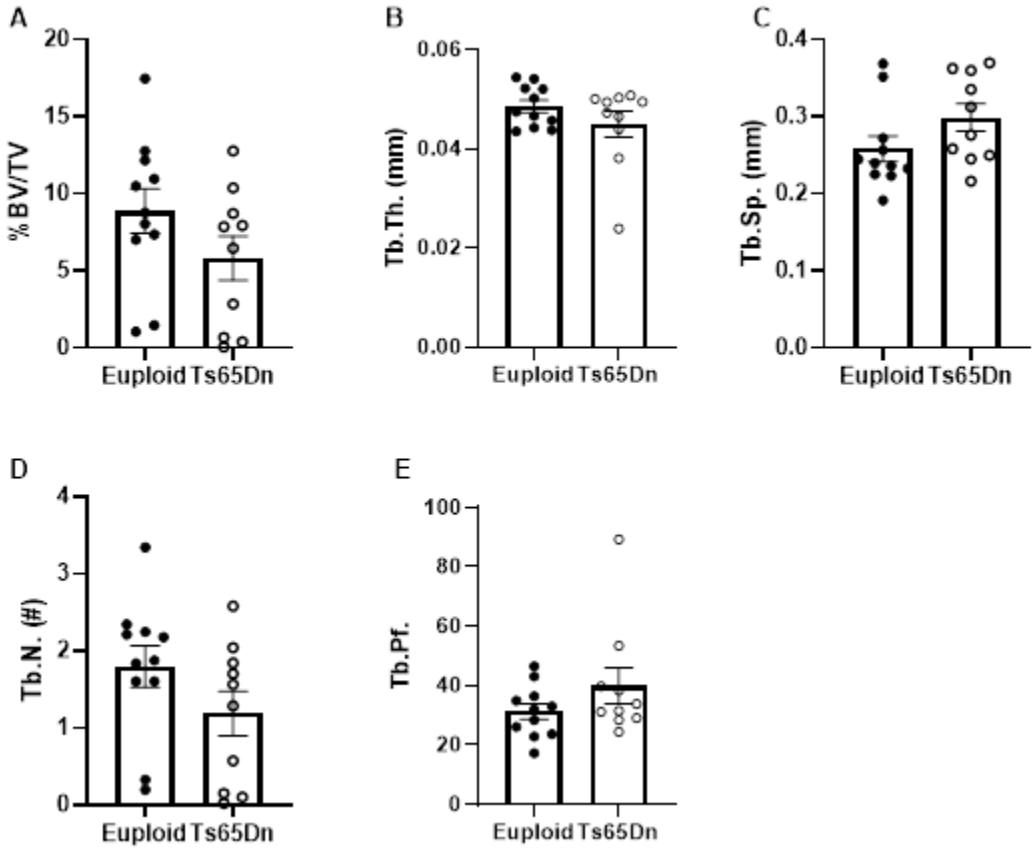

Figure 5. P15 trabecular geometry of Ts65Dn mice. Unpaired one-tailed t test *p≤0.01, **p≤0.001, ***p≤0.0001

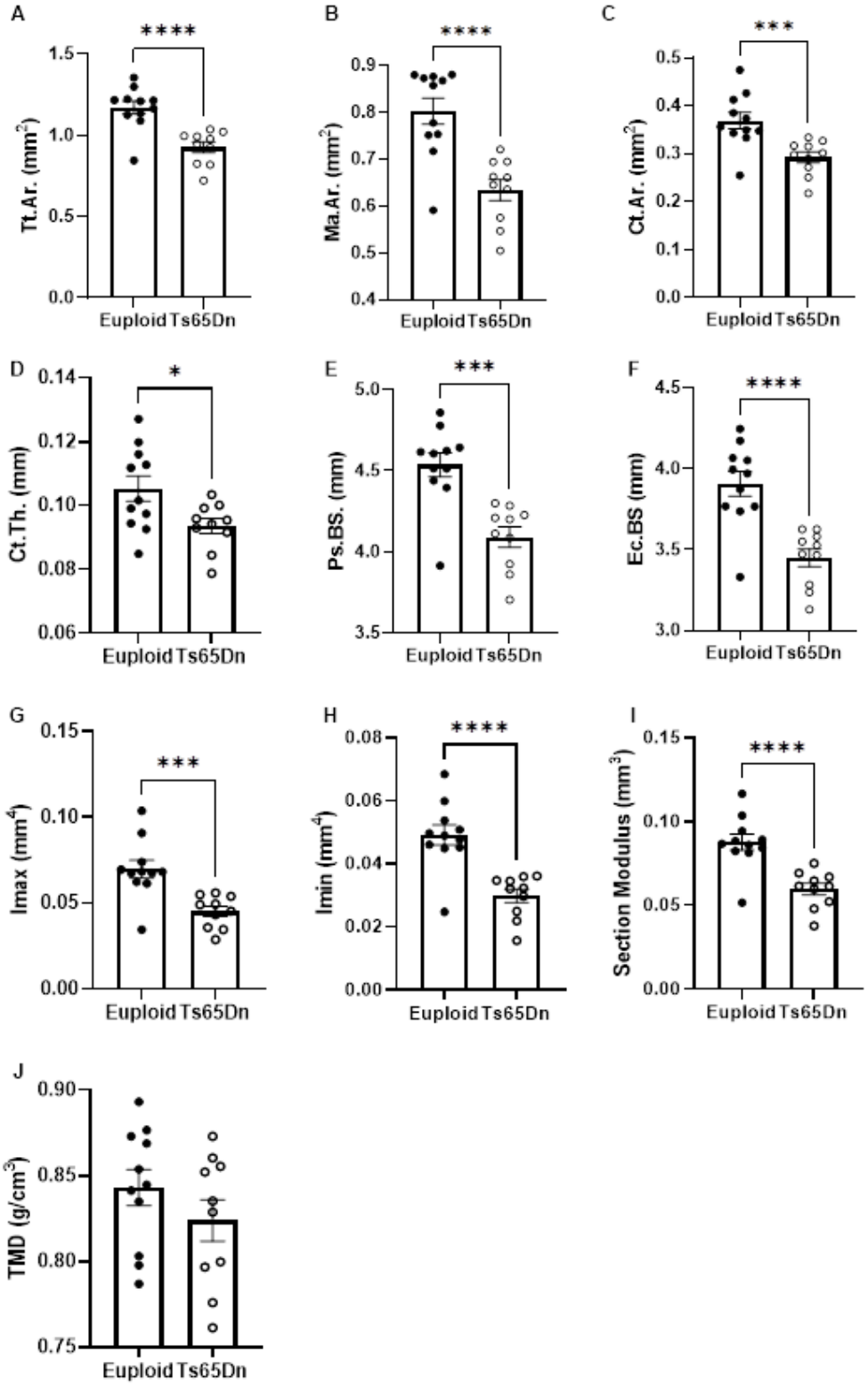

Figure 6. P15 cortical geometry of Ts65Dn mice. Unpaired one-tailed t test *p≤0.01, **p≤0.001, ***p≤0.0001

3.1.4 P18 Skeletal Analysis

Unpaired one-tailed t-tests showed significant defects in all trabecular and cortical geometry measures in male Ts65Dn mice. %BV/TV [t(17)=2.738, p=0.0070] (**Figure 7A**), Tb.Th. [t(17)=1.990, p=0.0315] (**Figure 7B**), Tb.N. [t(17)=2.834, p=0.0057] (**Figure 7D**) were reduced in Ts65Dn males at P18. Tb.Sp. [t(17)=2.408, p=0.0138] (**Figure 7C**) and Tb.Pf. [t(17)=2.755, p=0.0068] (**Figure 7E**) were increased in Ts65Dn. The cortical measures Tt.Ar. [t(17)=4.570, p=0.0001] (**Figure 8A**), Ma.Ar. [t(17)=3.977, p=0.0005] (**Figure 8B**), Ct.Ar. [t(17)=4.662, p=0.0001] (**Figure 8C**), Ct.Th. [t(17)=4.323, p=0.0002] (**Figure 8D**), Ps.BS. [t(17)=4.330, p=0.0002] (**Figure 8E**), Ec.BS [t(17)=3.762, p=0.0008] (**Figure 8F**), Imax [t(17)=4.514, p=0.0002] (**Figure 8G**), Imin [t(17)=4.847, p<0.0001] (**Figure 8H**), Section Modulus [t(17)=4.608, p=0.0001] (**Figure 8I**), and TMD [t(17)=4.615, p=0.0001] (**Figure 8J**) were all compromised in Ts65Dn mice compared to Euploid mice. Qualitatively, these results match the differences in trabecular and cortical phenotype between male Euploid and Ts65Dn mice reported at P42(Blazek, Abeysekera, et al., 2015), suggesting that trabecular skeletal defects emerge at P18.

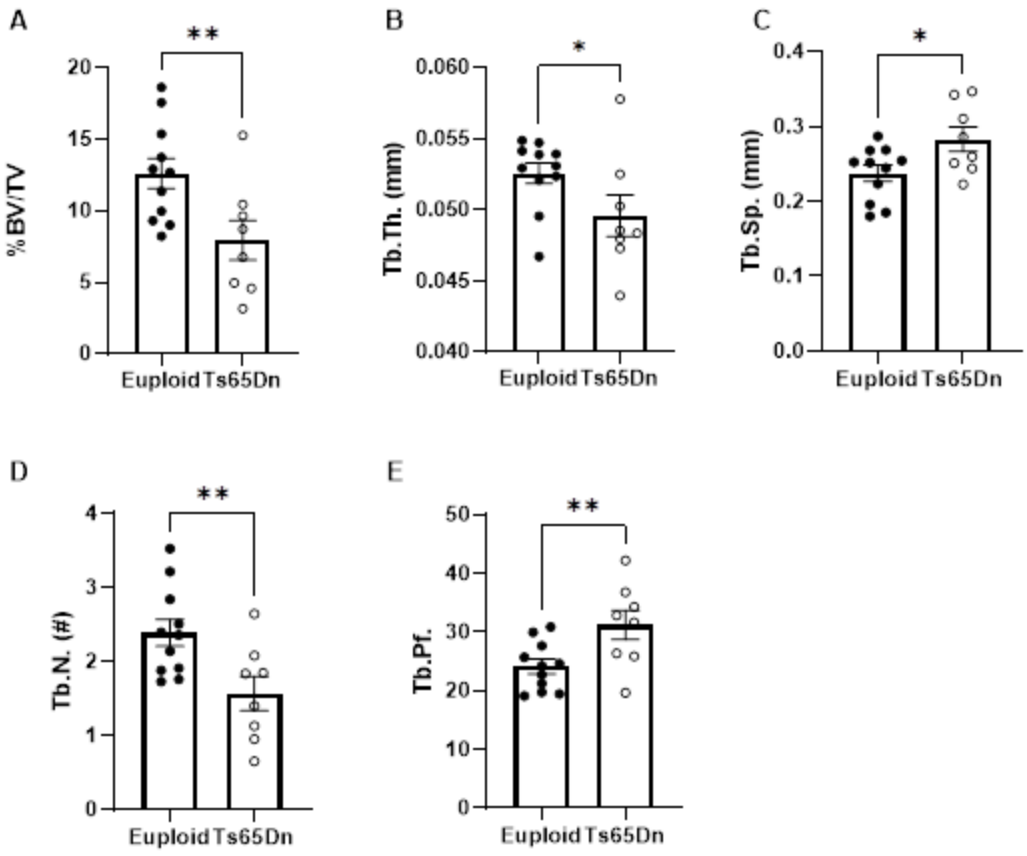

Figure 7. P18 trabecular geometry of Ts65Dn mice. Unpaired one-tailed t test *p≤0.01, **p≤0.001, ***p≤0.0001

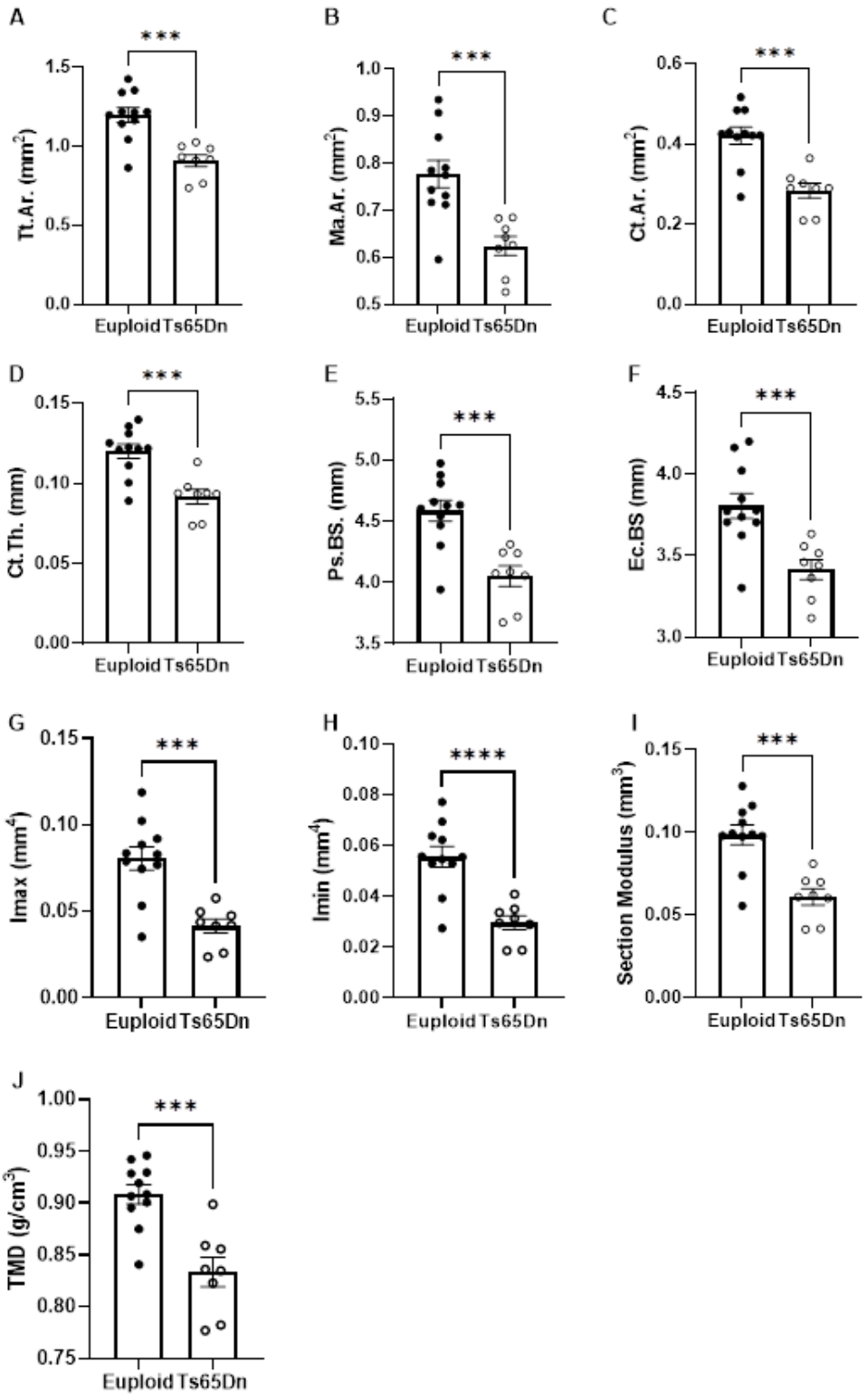

Figure 8. P18 cortical geometry of male Ts65Dn mice. Unpaired one-tailed t test *p≤0.01, **p≤0.001, ***p≤0.0001

3.1.5 P24 Skeletal Analysis

Unpaired one-tailed t-tests showed significant defects in P24 male Ts65Dn mice including: increased Tb.Pf [f(23)=1.961, p=0.0310] (**Figure 9E**), Tb.Th [t(23)=1.918, p=0.0338] (**Figure 9B**), Tt.Ar [t(23)=1.818, p=0.0411] (**Figure 10A**), Ct.Ar [t(23)=2.853, p=0.0045] (**Figure 10C**), Ct.Th [t(23)=3.349, p=0.0014] (**Figure 10D**), Ps.BS [t(23)=1.770, p=0.0450] (**Figure 10E**), Imax [t(23)=1.962, p=0.0310] (**Figure 10G**), Imin [t(23)=2.495, p=0.0101] (**Figure 10H**), Section Modulus [t(23)=2.171, p=0.0203] (**Figure 10I**), and TMD [t(23)=4.654, p<0.0001] (**Figure 10J**) in Ts65Dn femurs compared to Euploid. Analysis determined that there were no differences in %BV/TV [t(23)=0.7919, p=0.2183] (**Figure 9A**), Tb.Sp [t(23)=0.07676, p=0.4697] (**Figure 9C**), Tb.N [t(23)=0.4623, p=0.3241] (**Figure 9D**), Ma.Ar [t(23)=0.9479, p=0.1765] (**Figure 10B**), Ec.BS [t(23)=0.8094, p=0.2133] (**Figure 10F**), and in male Ts65Dn mice at 24 days of age. This is the first age that a defect in Tb.Th emerges. Trabecular measures in Ts65Dn seem to have caught up with Euploid at P24. The disappearance of the skeletal phenotype was unexpected and suggests differentially regulated genetic mechanisms that result in increased growth between P18 and P24 in Ts65Dn male mice. The increased growth rate leads to improved trabecular %BV/TB, Tb.Sp, and Tb.N at P24. With the exception of Ma.Ar and Ec.BS, cortical defects remain present in Ts65Dn at P24.

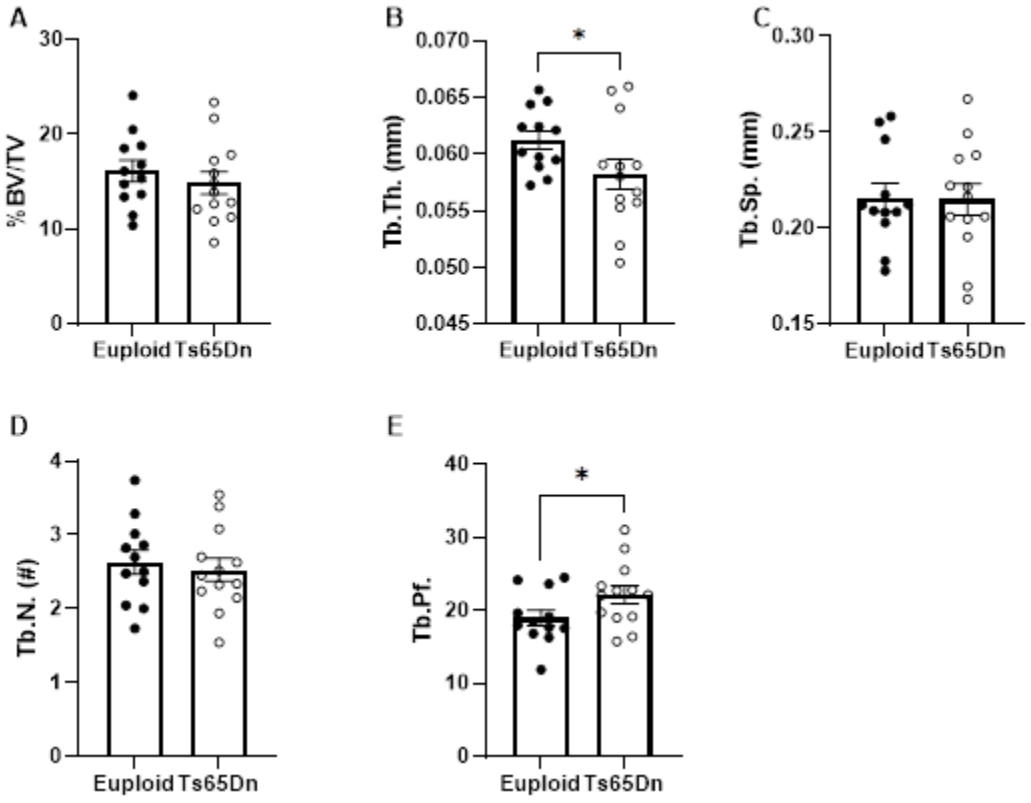

Figure 9. P24 trabecular geometry of male Ts65Dn mice. Unpaired one-tailed t test *p≤0.01, **p≤0.001, ***p≤0.0001

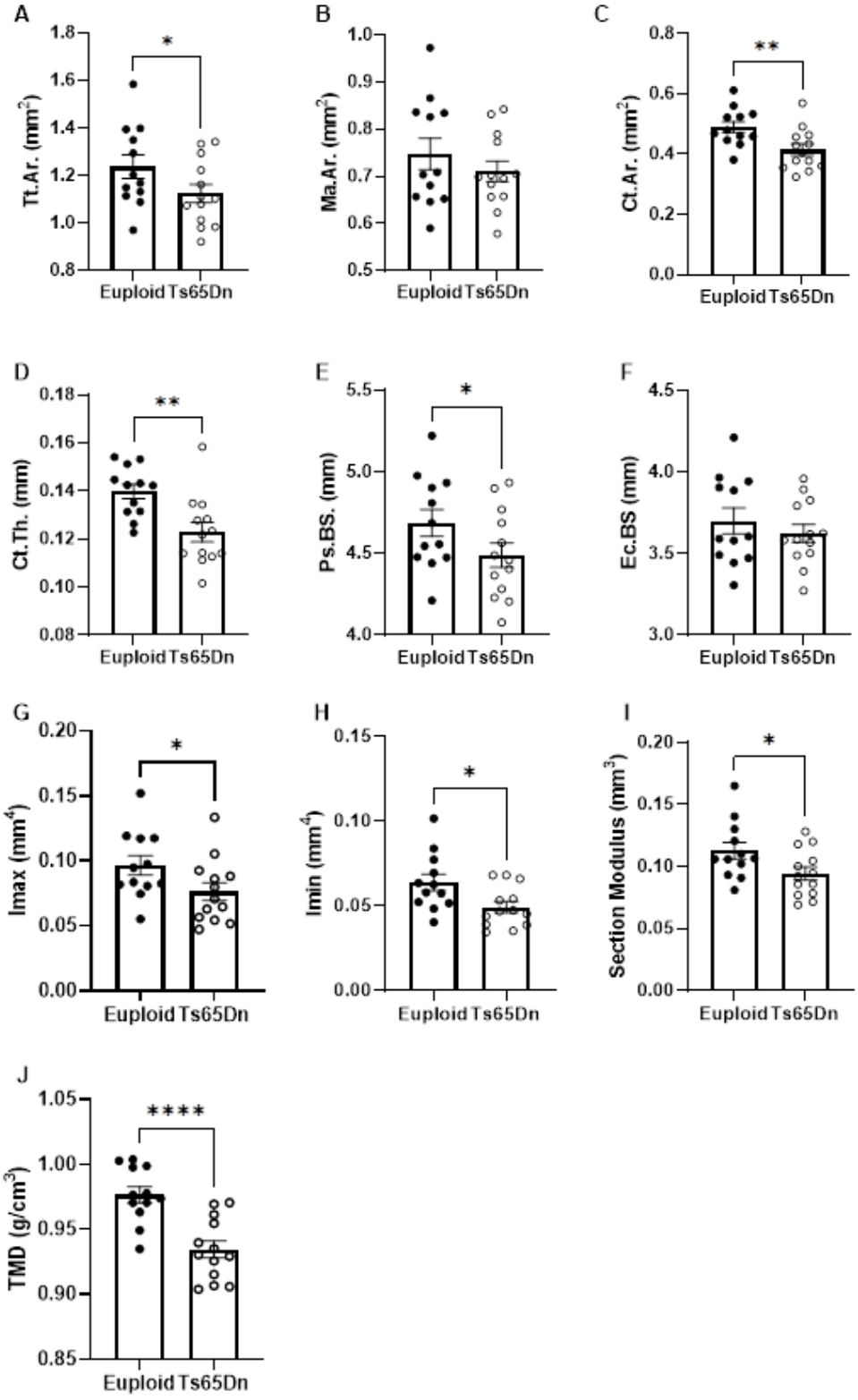

Figure 10. P24 cortical geometry of male Ts65Dn mice. Unpaired one-tailed t test *p≤0.01, **p≤0.001, ***p≤0.0001

3.1.6 P27 Skeletal Analysis

Unpaired one-tailed t-tests in male Ts65Dn mice at 27 days of age showed significant defects in most cortical measures including: Tt.Ar. [t(17)=4.157, p=0.0003] (**Figure 12.A**), Ma.Ar. [t(17)=3.998, p=0.0005] (**Figure 12.B**), Ct.Ar. [t(17)=2.052, p=0.0279] (**Figure 12.C**), Ps.BS. [t(17)=3.640, p=0.0010] (**Figure 12.E**), Ec.BS [t(17)=3.771, p=0.0008] (**Figure 12.F**), Imax [t(17)=2.709, p=0.0075] (**Figure 12.G**), Imin [t(17)=4.116, p=0.0004] (**Figure 12.H**), Section Modulus [t(17)=3.774, p=0.0008] (**Figure 12.I**), and TMD [t(17)=1.956, p=0.0335] (**Figure 12.J**). There were no differences in %BV/TV [t(17)=0.9048, p=0.1891] (**Figure 11.A**), Tb.Th. [t(17)=1.012, p=0.1630] (**Figure 11.B**), Tb.Sp. [t(17)=1.146, p=0.1339] (**Figure 11.C**), Tb.N. [t(17)=1.309, p=0.1039] (**Figure 11.D**), Tb.Pf. [t(17)=0.5095, p=0.3085] (**Figure 11.E**), Ct.Th. [t(17)=0.7272, p=0.2385] (**Figure 12.D**). Similar to P24, trabecular measures were not compromised at P27. Cortical defects remain with the exception of Ct.Th. These results suggest that the expected trabecular defects reported at P42(Blazek, Abeysekera, et al., 2015) must reemerge at a later age.

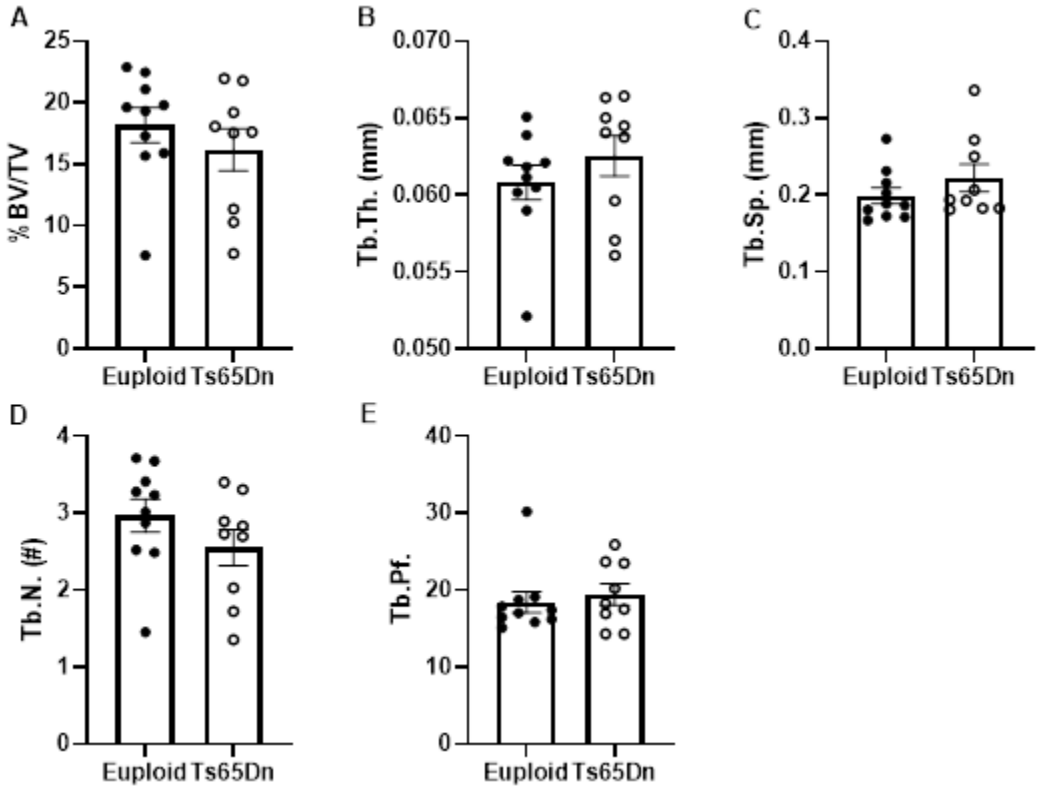

Figure 11. P27 trabecular geometry of male Ts65Dn mice. Unpaired one-tailed t test *p≤0.01, **p≤0.001, ***p≤0.0001

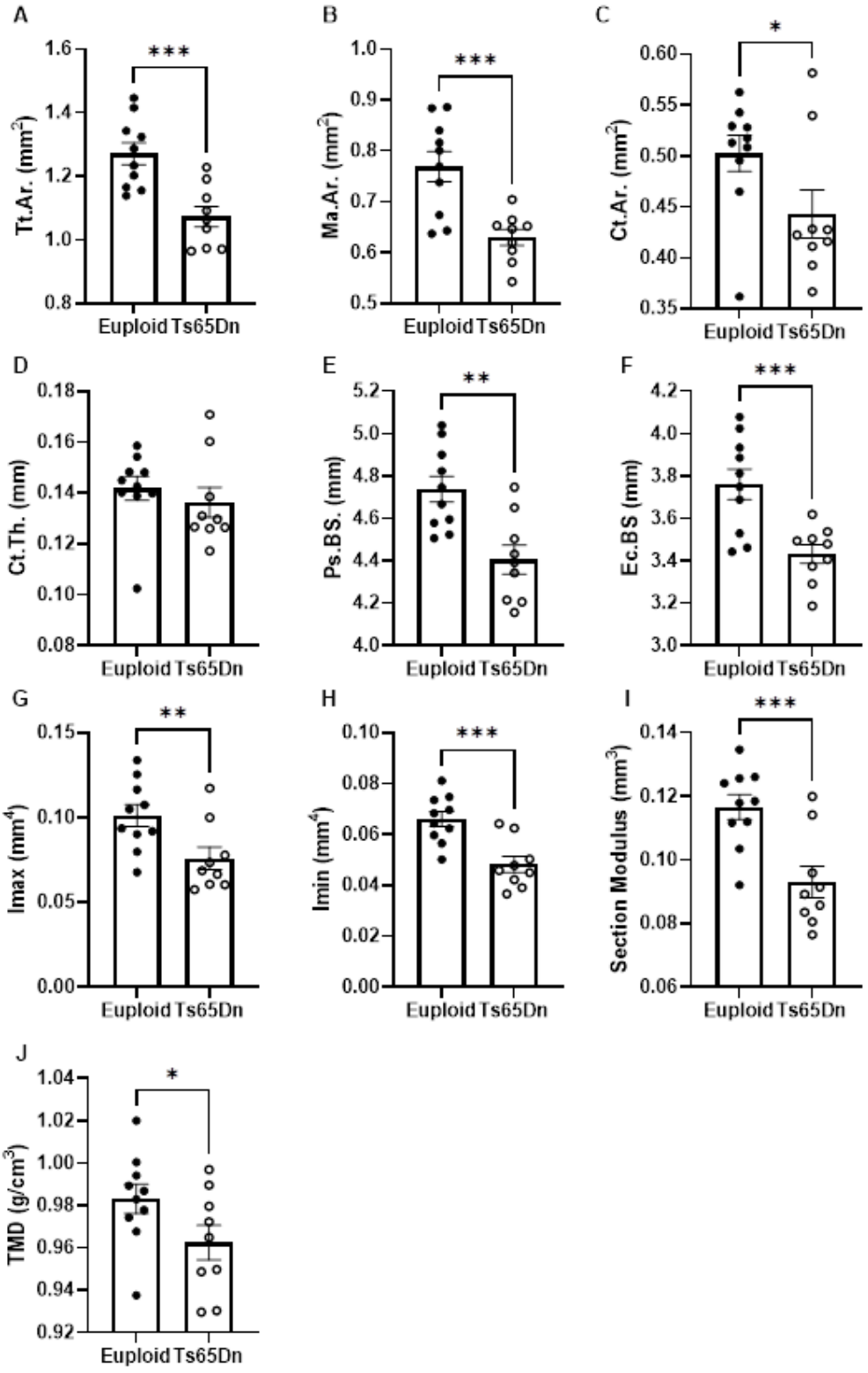

Figure 12. P27 cortical geometry of male Ts65Dn mice. Unpaired one-tailed t test *p≤0.01, **p≤0.001, ***p≤0.0001

3.1.7 P30 Skeletal Analysis

Unpaired one-tailed t-tests showed significant defects in almost all measures in P30 male Ts65Dn mice: increased Tb.Sp. [t(21)=2.482, p=0.0108] (**Figure 13.C**) and Tb.Pf. [t(21)=1.744, p=0.0479] (**Figure 13.E**), reduced %BV/TV [t(21)=2.505, p=0.0103] (**Figure 13.A**), Tb.N. [t(21)=2.717, p=0.0065] (**Figure 13.D**), Tt.Ar. [t(21)=3.678, p=0.0007] (**Figure 14A**), Ma.Ar. [t(21)=3.556, p=0.0009] (**Figure 14B**), Ct.Ar. [t(21)=3.467, p=0.0012] (**Figure 14C**), Ct.Th. [t(21)=2.937, p=0.0039] (**Figure 14D**), Ps.BS. [t(21)=3.405, p=0.0013] (**Figure 14E**), Ec.BS [t(21)=3.356, p=0.0015] (**Figure 14F**), Imax [t(21)=3.399, p=0.0014] (**Figure 14G**), Imin [t(21)=4.075, p=0.0003] (**Figure 14H**), Section Modulus [t(21)=3.934, p=0.0004] (**Figure 14I**), and TMD [t(21)=3.258, p=0.0019] (**Figure 14J**). The only measure that did not reach statistical significance was Tb.Th. [t(21)=0.9045, p=0.1880] (**Figure 13.B**). These results suggest that Euploid mice experience an increased growth rate between P27 and P30, while the growth rate of Ts65Dn males remains static. The increased growth of Euploid femurs affected almost all measures except Tb.Th, the only defect present at P42 in male Ts65Dn mice that has yet to reemerge.

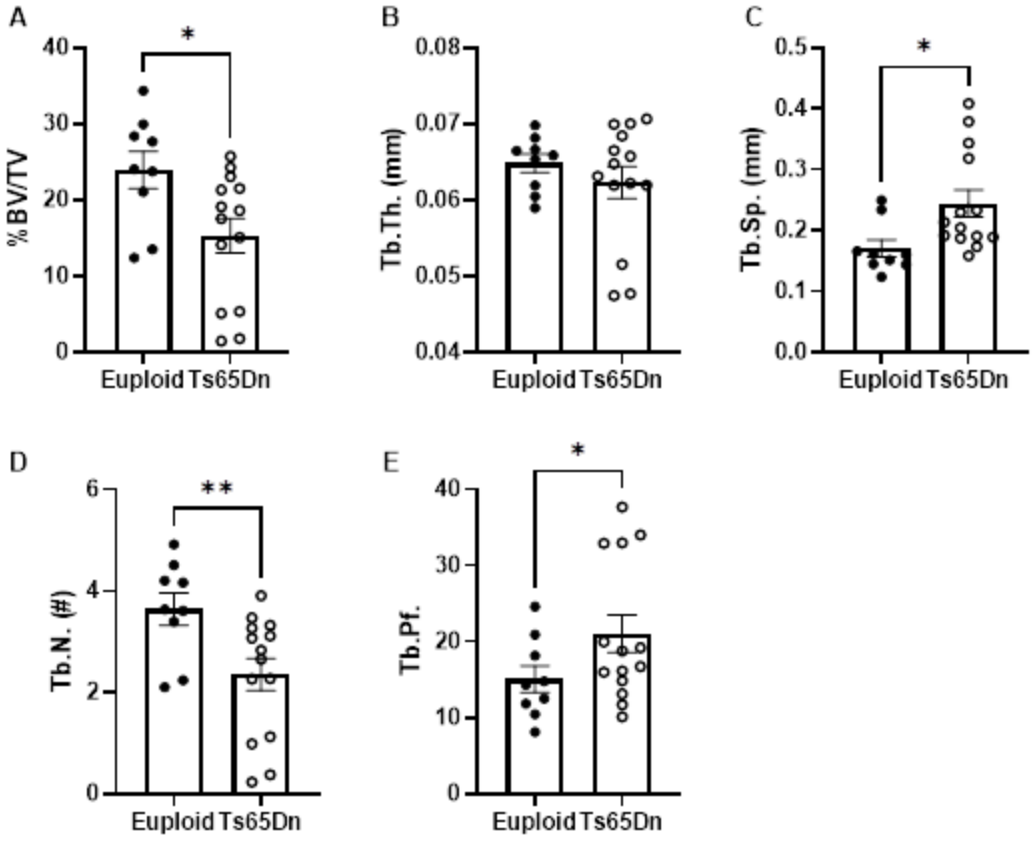

Figure 13. P30 trabecular geometry of male Ts65Dn mice. Unpaired one-tailed t test *p≤0.01, **p≤0.001, ***p≤0.0001

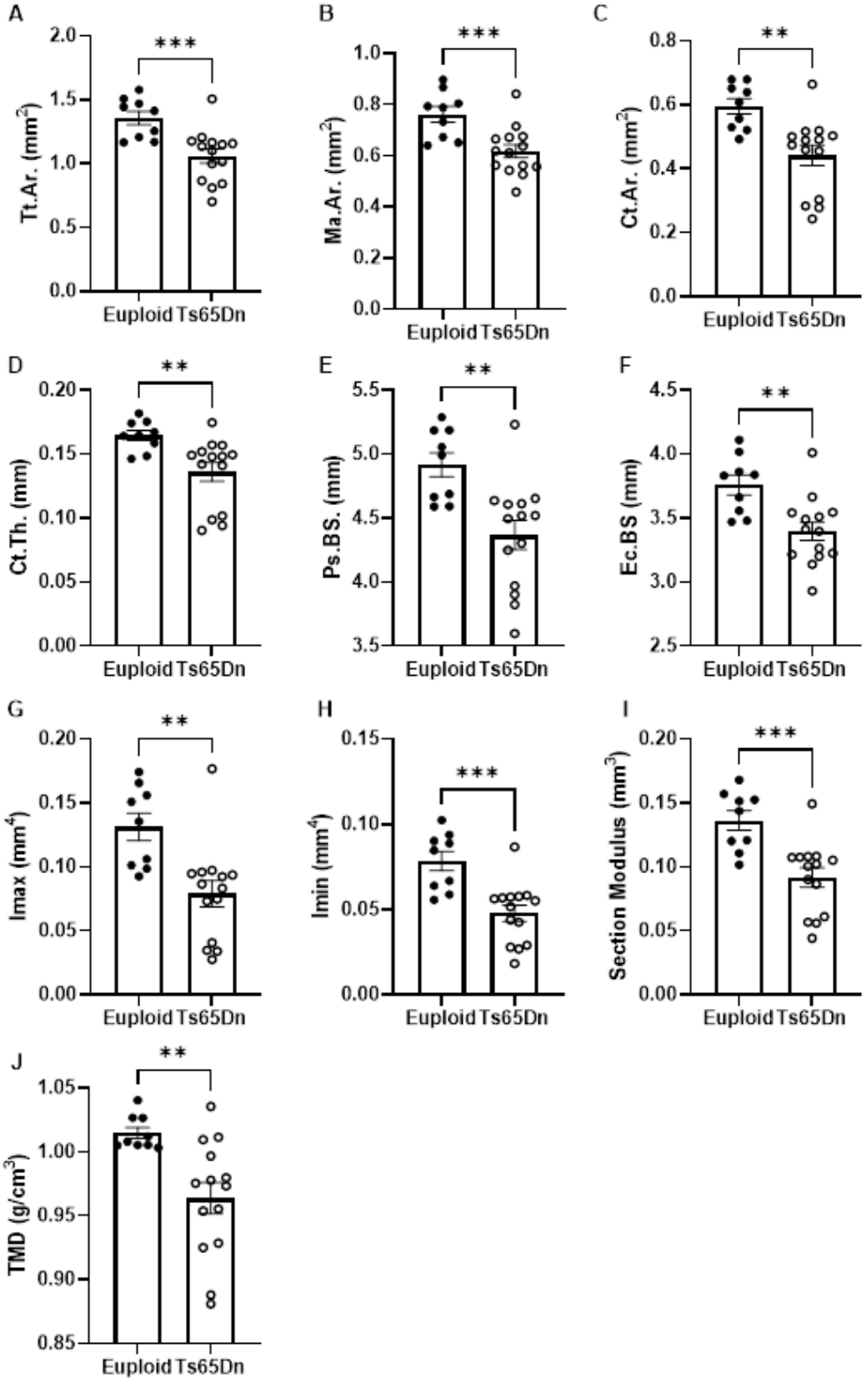

Figure 14. P30 cortical geometry of male Ts65Dn mice. Unpaired one-tailed t test *p≤0.01, **p≤0.001, ***p≤0.0001

3.1.8 P42 Skeletal Analysis

Structural geometry of the femur was assessed again at P42 to verify that the Ts65Dn mouse model has the same phenotype as previously described(Blazek, Abeysekera, et al., 2015) after crossing with *Dyrk1a*$^{+/fl}$, although mice were maintained on a 50-50 B6-C3H background to minimize genetic and phenotypic variability. Unpaired one-tailed t-tests showed significant defects in the following measures: Tb.Sp. [t(18)=1.890, p=0.0375] (**Figure 15C**) and Tb.Pf. [t(18)=3.031, p=0.0036] (**Figure 15E**) were increased, while %BV/TV [t(18)=2.104, p=0.0248] (**Figure 15A**), Tb.Th. [t(18)=1.994, p=0.0308] (**Figure 15B**), Tb.N. [t(18)=1.880, p=0.0382] (**Figure 15D**), Tt.Ar. [t(18)=5.976, p<0.0001] (**Figure 16A**), Ma.Ar. [t(18)=4.387, p=0.0002] (**Figure 16B**), Ct.Ar. [t(18)=3.817, p=0.0006] (**Figure 16C**), Ps.BS. [t(18)=5.084, p<0.0001] (**Figure 16E**), Ec.BS [t(18)=4.521, p=0.0001] (**Figure 16F**), Imax [t(18)=4.189, p=0.0003] (**Figure 16G**), Imin [t(18)=6.549, p<0.0001] (**Figure 16H**), Section Modulus [t(18)=6.063, p<0.0001] (**Figure 16I**), and TMD [t(18)=3.477, p=0.0013] (**Figure 16J**) were decreased. The only measure that was not significantly compromised in male Ts65Dn mice compared to Euploid littermates at P42 was Ct.Th. [t(18)=1.054, p=0.1528] (**Figure 16D**). The results demonstrate a skeletal phenotype in accordance with the previous study at P42(Blazek, Abeysekera, et al., 2015). Considering the results of all studies to date, it seems that lasting trabecular skeletal phenotypes emerge at P30 with the exception of Tb.Th, which emerges at P42(Blazek, Malik, et al., 2015; Fowler et al., 2012). However, these data do not preclude changes in growth rates between the time points characterized that would result in lack of differences in structural geometry between genotypes.

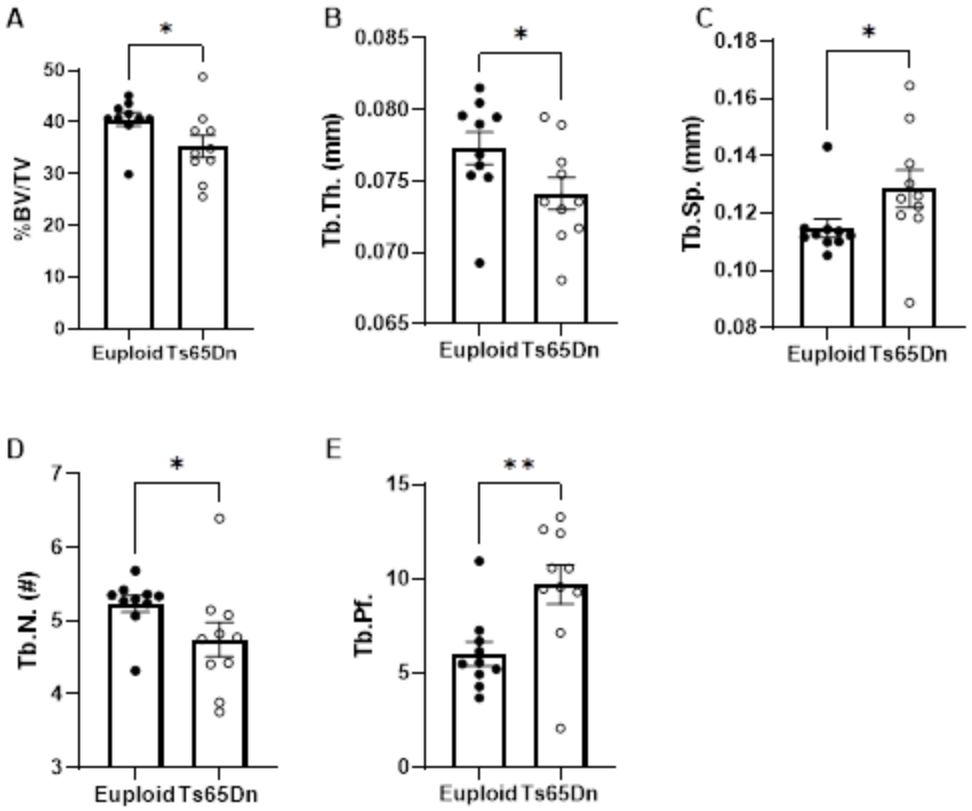

Figure 15. P42 trabecular geometry of male Ts65Dn mice. Unpaired one-tailed t test *p≤0.01, **p≤0.001, ***p≤0.0001

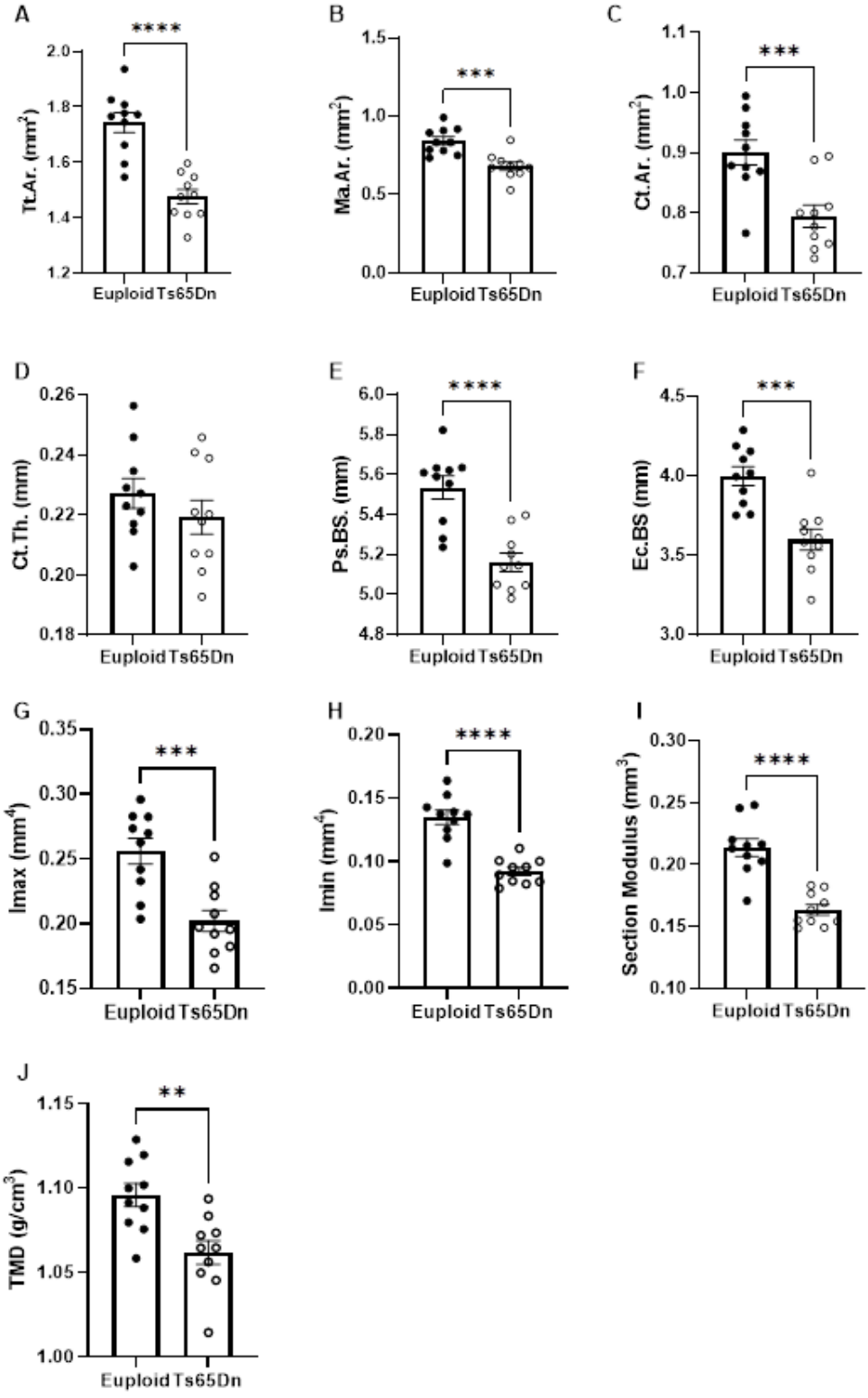

Figure 16. P42 cortical geometry of male Ts65Dn mice. Unpaired one-tailed t test *p≤0.01, **p≤0.001, ***p≤0.0001

3.1.9 Trends in Femur Growth During Postnatal Development

To understand the growth trajectory in developing male Ts65Dn femur structural geometry, line graphs of the means and SEM of key features were plotted over time. This perspective revealed a period of zero net growth in Ts65Dn males from P24 to P30 in %BV/TV (**Figure 17A.**), Tb.Sp. (**Figure 17C.**), Tb.N. (**Figure 17E.**), Tt.Ar. (**Figure 17B.**), Section Modulus (**Figure 17D.**), and TMD (**Figure 17F.**). These data prompted a deeper investigation into genetic mechanisms during the growth period spanning P12 to P42.

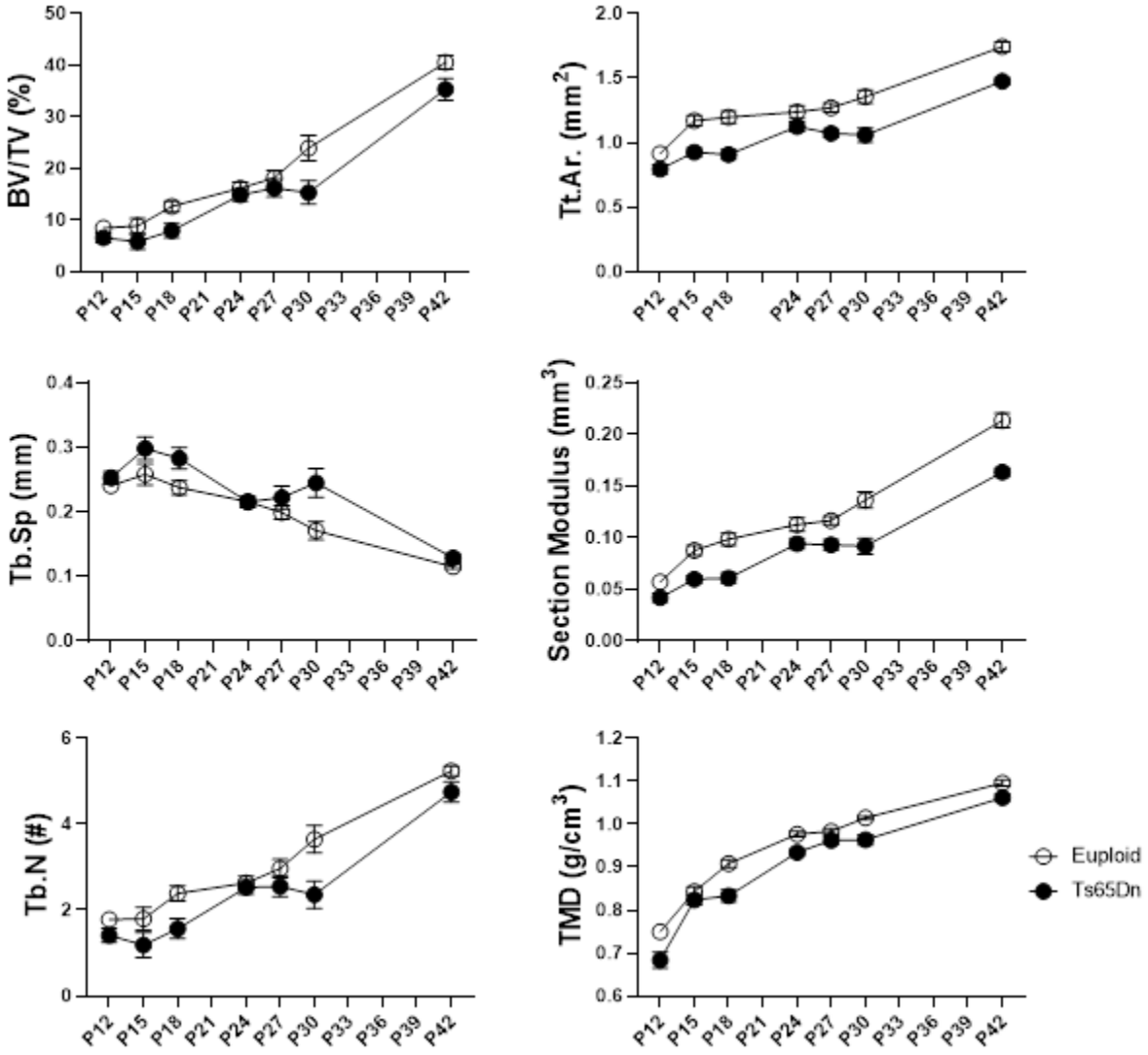

Figure 17. Mean and SEM of key features plotted over time. Points are means, error bars are SEM. Two-way ANOVA, Tukey's post hoc *p≤0.01, **p≤0.001, ***p≤0.0001.

3.2 Determining the Period of *Dyrk1a* Overexpression in Ts65Dn Male Mice

To test the hypothesis that *Dyrk1a* overexpression during postnatal development in male Ts65Dn mice is linked to the emergence of appendicular skeletal abnormalities, RNA was isolated from the midshafts of left femurs obtained from P12, 15, 18, 24, 27, and 30 Euploid and Ts65Dn mice (**Table 3**). Right femurs of mice were analyzed by μCT and RNA was isolated from matching left femurs to determine if *Dyrk1a* expression is linked to aberrant skeletal phenotypes.

Table 3. Sample sizes for each age of *Dyrk1a* expression analysis in male Ts65Dn femurs

***Dyrk1a* Expression in Male Ts65Dn Femurs During Development**		
Sample Sizes		
Age	**Euploid**	**Ts65Dn**
P12	7	9
P15	5	5
P18	7	8
P24	10	9
P27	7	7
P30	10	8

3.2.1 *Dyrk1a* Expression in Male Ts65Dn Femurs During Early Postnatal Development

Unpaired t-tests were used to determine *Dyrk1a* expression at time points assessed in the characterization of femur development. At P12, the male trisomic *Dyrk1a* Fold Change was determined to be 2.526 ± 0.4907 (euploid n=7, trisomic n=9; t(14)=2.062, p=0.0292) (**Figure 18A**.). The male trisomic *Dyrk1a* Fold Change at P15 was 1.165 ± 0.2291 (euploid n=5, trisomic n=5; t(8)=0.1134, p=0.4563) (**Figure 18B**.). *Dyrk1a* was overexpressed at P18; the Fold Change for male trisomic mice was 2.207 ± 0.4541 (euploid n=7, trisomic n=8; t(13)=2.226, p=0.0222) (**Figure 17C**.). At P24, the male trisomic *Dyrk1a* Fold Change value was determined to be 0.9841 ± 0.2591 (euploid n=10, trisomic n=9; t(17)=0.7553, p=0.2302) (**Figure 18D**.). The *Dyrk1a* Fold Change at P27 for trisomic male mice was 2.039 ± 0.4839 (euploid n=7, trisomic n=7; t(12)=1.184, p=0.1297) (**Figure 18E**.). The *Dyrk1a* Fold Change for Ts65Dn male mice at the final timepoint, P30, was 1.984 ± 0.4897 (euploid n=10, trisomic n=8; t(16)=1.918, p=0.0366) (**Figure 18F**.). While the *Dyrk1a* Fold Change of male Ts65Dn mice suggests overexpression at all timepoints except P15 and P24, statistical significance is only reached at P12, P18, and P30. Considering both *Dyrk1a* expression and the emergence of skeletal phenotypes, it seems that *Dyrk1a* expression is linked with trabecular defects.

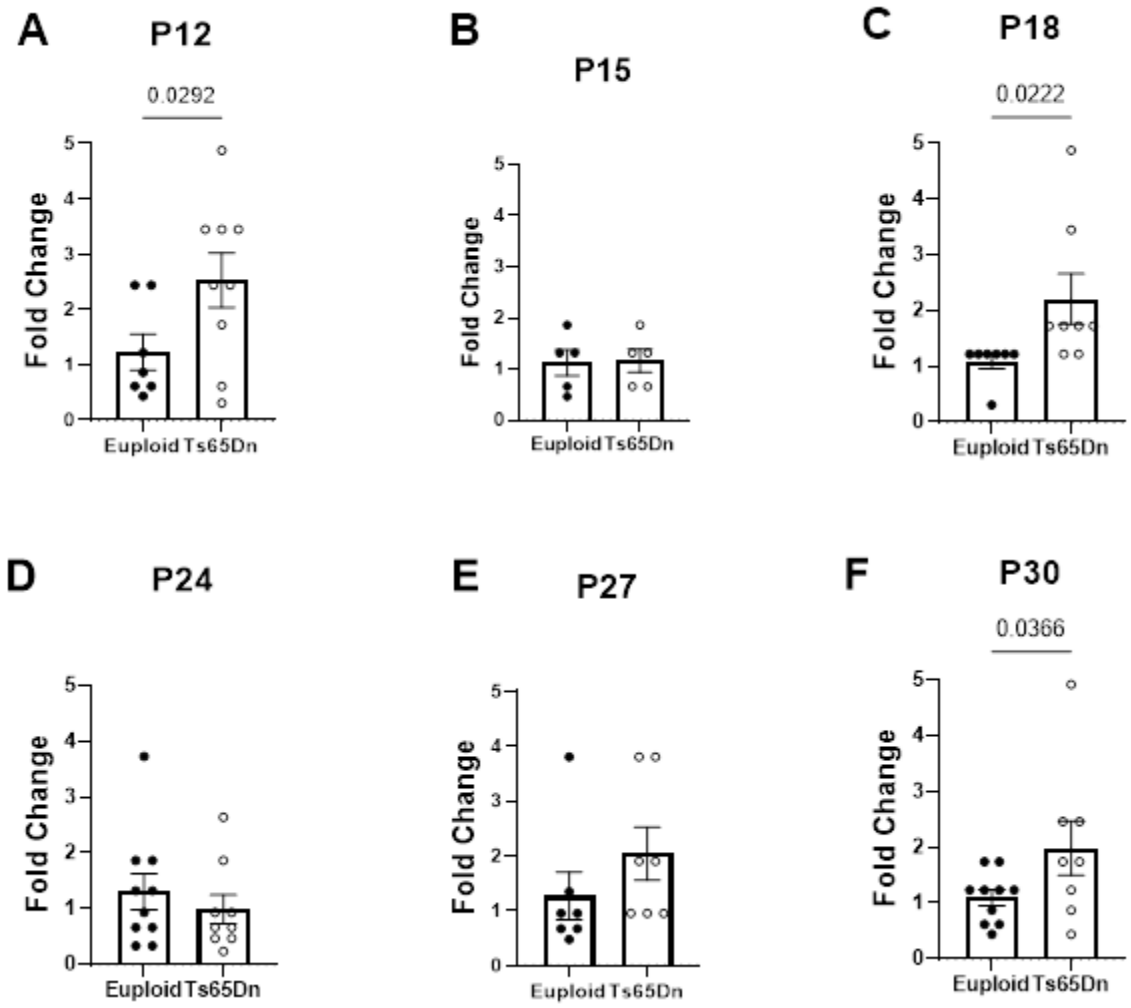

Figure 18. *Dyrk1a* expression in male Ts65Dn mice during early development. Unpaired one-tailed t test.

3.3 Aim 1.4 Inhibition of DYRK1A Prior to Emergence of Skeletal Defects

The static growth period identified previously led to the hypothesis that inhibition of DYRK1A in male Ts65Dn mice from weaning (P21) until P30 would prevent the emergence of trabecular defects. The DYRK1A inhibitor CX-4945 was chosen based on reports praising its relative specificity for DYRK1A, established safety(H. Kim et al., 2016), and osteogenic properties(Son et al., 2013).

CX-4945 trials revealed challenges in administration. Due to solubility constraints, the drug had to be dissolved in DMSO (250mM) and warmed before diluting to the working concentration (25mM) with PBS. The yellow suspension was kept warm in a 37°C heat block until administration. Intraperitoneal and subcutaneous injections from P21 to P29 similarly resulted in yellow precipitate at the injection site (**Figure 19.**). Evidence suggests that the drug precipitated at the injection site and was not bioavailable using either administration method. Oral gavage trials were more convincing; organs seemed unaffected (**Figure 20.**), feces were not discolored, and the gastric system appeared normal (**Figure 21.**).

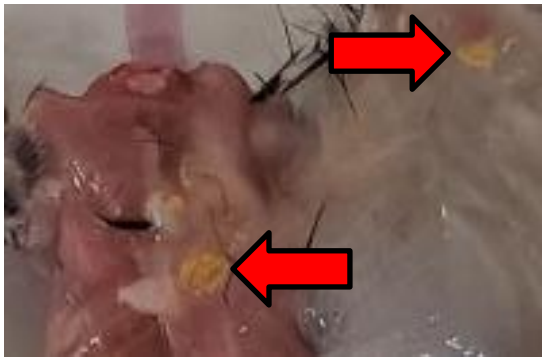

Figure 19. Necropsy of trial mice at P30 after CX-4945 injections from P21-P29 revealed precipitation at the site of injection (arrows).

Figure 20. Necropsy of trial mice at P30 after CX-4945 oral gavage from P21-P29 revealed no visible signs of toxicity in the spleen, liver, or kidneys.

Figure 21. Necropsy of trial mice at P30 after CX-4945 oral gavage from P21-P29 revealed no visible signs of toxicity gastrointestinal tract.

Euploid and Ts65Dn littermates were administered either a 75mg/kg/day CX-4945 suspension (90%PBS:10%DMSO) or the vehicle (90%PBS:10%DMSO) via oral gavage from P21 to P29. Mice were euthanized and femurs were collected for µCT analysis on P30 (**Table 4**). The weights of mice were recorded to calculate dosage and track health throughout the course of drug administration. Weights of mice were unaffected based on treatment but there was a difference based on genotypes (**Figure 22.**). Necropsy and weight results suggest that CX-4945 and Vehicle treatment via oral gavage was well-tolerated and visibly had no negative effects.

Table 4. Sample sizes for assessment of male P30 Ts65Dn femurs at P30 following DYRK1A inhibition with CX-4945 from P21-29.

Ts65Dn DYRK1A Inhibition Femur Geometry

Sample Sizes			
Euploid + Vehicle	**Euploid + CX-4945**	**Ts65Dn + Vehicle**	**Ts65Dn + CX-4945**
12	13	11	8

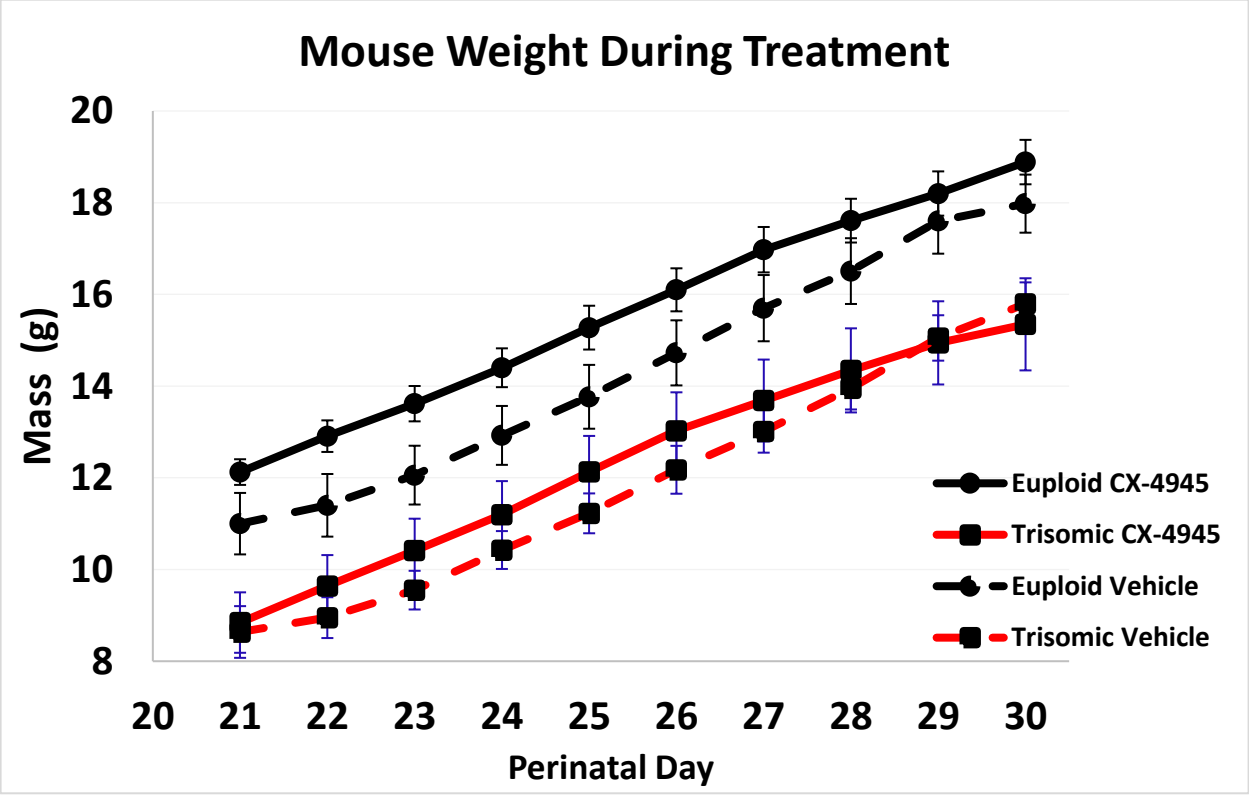

Figure 22. Mouse weight during the course of CX or Vehicle treatment from P21 to P29 in Euploid and Ts65Dn male mice.

3.3.1 Characterize the Femur Geometry of P30 Male Ts65Dn Mice Treated with CX-4945

Two-way ANOVA of Euploid and Ts65Dn treated with either CX-4945 (suspension in 90%PBS, 10%DMSO) or vehicle (90%PBS, 10%DMSO) was utilized to determine effects of genotype, gene dosage, and interactions affecting bone geometry (**Table 5**). Analysis of femur geometry revealed a main effect of genotype in %BV/TV [F(1,40)]=10.03, p=0.0029] (**Figure 23A.**), Tb.Sp. [F(1,40)=12.54, p=0.0010] (**Figure 23C.**), Tb.N. [F(1,40)=12.01, p=0.0013] (**Figure 23D.**), Tb.Pf. [F(1,40)=4.752, p=0.0352] (**Figure 23E.**), Tt.Ar. [F(1,40)=21.02, p<0.0001] (**Figure 24A.**), Ma.Ar. [F(1,40)=15.16, p=0.0004] (**Figure 24B.**), Ct.Ar. [F(1,40)=21.23, p<0.0001] (**Figure 24C.**), Ct.Th. [F(1,40)=12.02, p=0.0012] (**Figure 24D.**), Ps.BS [F(1,40)=19.14, p<0.0001] (**Figure 24E.**), Ec.BS [F(1,40)=15.72, p=0.0003] (**Figure 24F.**), Imax [F(1,40)=19.11, p<0.0001] (**Figure 24G.**), Imin [F(1,40)=25.88, p<0.0001] (**Figure 24H.**), Section Modulus [F(1,40)=24.16, p<0.0001] (**Figure 24I.**), and TMD [F(1,40)=15.42, p=0.0003] (**Figure 24.**). An interactive effect was observed in Tb.Pf. [F(1,40)=4.268, p=0.0454] (**Figure 23E.**) (**Table 10.**).

Tukey's multiple comparison post hoc analysis showed that Ts65Dn mice receiving the vehicle did not have impaired trabecular bone geometry compared to Euploid mice receiving the vehicle (**Figure 23.**). The only cortical defects that reached statistical significance were Tt.Ar. (p=0.0445) (**Figure 24A.**), Ct.Ar. (p=0.0332) (**Figure 24C.**), Imin (p=0.0170) (**Figure 24H.**), Section Modulus (p=0.0220) (**Figure 24I.**), and TMD (p=0.0198) (**Figure 24J.**). Post hoc analysis also revealed the source of the interactive effect: Tb.Pf. was significantly lower in the Euploid+CX-4945 group compared to the Ts65Dn+CX-4945 group (p=0.0297), suggesting better trabecular organization in the Euploid mice. By all measures, a treatment regime of 75mg/kg/day CX-4945 (suspension in 90%PBS:10%DMSO) via oral gavage from P21 to P29 directed at inhibiting DYRK1A did not improve skeletal defects at P30 in male Ts65Dn mice.

Table 5. ANOVA for P30 male Ts65Dn femurs following CX-4945 treatment from P21 to P30. [a] Main effect of genotype; [b] Main effect of treatment; [c] Interactive effect

Measure	Source of Variation		
	Genotype	Treatment	Interactive
%BV/TV	F (1, 40) = 10.03, p=0.0943	F (1, 40) = 1.764, p=0.1917	F (1, 40) = 2.937, p=0.0943
Tb.Th	F (1, 40) = 0.2911, p=0.5924	F (1, 40) = 0.0007795, p=0.9779	F (1, 40) = 1.960, p=0.1692
Tb.Sp [a]	F (1, 40) = 12.54, p=0.0010	F (1, 40) = 2.711, p=0.1075	F (1, 40) = 0.4252, p=0.5181
Tb.N [a]	F (1, 40) = 12.01, p=0.0013	F (1, 40) = 2.216, p=0.1444	F (1, 40) = 2.272, p=0.1396
Tb.Pf [a,c]	F (1, 40) = 4.752, p=0.0352	F (1, 40) = 0.7875, p=0.3801	F (1, 40) = 4.268, p=0.0454
Tt.Ar [a]	F (1, 40) = 21.02, p<0.0001	F (1, 40) = 0.04211, p=0.8384	F (1, 40) = 0.7547, p=0.3902
Ma.Ar [a]	F (1, 40) = 15.16, p=0.0004	F (1, 40) = 0.3990, p=0.5312	F (1, 40) = 0.7408, p=0.3945
Ct.Ar [a]	F (1, 40) = 21.23, p<0.0001	F (1, 40) = 0.1208, p=0.7300	F (1, 40) = 0.5244, p=0.4732
Ct.Th [a]	F (1, 43) = 12.02, p=0.0012	F (1, 43) = 1.169, p=0.2856	F (1, 43) = 0.07773, p=0.7817
Ps.BS [a]	F (1, 40) = 19.14, p<0.0001	F (1, 40) = 0.04154, p=0.8395	F (1, 40) = 0.8061, p=0.3747
Ec.BS [a]	F (1, 40) = 15.72, p=0.0003	F (1, 40) = 0.3961, p=0.5327	F (1, 40) = 1.027, p=0.3171
Imax [a]	F (1, 40) = 19.11, p<0.0001	F (1, 40) = 0.05307, p=0.8190	F (1, 40) = 0.7638, p=0.3873
Imin [a]	F (1, 40) = 25.88, p<0.0001	F (1, 40) = 0.07200, p=0.7898	F (1, 40) = 0.7088, p=0.4048
Section Modulus [a]	F (1, 40) = 24.16, p<0.0001	F (1, 40) = 0.06131, p=0.8057	F (1, 40) = 0.6528, p=0.4239
TMD [a]	F (1, 40) = 15.42, p=0.0003	F (1, 40) = 1.437, p=0.2377	F (1, 40) = 0.05631, p=0.8136

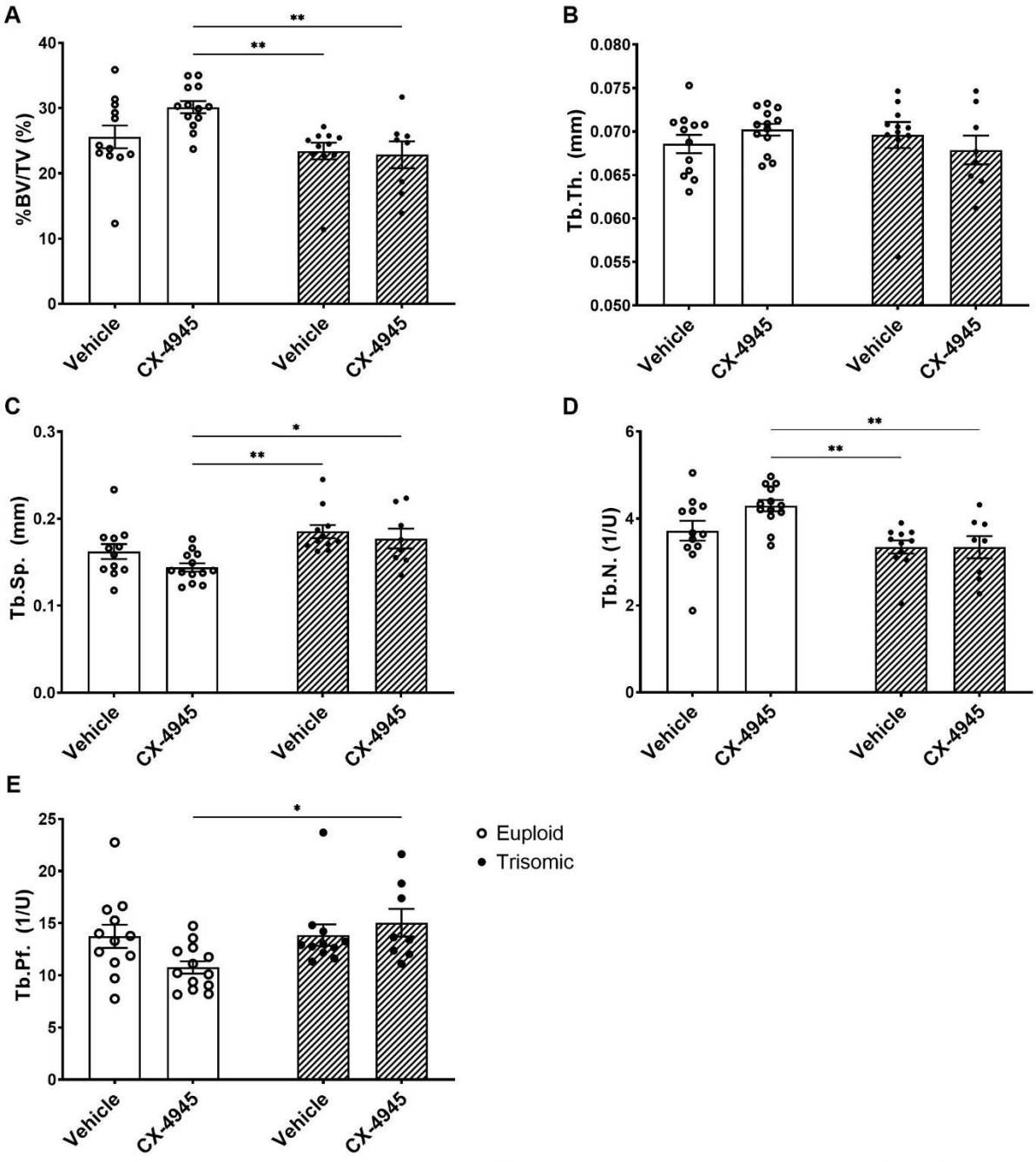

Figure 23. Trabecular geometry of P30 male Ts65Dn mice treated with CX-4945 or vehicle from P21-P30. Mean and SEM shown. Two-way ANOVA and Tukey's post hoc *p≤0.05, **p≤0.01, ***p≤0.001, ****p≤0.0001

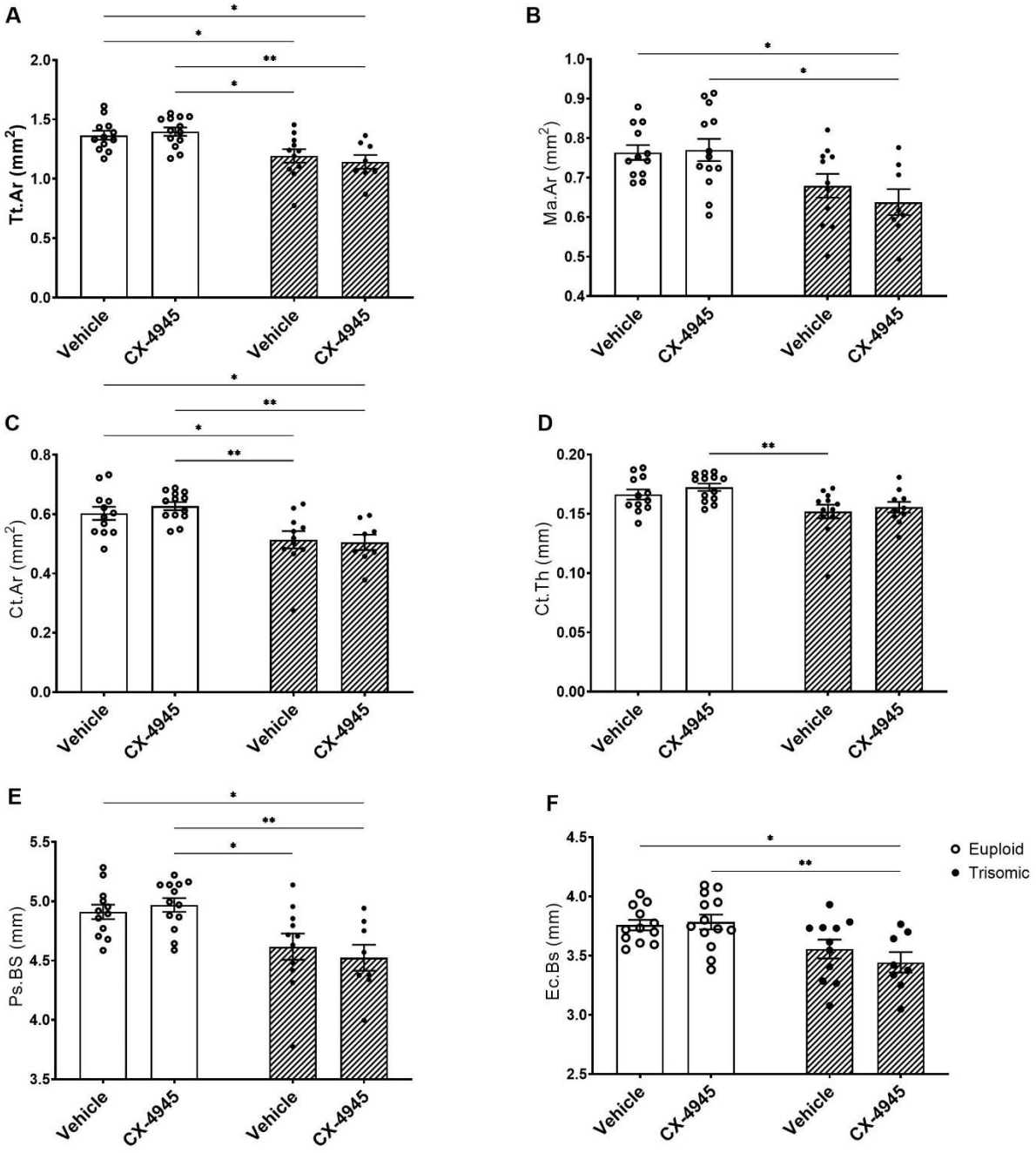

Figure 24. Cortical geometry of P30 male Ts65Dn mice treated with CX-4945 or vehicle from P21-P30. Mean and SEM shown. Two-way ANOVA and Tukey's post hoc *p≤0.05, **p≤0.01, ***p≤0.001, ****p≤0.0001

Figure 24. continued

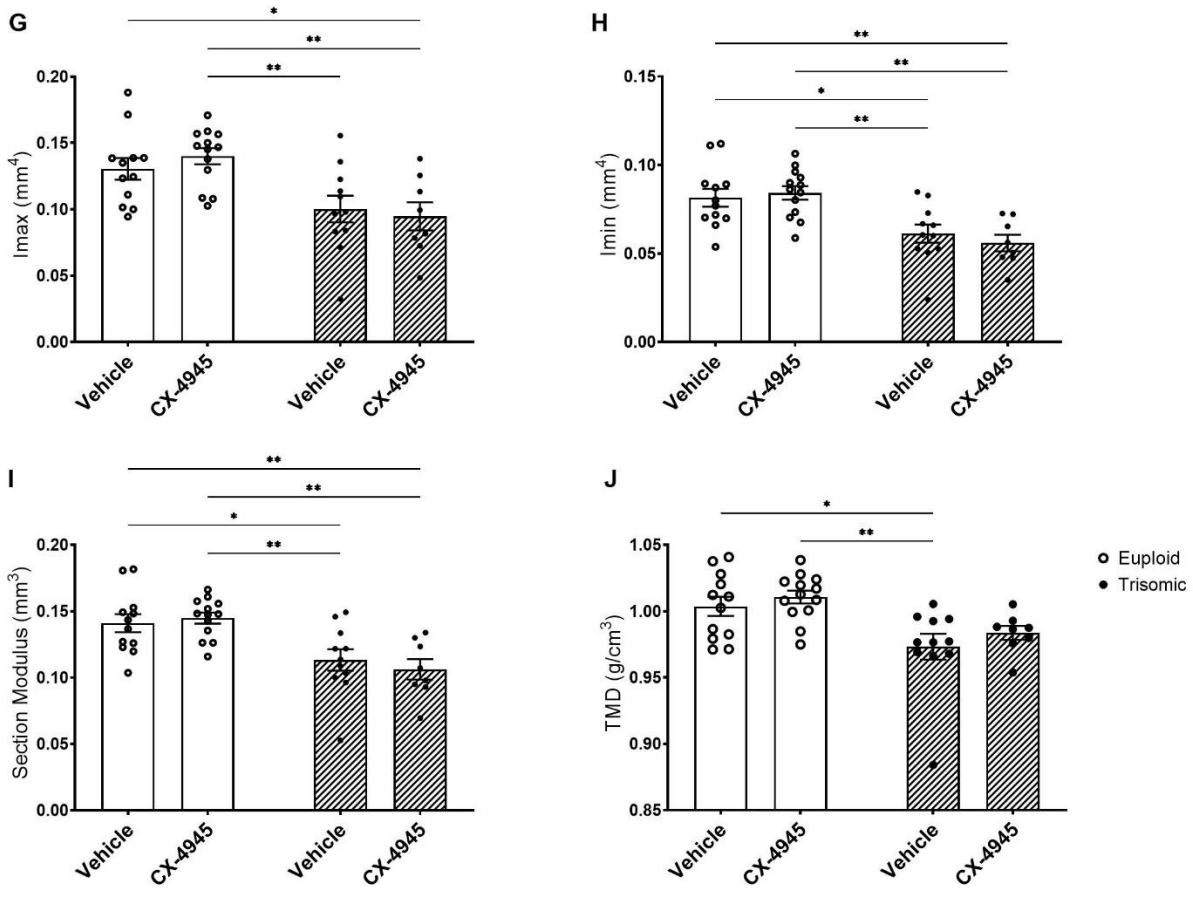

3.4 Determine if Reduction of *Dyrk1a* Copy Number in Male Ts65Dn Mice Prior to the Emergence of Trabecular Defects Rescues the Abnormal Phenotype

While *Dyrk1a* is overexpressed at P12 (p=0.0292), it doesn't seem to correlate with trabecular phenotypes and the time point is before the first large increase in growth rate. Considering previous reports and experiments that showed: 1) reduction of *Dyrk1a* in otherwise trisomic mice from conception results in improved trabecular phenotypes at P42(Blazek, Abeysekera, et al., 2015) 2) significant and lasting femur defects emerge at P30 after a six-day period of zero net growth (**Figure 17.**) and 3) *Dyrk1a* is overexpressed when trabecular defects are present at P12 (%BV/TV [t(16)=1.642, p=0.0600] (**Figure 3A**) and Tb.N [t(16)=1.735, p=0.0510] (**Figure 3D**)), P18 (%BV/TV [t(17)=2.738, p=0.0070] (**Figure 7A**), Tb.Th. [t(17)=1.990, p=0.0315] (**Figure 7B**), Tb.N. [t(17)=2.834, p=0.0057] (**Figure 7D**)) and P30 (%BV/TV [t(21)=2.505, p=0.0103] (**Figure 13.A**), Tb.N. [t(21)=2.717, p=0.0065] (**Figure 13.D**), Tb.Sp. [t(21)=2.482, p=0.0108] (**Figure 13.C**), and Tb.Pf. [t(21)=1.744, p=0.0479] (**Figure 13.E**)), we hypothesized that normalization of *Dyrk1a* copy number at P21 would prevent the emergence of trabecular defects at P30. To explore this hypothesis, Ts65Dn mice were crossed with *Dyrk1a*$^{+/fl}$ and progeny crossed with a doxycycline-inducible Cre promotor model rtTA^{+}, TetOCre^{+}. In progeny, doxycycline administration activates Cre expression to excise exon 5 and 6 in one allele of *Dyrk1a* leaving the protein product non-functional. Doxycycline administration at weaning (P21) reduced *Dyrk1a* functional copy number in trisomic male Ts65Dn, *Dyrk1a*$^{+/fl}$, rtTA^{+}, TetOCre^{+} mice at P30 (**Figure 25**). From this point forward, these mice will be referred as Euploid, *Dyrk1a*$^{+/fl}$, Cre –; Euploid, *Dyrk1a*$^{+/fl}$, Cre +; Ts65Dn, *Dyrk1a*$^{+/fl}$, Cre –; Ts65Dn, *Dyrk1a*$^{+/fl}$, Cre +; to indicate the ploidy and active copies of *Dyrk1a* (two, one, three, and three, respectively) of the experimental mice.

Table 6. *Dyrk1a* sample sizes for geometric and mechanical measures in male P30 Ts65Dn, *Dyrk1a*$^{+/fl}$ femurs following gene dosage reduction through Cre-loxp induction by doxycycline administration from P21-29.

Conditional *Dyrk1a* Dosage Reduction in Male Ts65Dn Mice

a

P30 Femur Structural Geometry Analysis				
Genotype	**Euploid, *Dyrk1a*$^{+/fl}$**	**Euploid, *Dyrk1a*$^{+/fl}$**	**Ts65Dn, *Dyrk1a*$^{+/fl}$**	**Ts65Dn, *Dyrk1a*$^{+/fl}$**
rtTA, Cre	-	+	-	+
Functional *Dykr1a*	++	+ -	+++	++ -
Sample Size	10	7	10	5

b

P30 Femur Mechanical Analysis				
Genotype	**Euploid, *Dyrk1a*$^{+/fl}$**	**Euploid, *Dyrk1a*$^{+/fl}$**	**Ts65Dn, *Dyrk1a*$^{+/fl}$**	**Ts65Dn, *Dyrk1a*$^{+/fl}$**
rtTA, Cre	-	+	-	+
Functional *Dykr1a*	++	+ -	+++	++ -
Sample Size	6	4	6	5

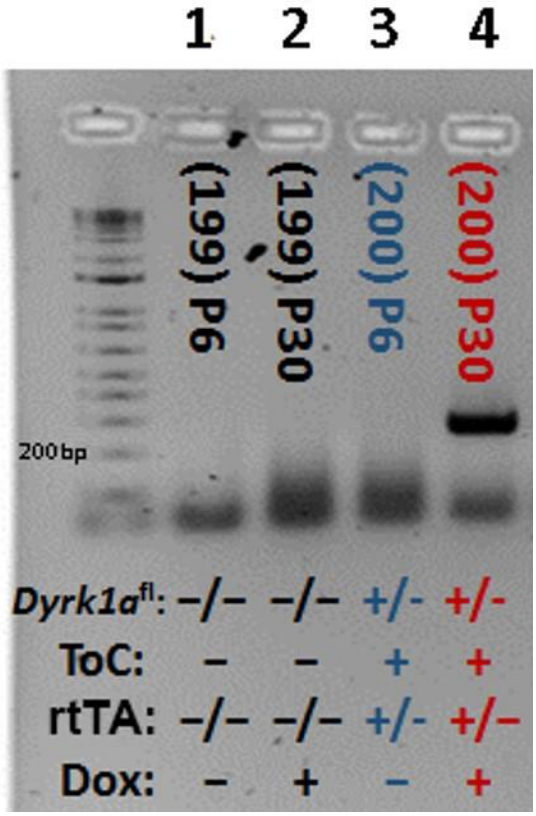

Figure 25. PCR verification of Cre-loxp excision of exon 5-6 in male Ts65Dn, *Dyrk1a*$^{+/fl}$, rtTA^{+}, tetOcre^{+} mice. The numbers in parenthesis correspond to the mouse identification number. The age of the mouse follows, signifying perinatal day 6 (P6) or P30. The genotypes of the mice are indicated in the respective column. PCR was performed on DNA obtained at each age; at P6 before doxycycline administration and P30, after the mouse had received doxycycline for 9 consecutive days in chow. A 214bp amplicon is produced in the presence of a truncated *Dyrk1a* allele.

3.4.1 Characterize the Femur Geometry of P30 Male Ts65Dn, *Dyrk1a*$^{+/fl}$ Mice

Right femurs from experimental mice were analyzed by μCT (**Table 6a.**). Two-way ANOVA of Euploid, *Dyrk1a*$^{+/fl}$, Cre –, Euploid, *Dyrk1a*$^{+/fl}$, Cre + (one functional copy of *Dyrk1a* in an otherwise wild type mouse following doxycycline administration), Ts65Dn, *Dyrk1a*$^{+/fl}$, Cre –, and Ts65Dn, *Dyrk1a*$^{+/fl}$, Cre + (two functional copies of *Dyrk1a* in an otherwise trisomic mouse following doxycycline administration from P21 to P30) mice was utilized to determine effects of genotype, gene dosage, and interactions affecting bone geometry. Details of the analysis are organized on **Table 7**.

Analysis of P30 male Ts65Dn femur geometry revealed an effect of genotype for every measure: %BV/TV (**Figure 26A.**), Tb.Th (**Figure 26B.**), Tb.Sp (**Figure 26C.**), Tb.N (**Figure 26D.**), Tb.Pf (**Figure 26E.**), Tt.Ar (**Figure 27A.**), Ma.Ar (**Figure 27B.**), Ct.Ar (**Figure 27C.**), Ct.Th (**Figure 27D.**), Ps.BS (**Figure 27E**), Ec.BS (**Figure 27F.**), Imax (**Figure 27G.**), Imin (**Figure 27H.**), Section Modulus (**Figure 27I.**), and TMD (**Figure 27J.**). There was no effect of gene dosage, but there was an interaction for Tb.N.

Tukey's multiple comparison post hoc tests confirmed reductions in male Ts65Dn, *Dyrk1a*$^{+++}$ trabecular and cortical measures including %BV/TV ($p=0.0555$) (**Figure 26A.**), Tb.Sp ($p=0.0324$) (**Figure 26C.**),Tt.Ar ($p<0.0001$) (**Figure 27A.**), Ma.Ar ($p=0.0009$) (**Figure 27B.**), Ct.Ar ($p<0.0001$) (**Figure 27C.**), Ct.Th ($p=0.0001$) (**Figure 27D.**), Ps.BS ($p<0.0001$) (**Figure 27E**), Ec.BS ($p=0.0003$) (**Figure 27F.**), Imax ($p=0.0002$) (**Figure 27G.**), Imin ($p<0.0001$) (**Figure 27H.**), Section Modulus ($p<0.0001$) (**Figure 27I.**), and TMD ($p=0.0008$) (**Figure 27J.**) compared to Euploid, *Dyrk1a*$^{++}$ littermates. Other trabecular measures Tb.Th ($p=0.1104$) (**Figure 26B.**) and Tb.N ($p=0.0933$) (**Figure 26D.**) were reduced but did not reach statistical significance. Contrary to the hypothesis, reduction of a functional *Dyrk1a* gene in trisomic mice at the time of weaning (P21) by administration of doxycycline to activate cre-loxp excision of *Dyrk1a* exon 5-6 failed to improve any trabecular or cortical phenotypes when comparing Ts65Dn, *Dyrk1a*$^{+++}$ and Ts65Dn, *Dyrk1a*$^{++-}$ measures. Reduction of *Dyrk1a* gene dosage in Euploid mice from P21 to P30 had no effect on femur geometry.

Table 7. ANOVA results for P30 male Ts65Dn, *Dyrk1a*$^{+/fl}$ femurs following gene dosage reduction from P21 to P30. [a] Main effect of genotype; [b] Main effect of gene dosage; [c] Interactive effect

Measure	Source of Variation		
	Genotype	Gene Dosage	Interaction
%BV/TV [a]	F (1, 28) = 18.59, p=0.0002	F (1, 28) = 0.1287, p=0.7725	F (1, 28) = 1.114, p=0.3002
Tb.Th [a]	F (1, 28) = 5.329, p=0.0286	F (1, 28) = 2.104, p=0.1580	F (1, 28) = 0.2992, p=0.5887
Tb.Sp [a]	F (1, 28) = 21.95, p<0.0001	F (1, 28) = 0.6292, p=0.4343	F (1, 28) = 1.292, p=0.2653
Tb.N [a,c]	F (1, 28) = 26.76, p<0.0001	F (1, 28) = 0.1891, p=0.6670	F (1, 28) = 4.911, p=0.0350
Tb.Pf [a]	F (1, 28) = 9.649, p=0.0043	F (1, 28) = 1.239, p=0.2751	F (1, 28) = 0.9560, p=0.3366
Tt.Ar [a]	F (1, 28) = 31.86, p<0.0001	F (1, 28) = 0.1637, p=0.6889	F (1, 28) = 0.2890, p=0.5951
Ma.Ar [a]	F (1, 28) = 21.02, p<0.0001	F (1, 28) = 4.616e-005, p=0.9946	F (1, 28) = 0.2965, p=0.5904
Ct.Ar [a]	F (1, 28) = 36.55, p<0.0001	F (1, 28) = 0.6727, p=0.4190	F (1, 28) = 0.1990, p=0.6590
Ct.Th [a]	F (1, 28) = 32.37, p<0.0001	F (1, 28) = 1.180, p=0.2866	F (1, 28) = 0.06279, p=.8040
Ps.BS	F (1, 28) = 30.80, p<0.0001	F (1, 28) = 0.2946, p=0.5916	F (1, 28) = 0.3662, p=0.5500
Ec.BS	F (1, 28) = 24.96, p<0.0001	F (1, 28) = 0.004613, p=0.9463	F (1, 28) = 0.3878, p=0.5385
Imax	F (1, 28) = 27.45, p<0.0001	F (1, 28) = 0.6328, p=0.4330	F (1, 28) = 0.3448, p=0.5618
Imin	F (1, 28) = 30.02, p<0.0001	F (1, 28) = 0.3046, p=0.5854	F (1, 28) = 0.4340, p=0.5154
Section Modulus	F (1, 28) = 37.15, p<0.0001	F (1, 28) = 0.3148, p=0.5792	F (1, 28) = 0.2334, p=0.6328
TMD	F (1, 28) = 30.79, p<0.0001	F (1, 28) = 1.344, p=0.2561	F (1, 28) = 0.1271, p=0.7241

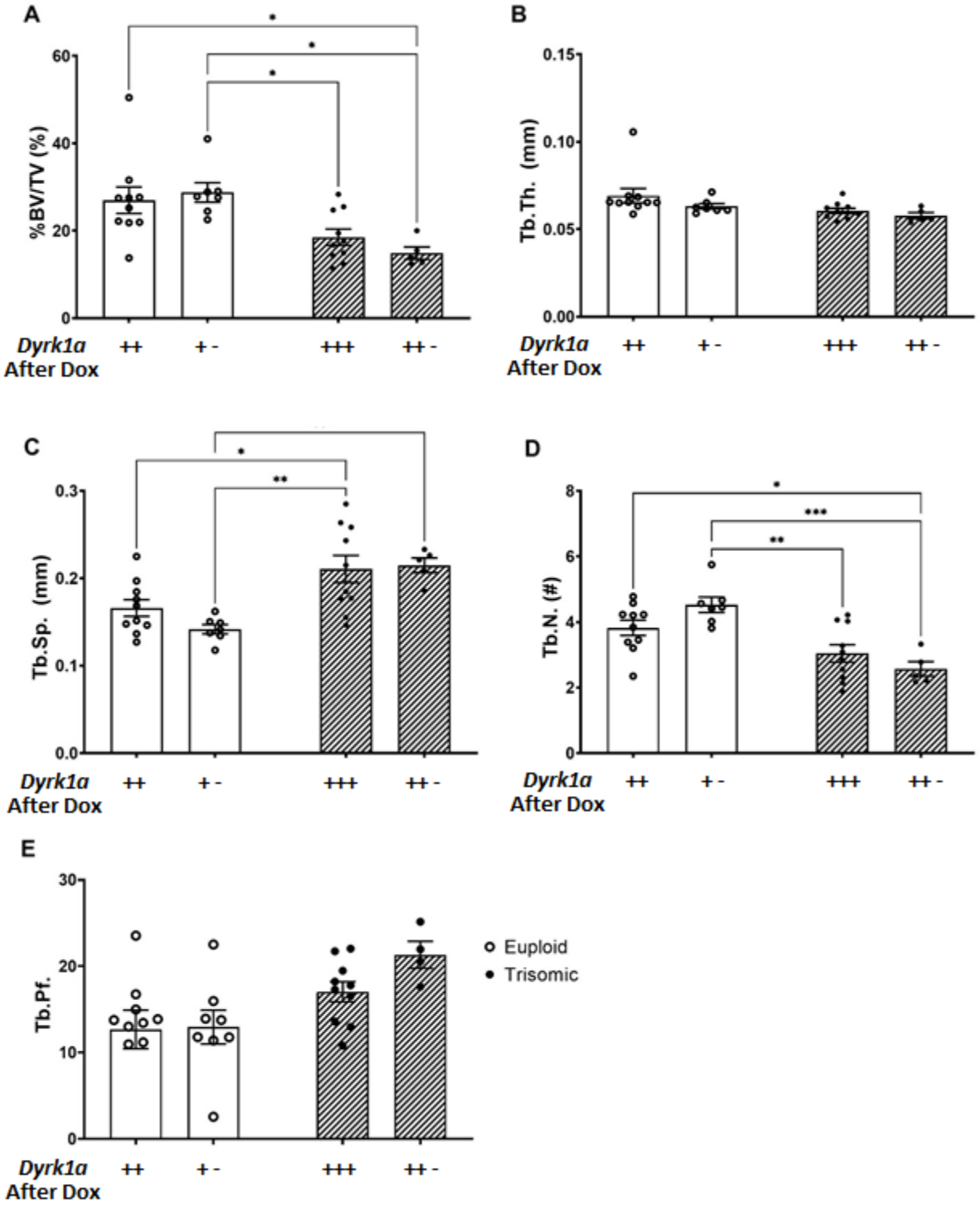

Figure 26. Trabecular geometry of P30 male Ts65Dn, *Dyrk1a*$^{+/fl}$ after gene dosage reduction through Cre-loxp induction by doxycycline administration from P21-P29. Two-way ANOVA, Tukey's post hoc *p≤0.05, **p≤0.01, ***p≤0.001, ****p≤0.0001.

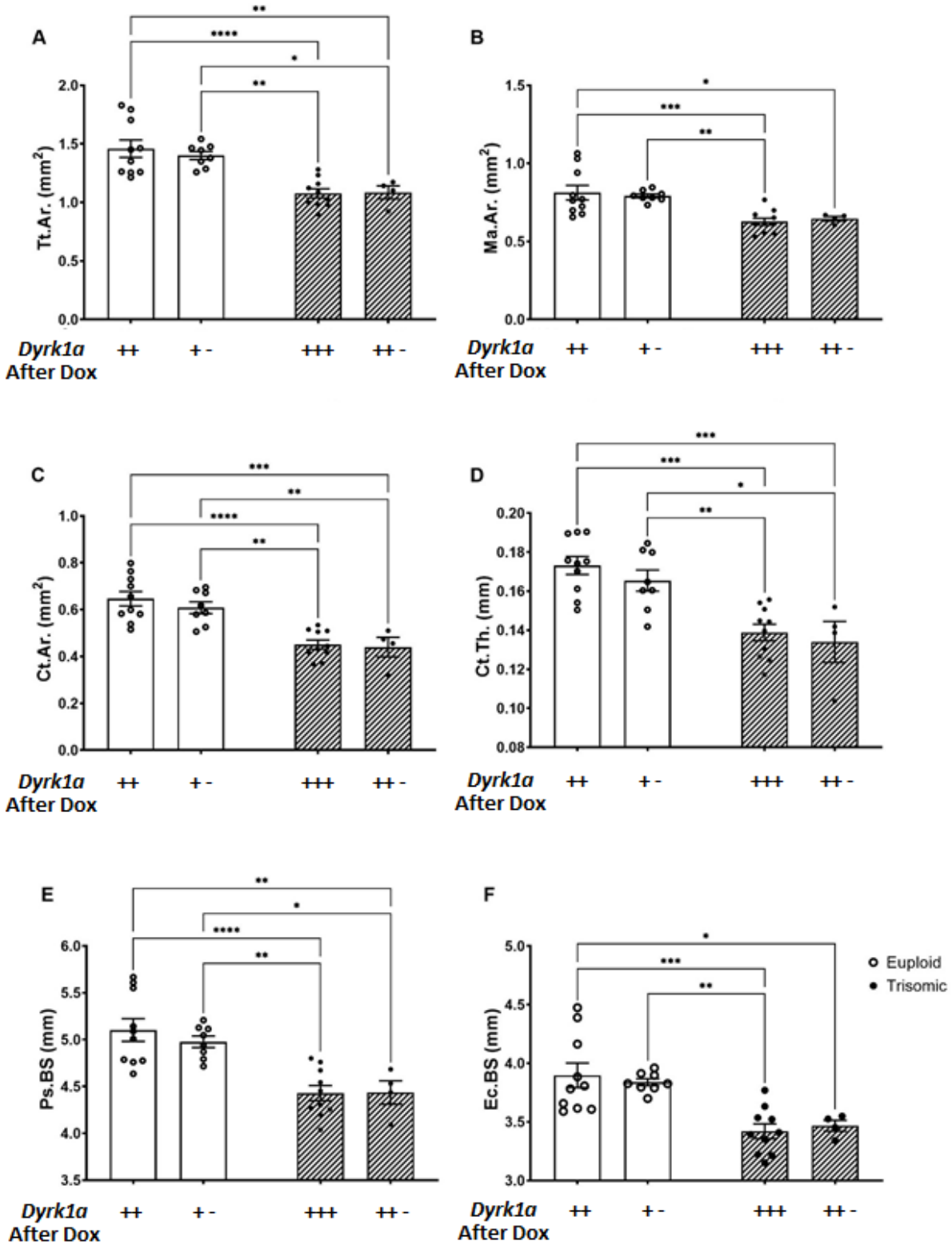

Figure 27. Cortical geometry of P30 male Ts65Dn, *Dyrk1a*$^{+/fl}$ after gene dosage reduction through Cre-loxp induction by doxycycline administration from P21-P29. Two-way ANOVA, Tukey's post hoc *p≤0.05, **p≤0.01, ***p≤0.001, ****p≤0.0001.

Figure 27. continued

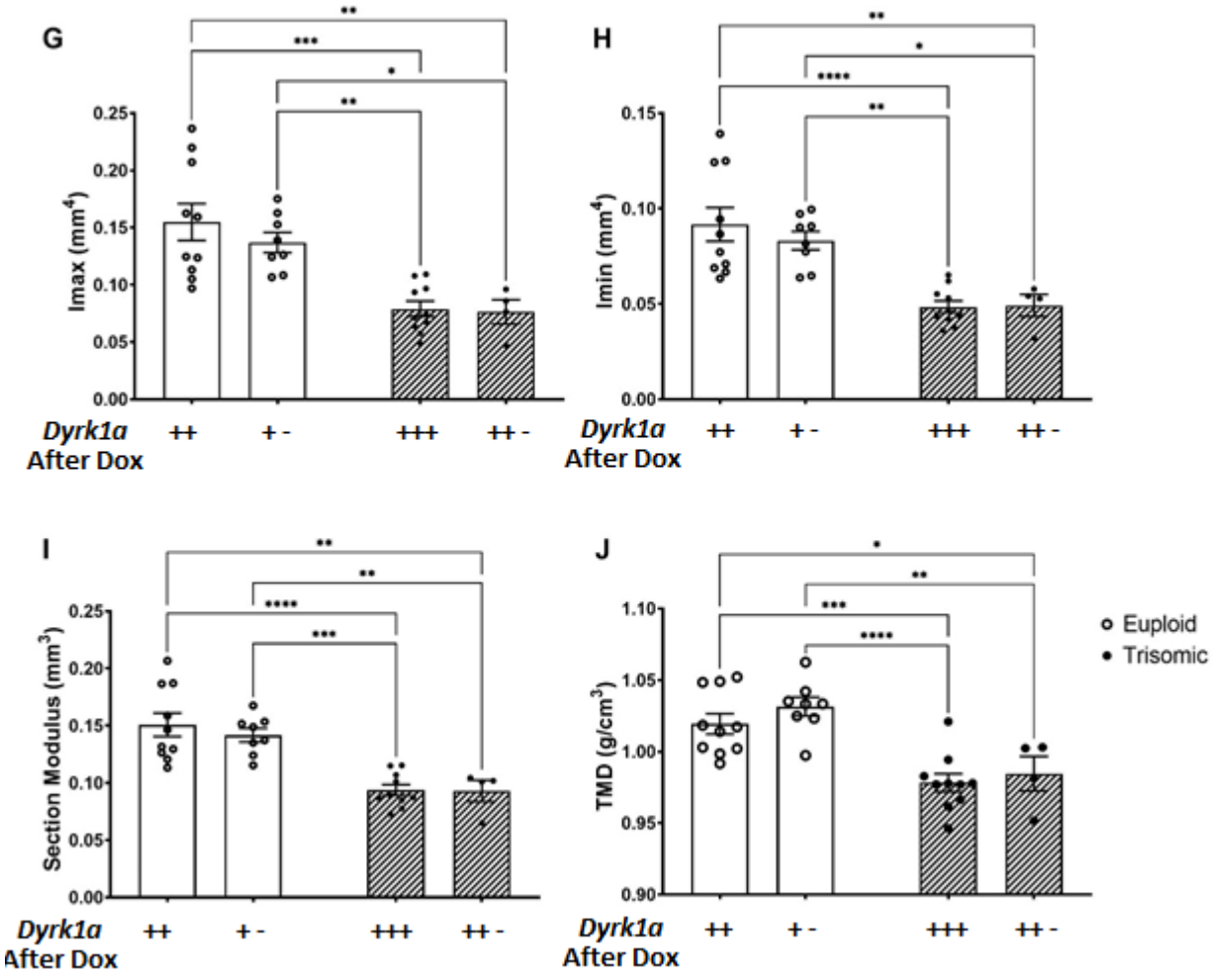

3.4.2 Determine if Mechanical Properties are Affected by Gene Dosage Normalization of *Dyrk1a* at P30 in Ts65Dn, *Dyrk1a*$^{+/fl}$ Mice

Three-point bending was utilized to assess mechanical properties in Ts65Dn, *Dyrk1a*$^{+/fl}$, femurs (**Table 6B., Table 8.**). Two-way ANOVA of Euploid, *Dyrk1a*$^{+/fl}$, Cre –; Euploid, *Dyrk1a*$^{+/fl}$, Cre +; Ts65Dn, *Dyrk1a*$^{+/fl}$, Cre –; Ts65Dn, *Dyrk1a*$^{+/fl}$, Cre + (the same mice described above) mice was utilized to determine effects of genotype, gene dosage, and interactions affecting mechanical properties (**Table 9**).

Analysis revealed a genotype effect on Ultimate Force [$F(1,17)=33.60$, $p<0.0001$] (**Figure 28B.**), Postyield Displacement [$F(1,17)=11.57$, $p=0.0034$] (**Figure 28D.**), Total Displacement [$F(1,17)=11.55$, $p=0.0034$] (**Figure 28E.**), Stiffness [$F(1,17)=22.52$, $p=0.0002$] (**Figure 28F.**), Total Strain [$F(1,17)=0.0117$, $p=0.0117$] (**Figure 21M.**), Toughness [$F(1,17)=0.0046$, $p=0.0046$] (**Figure 28P.**), and Failure Force [$F(1,17)=20.47$, $p=0.0003$] (**Figure 28Q.**). No gene dosage effect was observed. An interaction was observed in Ultimate Strain [$F(1,17)=5.747$, $p=0.0283$], but not in any other measures (**Table 9**).

Tukey's multiple comparison post hoc tests identified significant differences between Euploid and Ts65Dn mice without gene copy reduction in many mechanical measures including: Ultimate Force ($p=0.0009$) (**Figure 28B**), Stiffness ($p=0.0121$) (**Figure 28F**), and Failure Force ($p=0.0269$) (**Figure 28Q**). Reduction of *Dyrk1a* gene dosage from P21 to P30 in Ts65Dn mice failed to improve any mechanical measures. Mechanical measures in euploid mice were not significantly affected by only a single functional copy of *Dyrk1a* after P21.

Table 8. Means and SEM for mechanical analysis of male Ts65Dn, *Dyrk1a*$^{+/fl}$ femurs at P30 following gene dosage reduction at P21. Disp. = Displacement. [a] Main effect of genotype; [b] Main effect of gene dosage; [c] Interactive effect

Measure	Euploid, *Dyrk1a*$^{+/fl}$	Euploid, *Dyrk1a*$^{+/fl}$	Ts65Dn, *Dyrk1a*$^{+/fl}$	Ts65Dn, *Dyrk1a*$^{+/fl}$
rtTA, Cre	-	+	-	+
Functional *Dyrk1a*	++	+ -	+++	++ -
Sample Size	6	4	6	5
Yield Force (N)	3.91 ± 1.39	7.09 ± 0.89	3.59 ± 0.56	4.11 ± 0.38
Ultimate Force (N)[a]	13.09 ± 0.73	12.93 ± 0.44	8.78 ± 0.48	9.20 ± 0.91
Disp. to Yield (µm)	63.83 ± 19.66	113 ± 5.05	92.17 ± 11.56	100 ± 1.38
Postyield Disp. (µm)[a]	786.33 ± 94.44	469.75 ± 67.83	1240.67 ± 149.18	1026 ± 215.16
Total Disp. (µm)[a]	850.17 ± 107.81	582.75 ± 70.39	1332.83 ± 147.11	1126 ± 14.48
Stiffness (N/mm)[a]	61.37 ± 4.29	64.96 ± 6.39	40.98 ± 2.83	43.49 ± 4.51
Work to Yield (mJ)	.20 ± 0.09	0.43 ± 0.06	0.20 ± 0.04	0.23 ± 0.02
Postyield Work (mJ)	7.44 ± 0.66	5.03 ± 0.73	7.06 ± 0.59	7.16 ± 1.42
Total Work (mJ)	7.64 ± 0.74	5.46 ± 0.74	7.25 ± 0.59	7.39 ± 1.42
Yield Stress (MPa)	22.87 ± 8.86	45.71 ± 4.92	36.90 ± 6.34	37.61 ± 1.92
Ultimate Stress (MPa)	75.84 ± 3.56	84.05 ± 3.95	89.57 ± 4.55	83.64 ± 2.80
Strain to Yield (me)	30.65 ± 9.25	52.52 ± 3.19	37.97 ± 4.83	42.36 ± 0.45
Total Strain (me)[a]	407.05 ± 40.73	271.23 ± 36.39	543.33 ± 54.33	478.59 ± 91.50
Modulus (GPa)	0.75 ± 0.10	0.91 ± 0.09	1.03 ± 0.10	0.94 ± 0.05
Resilience (MPa)	0.56 ± 0.25	1.27 ± 0.16	0.84 ± 0.18	0.88 ± 0.05
Toughness (MPa)[a]	21.52 ± 2.15	16.16 ± 1.38	30.88 ± 3.19	28.02 ± 4.74
Failure Force (N)[a]	8.67 ± 1.24	10.17 ± 0.97	4.80 ± 0.67	5.53 ± 0.55
Ultimate Disp.(µm)	411.17 ± 22.88	359 ± 36.57	401.83 ± 22.29	449 ± 13.81
Failure Stress (MPa)	48.84 ± 4.90	67.16 ± 9.50	48.00 ± 4.97	50.34 ± 2.14
Ultimate Strain (me)[c]	200.33 ± 13.90	166.06 ± 16.0	165.23 ± 9.97	190.75 ± 9.08

Table 9. ANOVA results table for mechanical analysis of male Ts65Dn, *Dyrk1a*$^{+/fl}$, rtTA^{+}, TetOCre^{+} femurs. Disp. = Displacement. [a] Main effect of genotype; [b] Main effect of gene dosage; [c] Interactive effect

Measure	Source of Variation		
	Genotype	Gene Dosage	Interaction
Yield Force (N)	F (1, 17) = 2.969, p=0.1030	F (1, 17) = 3.731, p=0.0703	F (1, 17) = 1.932, p=0.1825
Ultimate Force (N) [a]	F (1, 17) = 33.60, p<0.0001	F (1, 17) = 0.03593, p=0.8519	F (1, 17) = 0.1803, p=0.6765
Disp. to Yield (µm)	F (1, 17) = 0.3200, p=0.5790	F (1, 17) = 4.422, p=0.0507	F (1, 17) = 2.325, p=0.1457
Postyield Disp. (mm) [a]	F (1, 17) = 11.57, p=0.0034	F (1, 17) = 3.196, p=0.0917	F (1, 17) = 0.1176, p=0.7358
Total Disp. (mm) [a]	F (1, 17) = 11.55, p=0.0034	F (1, 17) = 2.468, p=0.1346	F (1, 17) = 0.04028, p=0.8433
Stiffness (N/mm) [a]	F (1, 17) = 22.52, p=0.0002	F (1, 17) = 0.4775, p=0.4989	F (1, 17) = 0.01496, p=0.9041
Work to Yield (mJ)	F (1, 17) = 2.705, p=0.1184	F (1, 17) = 4.142, p=0.0577	F (1, 17) = 2.501, p=0.1322
Postyield Work (mJ)	F (1, 17) = 0.9421, p=0.3453	F (1, 17) = 1.651, p=0.2160	F (1, 17) = 1.958, p=0.1797
Total Work (mJ)	F (1, 17) = 0.6977, p=0.4152	F (1, 17) = 1.244, p=0.2802	F (1, 17) = 1.581, p=0.2256
Yield Stress (MPa)	F (1, 17) = 0.1936, p=0.6655	F (1, 17) = 3.068, p=0.0979	F (1, 17) = 2.707, p=0.1183
Ultimate Stress (MPa)	F (1, 17) = 2.877, p=0.1081	F (1, 17) = 0.08480, p=0.7744	F (1, 17) = 3.240, p=0.0896
Strain to Yield (me)	F (1, 17) = 0.05181, p=0.8227	F (1, 17) = 4.413, p=0.0509	F (1, 17) = 1.954, p=0.1802
Total Strain (me) [a]	F (1, 17) = 7.968, p=0.0117	F (1, 17) = 0.3408, p=0.1178	F (1, 17) = 2.714, p=0.5670
Modulus (GPa)	F (1, 17) = 2.612, p=0.1244	F (1, 17) = 0.1172, p=0.7363	F (1, 17) = 1.922, p=0.1836
Resilience (MPa)	F (1, 17) = 0.08099, p=0.7794	F (1, 17) = 3.932, p=0.0638	F (1, 17) = 3.004, p=0.1012
Toughness (MPa) [a]	F (1, 17) = 10.65, p=0.0046	F (1, 17) = 1.602, p=0.2227	F (1, 17) = 0.1476, p=0.7056
Failure Force (N) [a]	F (1, 17) = 20.47, p=0.0003	F (1, 17) = 1.415, p=0.2506	F (1, 17) = 0.1679, p=0.6871
Ultimate Disp. (µm)	F (1, 17) = 2.797, p=0.1127	F (1, 17) = 0.01075, p=0.9186	F (1, 17) = 4.242, p=0.0551
Failure Stress (MPa)	F (1, 17) = 2.567, p=0.1276	F (1, 17) = 3.515, p=0.0781	F (1, 17) = 2.099, p=0.1655
Ultimate Strain (me)	F (1, 17) = 0.1740, p=0.6818	F (1, 17) = 0.1231, p=0.7300	F (1, 17) = 5.747, p=0.0283

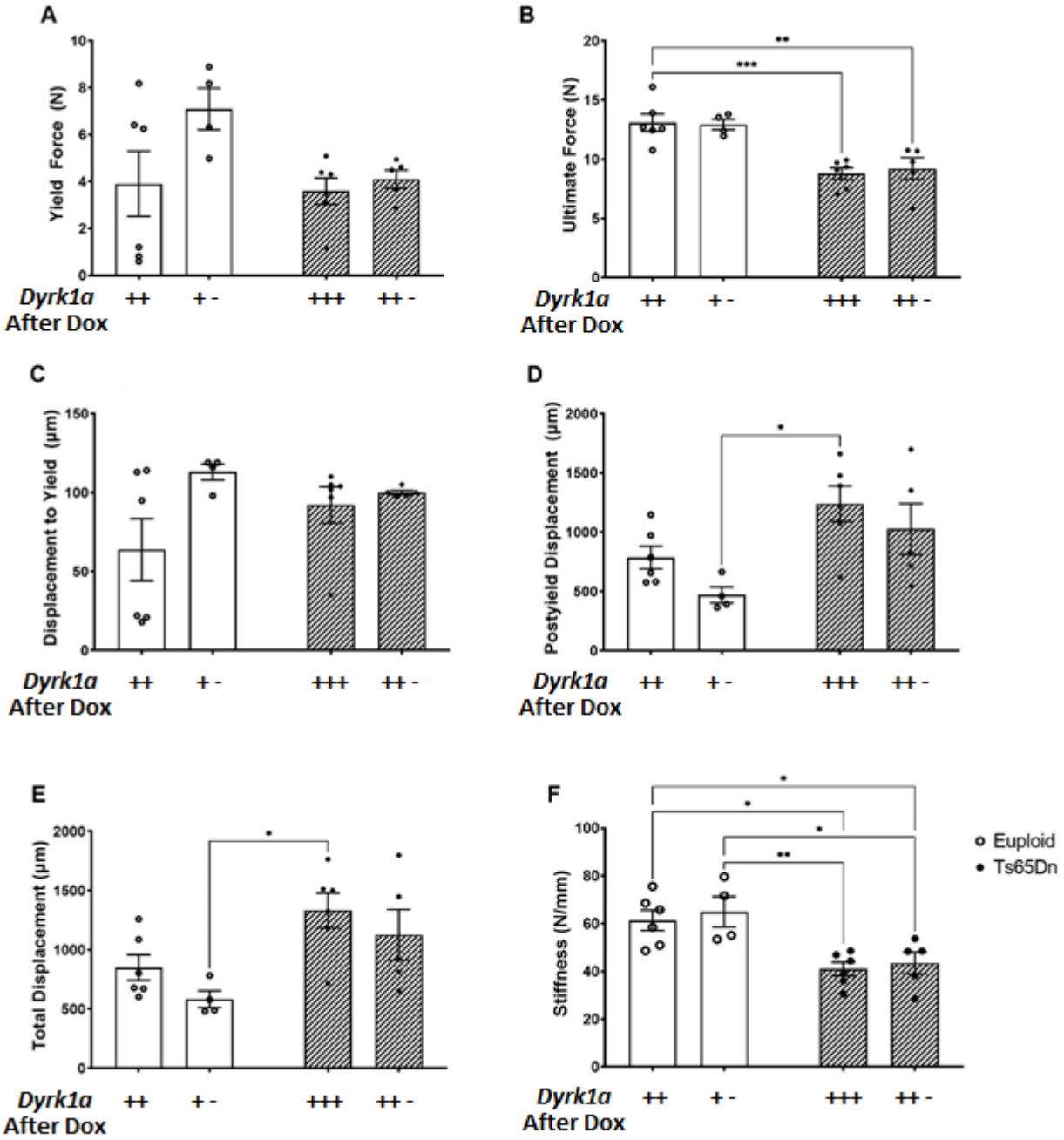

Figure 28. Three-point bending mechanical analysis of male P30 Ts65Dn, Dyrk1a+/fl femurs following gene dosage reduction through Cre-loxp induction by doxycycline administration from P21-29. Bars are means, error bars are SEM. Two-way ANOVA, Tukey's post hoc *p≤0.05, **p≤0.01, ***p≤0.001, ****p≤0.0001.

Figure 28. continued

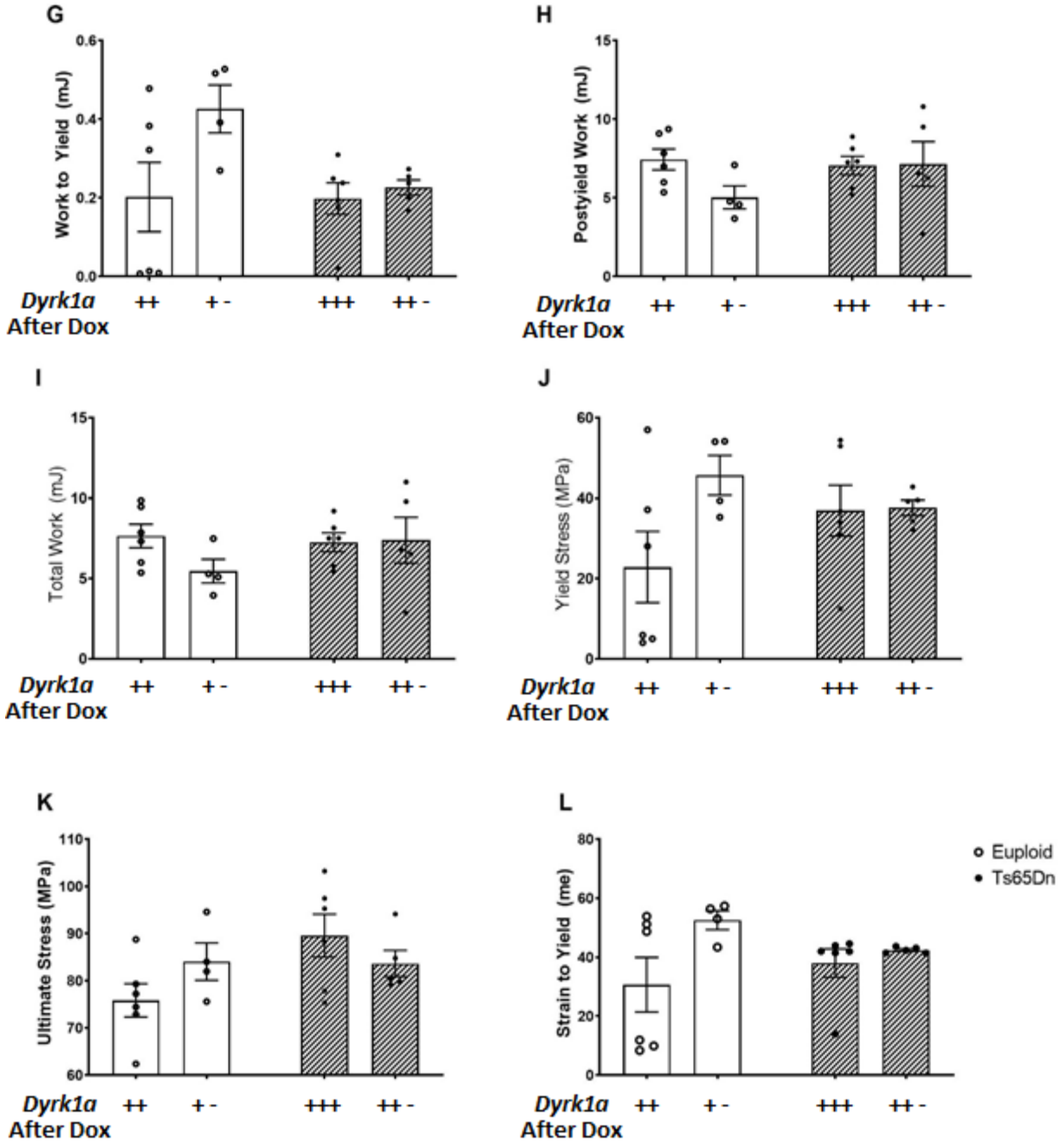

Figure 28. continued

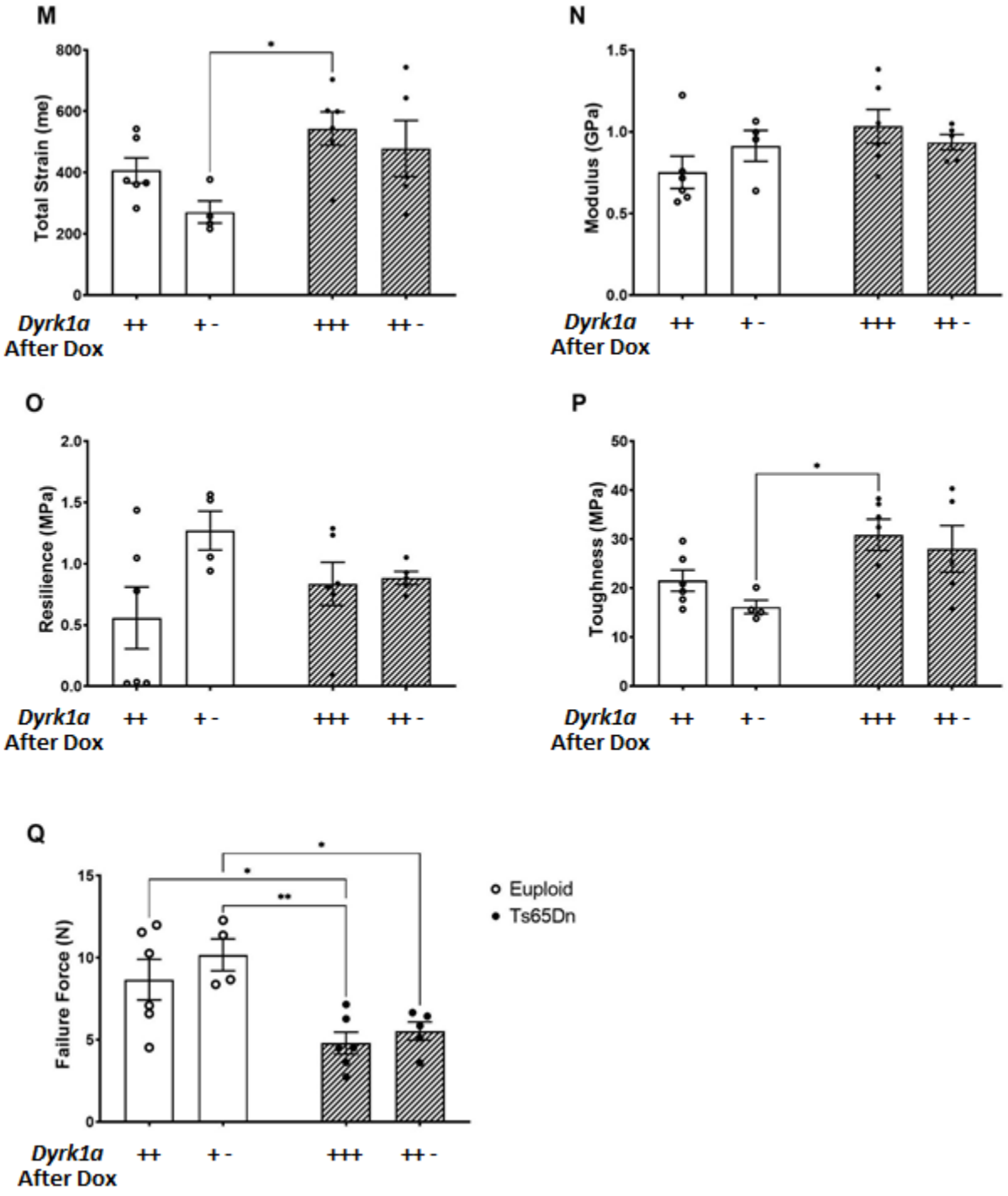

Figure 28. continued

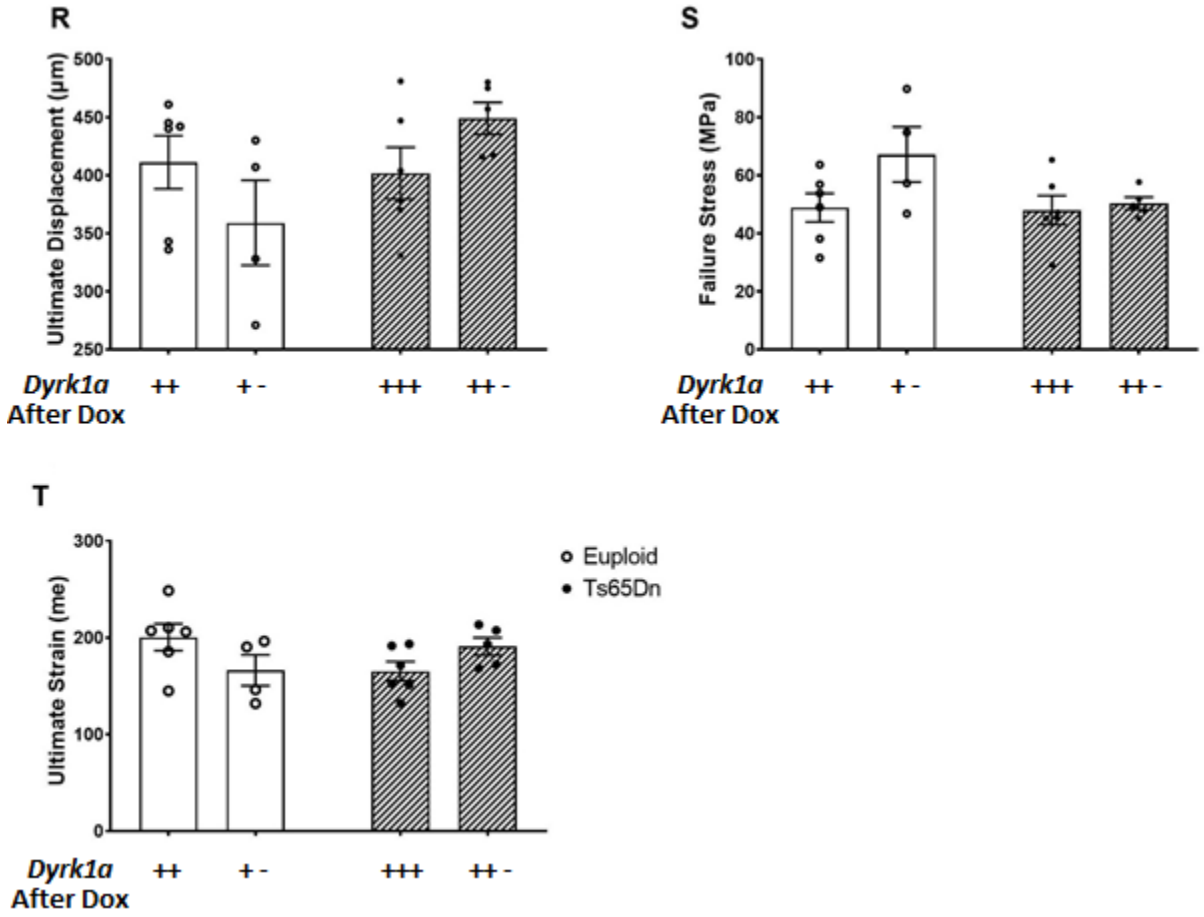

3.4.3 Verify Reduced *Dyrk1a* Gene Expression in P30 Male Ts65Dn, *Dyrk1a*$^{+/fl}$ Mice

To verify that reduction of *Dyrk1a* copy number was reduced *Dyrk1a* expression in P30 male Ts65Dn, *Dyrk1a*$^{+/fl}$, *rtTA*$^{+}$, *Cre*$^{+}$ mice that received doxycycline in chow at weaning (P21), RNA was isolated from left femurs of experimental mice for qPCR gene expression analysis (**Table 10**). All RNA samples were derived from femurs opposite of those used for μCT skeletal analysis and mechanical testing. This strain loses exons 5-6 of *Dyrk1a* following cre-loxp activation, rendering the transcript and translated protein nonfunctional. A difference in expression between Euploid and Ts65Dn mice missing exon 5-6 was hypothesized to be detectable by targeting the *Dyrk1a* mRNA product spanning exons 5-6 in these mice. There was no statistical difference in the expression of *Dyrk1a* exon 5-6 between male Ts65Dn mice confirmed by PCR to have *Dyrk1a* exon 5-6 excised and trisomic mice without the excision (**Figure 29**). There are three possible explanations to explain the results of these data: 1) a feedback mechanism compensating for loss of an allele of *Dyrk1a* 2) an effect of doxycycline on *Dyrk1a* expression 3) reduced statistical power compared to structural geometry and mechanical testing analyses. However, without the data to support these hypotheses, the explanation remains unknown.

Table 10. Sample sizes for assessment of *Dyrk1a* expression in male P30 Ts65Dn, *Dyrk1a*$^{+/fl}$ femurs following gene dosage reduction through Cre-loxp induction by doxycycline administration from P21-29.

P30 Ts65Dn, *Dyrk1a*$^{+/fl}$ Gene Expression				
Genotype	**Euploid, *Dyrk1a*$^{+/fl}$**	**Euploid, *Dyrk1a*$^{+/fl}$**	**Ts65Dn, *Dyrk1a*$^{+/fl}$**	**Ts65Dn, *Dyrk1a*$^{+/fl}$**
rtTA, Cre	-	+	-	+
Functional *Dyrk1a*	++	+ -	+++	++ -
Sample Size	4	3	5	4

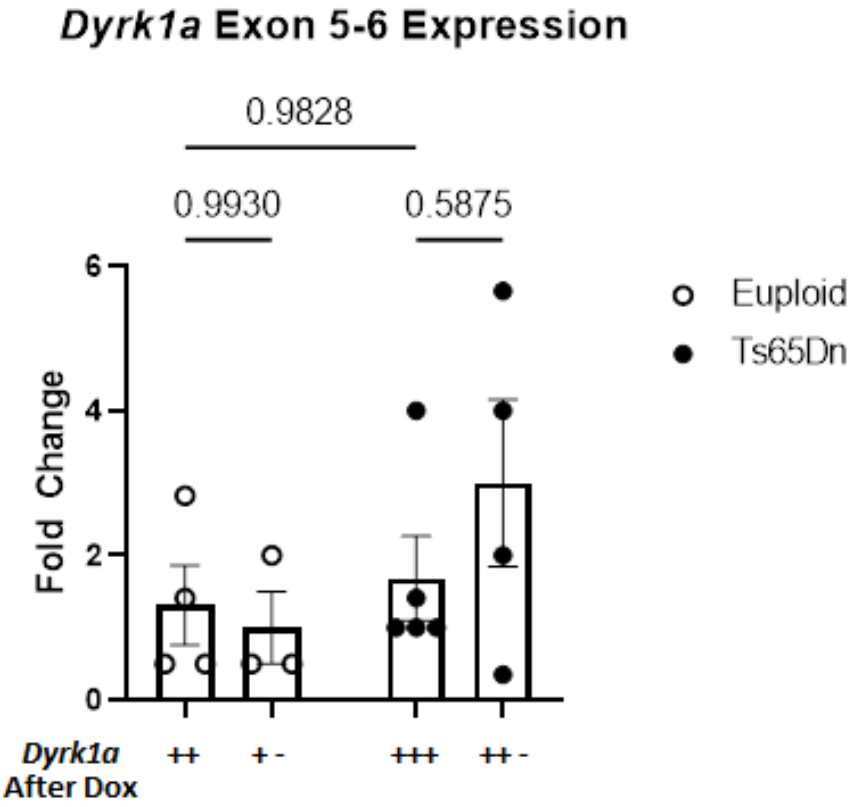

Figure 29. Expression of Dyrk1a exon5-6 in P30 male Ts65Dn, Dyrk1a+/fl femurs. Cre - mice did not have genotypes capable of Cre-Loxp recombination.Cre + mice were verified to possess a truncated Dyrk1a allele at P30. Bars represent means and error bars are SEM. Two-way ANOVA, Tukey's post hoc *p≤0.05, **p≤0.01, ***p≤0.001, ****p≤0.0001

3.5 Aim 1.3a Determine if Reduction of *Dyrk1a* Copy Number in Male Ts65Dn Mice from Conception Prevents the Emergence of Appendicular Skeletal Defects

Previous experiments that reduced the functional *Dyrk1a* gene dosage from three alleles to two alleles in otherwise trisomic male mice from the point of conception demonstrated a significant improvement in trabecular phenotypes by P42(Blazek, Abeysekera, et al., 2015). Euploid mice with two functional copies of *Dyrk1a* are identified as Euploid, $Dyrk1a^{+/+}$; mice with reduced gene dosage are identified as Euploid, $Dyrk1a^{+/-}$; Ts65Dn mice with three functional copies of *Dyrk1a* are identified as Ts65Dn, $Dyrk1a^{+/+}$; Ts65Dn mice with reduced gene dosage (two functional copies on an otherwise trisomic background) are identified as Ts65Dn, $Dyrk1a^{+/-}$ Reduction of *Dyrk1a* gene copy number in these mice was verified by PCR (**Figure 30**.). This apparent rescue led to the hypothesis that reducing gene dosage of *Dyrk1a* in otherwise trisomic male mice from conception mitigates the emergence of abnormal trabecular phenotypes at P30. Femurs obtained from all four genotypes at P30 were analyzed by μCT (**Table 11a.**) as described in Aim 1.1 and subjected to mechanical analysis at the same time as Ts65Dn, $Dyrk1a^{+/fl}$ femurs (**Table 11b.**).

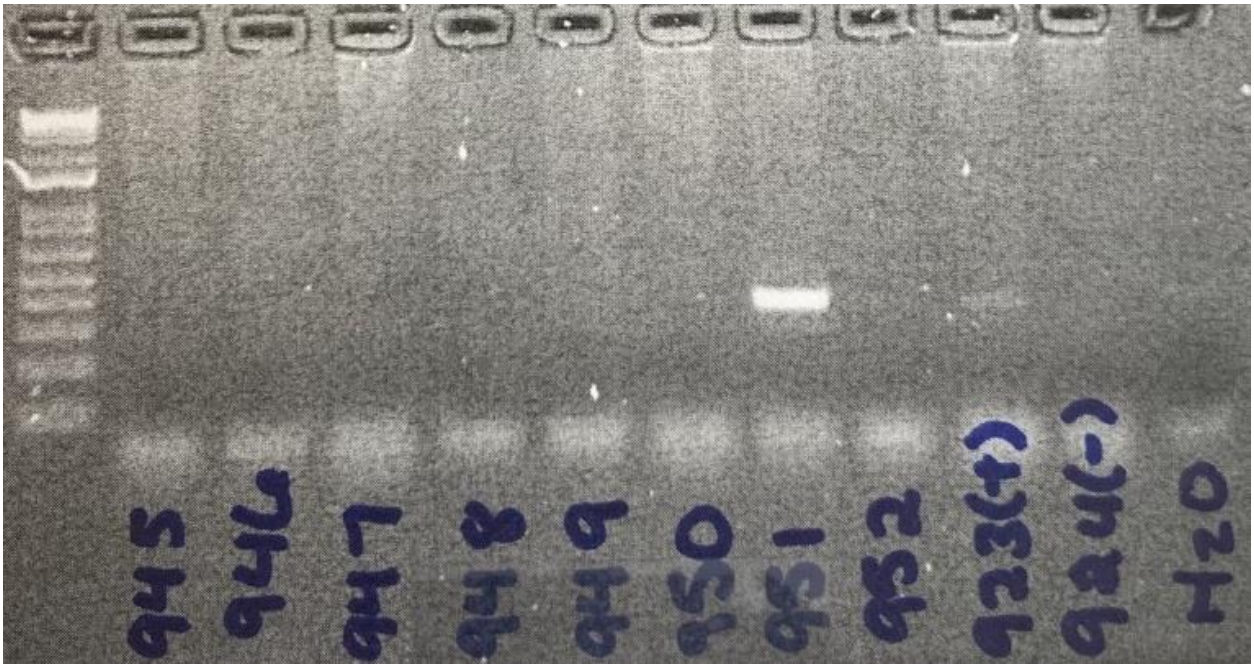

Figure 30. PCR verification of *Dyrk1a* gene copy reduction in Ts65Dn, $Dyrk1a^{+/-}$ mice. Number 951 and the control 923 are positive for the reduction whereas the others are all negative.

Table 11. Sample sizes for geometric (a) and mechanical measures (b) in P30 male Ts65Dn, *Dyrk1a*$^{+/-}$ femurs following gene dosage reduction at conception.

***Dyrk1a* Dosage Reduction from Conception in Male Ts65Dn Mice**

a

P30 Femur Structural Geometry Analysis				
Genotype	**Euploid, *Dyrk1a*$^{+/+}$**	**Euploid, *Dyrk1a*$^{+/-}$**	**Ts65Dn, *Dyrk1a*$^{+/+}$**	**Ts65Dn, *Dyrk1a*$^{+/-}$**
Functional Dyrk1a	++	+ -	+++	+ -
Sample Size	11	6	9	9

b

P30 Femur Mechanical Analysis				
Genotype	**Euploid, *Dyrk1a*$^{+/+}$**	**Euploid, *Dyrk1a*$^{+/-}$**	**Ts65Dn, *Dyrk1a*$^{+/+}$**	**Ts65Dn, *Dyrk1a*$^{+/-}$**
Functional Dyrk1a	++	+ -	+++	+ -
Sample Size	9	3	9	8

3.5.1 Characterize the Femur Geometry of P30 Male Ts65Dn, *Dyrk1a*$^{+/-}$ Mice

Two-way ANOVA of femur geometry revealed an effect of genotype on %BV/TV (**Figure 31A.**), Tb.Sp (**Figure 31C.**), Tb.N (**Figure 31D.**), Tb.Pf (**Figure 31E.**), Tt.Ar (**Figure 32A.**), Ma.Ar (**Figure 32B.**), Ct.Ar (**Figure 32C.**), Ct.Th (**Figure 32D.**), Ps.BS (**Figure 32E.**), Ec.BS (**Figure 32F.**), Section Modulus (**Figure 32I.**), and TMD (**Figure 32J.**). An effect of gene dosage was observed in %BV/TV, Tb.Th (**Figure 31B.**), Ma.Ar, and Ec.BS. A genotype x gene dosage interaction was detected in %BV/TV, Tb.Th, Ma.Ar, and Ec.BS (**Table 12**).

Tukey's post hoc analyses identified several defects in trabecular and cortical geometry in male Ts65Dn, *Dyrk1a*$^{+++}$ male mice at P30 including: significantly reduced %BV/TV (p=0.0001) (**Figure 31A.**), Tb.Th (p=0.0001) (**Figure 31B.**), Tb.N (p=0.0062) (**Figure 31D.**), Ma.Ar (p=0.0003) (**Figure 32B.**), Ps.BS (p=0.0379) (**Figure 32E.**), Ec.BS (p=0.0007) (**Figure 32F.**), and TMD (p=0.0216) (**Figure 32J.**), and increased Tb.Sp (p=0.0007) (**Figure 31C.**) and Tb.Pf (p=0.0070) (**Figure 31E.**) compared to Euploid, *Dyrk1a*$^{+/+}$ littermates. Contrary to the hypothesis, reduction of *Dyrk1a* copy number from conception failed to improve any trabecular or cortical measures in male Ts65Dn, *Dyrk1a*$^{++-}$ mice. Reduction of *Dyrk1a* in euploid mice significantly reduced %BV/TV (p=0.0101) through significant reduction of Tb.Th (p<0.0001). Cortical bone

was less adversely affected by reduced copy number with only Ma.Ar ($p=0.0133$) and Ec.BS ($p=0.0115$) being reduced compared to euploid mice with two functional alleles of *Dyrk1a*.

Table 12. ANOVA results for P30 male Ts65Dn, *Dyrk1a*$^{+/-}$ femur structural geometry following gene dosage reduction from conception. [a] Main effect of genotype; [b] Main effect of gene dosage; [c] Interactive effect

Measure	Source of Variation		
	Genotype	Gene Dosage	Interaction
%BV/TV [a,b,c]	F (1, 31) = 13.95, p=0.0008	F (1, 31) = 4.576, p=0.0404	F (1, 31) = 7.924, p=0.0084
Tb.Th [b,c]	F (1, 31) = 2.423, p=0.1297	F (1, 31) = 7.325, p=0.0110	F (1, 31) = 23.67, p<0.0001
Tb.Sp [a]	F (1, 31) = 23.72, p<0.0001	F (1, 31) = 3.135, p=0.0865	F (1, 31) = 0.6965, p=0.4103
Tb.N [a]	F (1, 31) = 13.21, p=0.0010	F (1, 31) = 1.170, p=0.2878	F (1, 31) = 0.9979, p=0.3255
Tb.Pf [a,c]	F (1, 31) = 4.865, p=0.0350	F (1, 31) = 1.260, p=0.2703	F (1, 31) = 5.606, p=0.0243
Tt.Ar [a]	F (1, 31) = 8.462, p=0.0067	F (1, 31) = 0.3099, p=0.5817	F (1, 31) = 0.07034, p=0.7926
Ma.Ar [a,b,c]	F (1, 31) = 11.78, p=0.0017	F (1, 31) = 4.844, p=0.0353	F (1, 31) = 6.720, p=0.0144
Ct.Ar [a]	F (1, 31) = 4.542, p=0.0411	F (1, 31) = 1.147, p=0.2925	F (1, 31) = 0.7540, p=0.3919
Ct.Th [a]	F (1, 31) = 6.586, p=0.0153	F (1, 31) = 0.5197, p=0.4764	F (1, 31) = 0.04324, p=0.8366
Ps.BS [a]	F (1, 31) = 11.62, p=0.0018	F (1, 31) = 0.03173, p=0.8598	F (1, 31) = 0.07371, p=0.7878
Ec.BS [a,b,c]	F (1, 31) = 9.750, p=0.0039	F (1, 31) = 5.466, p=0.0260	F (1, 31) = 6.450, p=0.0163
Imax	F (1, 31) = 2.223, p=0.1461	F (1, 31) = 2.112, p=0.1562	F (1, 31) = 2.094, p=0.1579
Imin	F (1, 31) = 3.428, p=0.0736	F (1, 31) = 1.547, p=0.2230	F (1, 31) = 1.317, p=0.2599
Section Modulus [a]	F (1, 31) = 5.375, p=0.0272	F (1, 31) = 0.7725, p=0.3862	F (1, 31) = 0.3807, p=0.5417
TMD [a]	F (1, 31) = 5.115, p=0.0309	F (1, 31) = 0.05956, p=0.8088	F (1, 31) = 2.987, p=0.0939

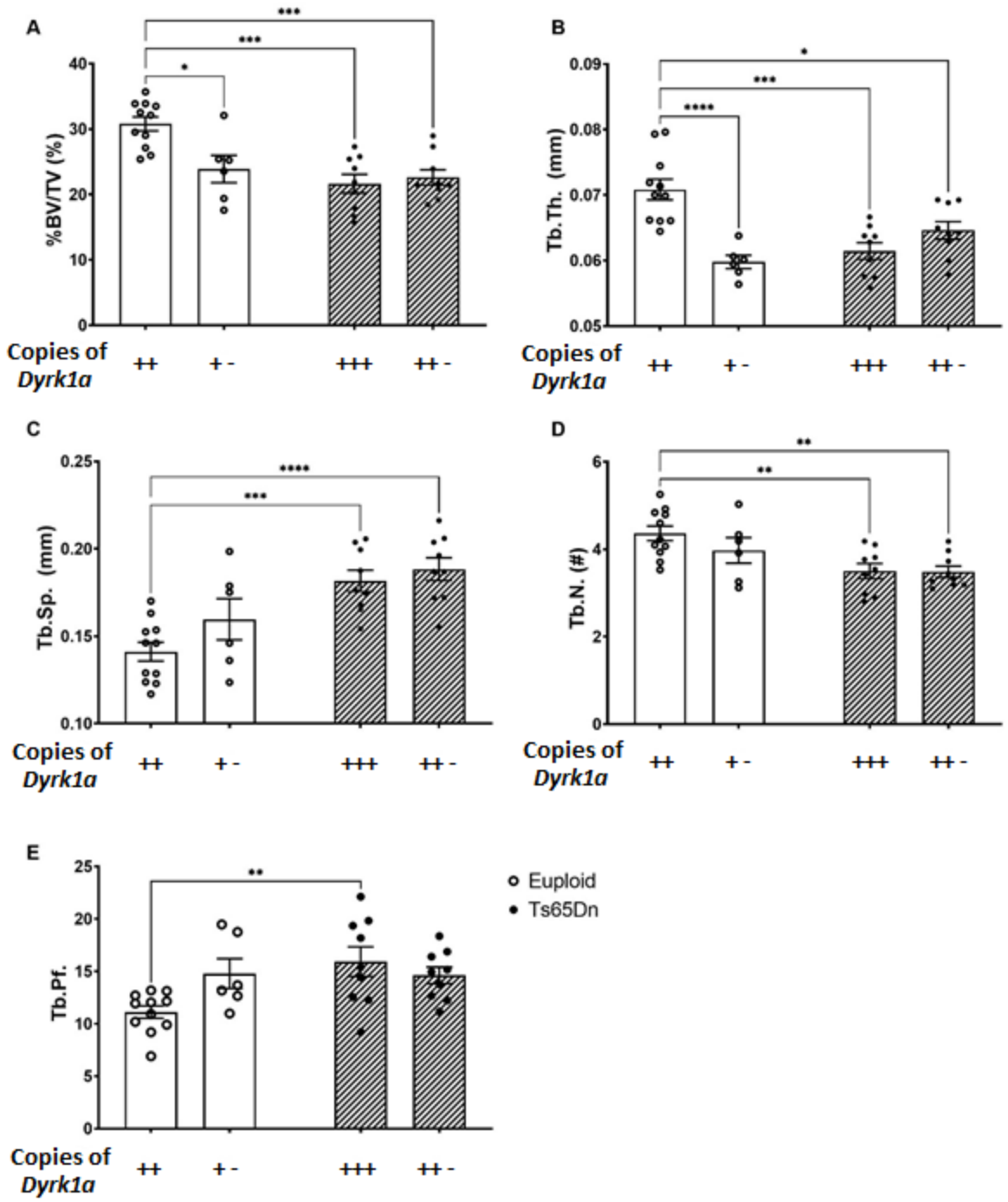

Figure 31. Trabecular geometry measures of P30 male Ts65Dn, Dyrk1a+/- femurs. Dyrk1a +/+ have two intact Dyrk1a alleles; Dyrk1a +/- have one truncated Dyrk1a allele, verified by PCR. Bars represent means and error bars are SEM. Two-way ANOVA and Tukey's post hoc *p≤0.05, **p≤0.01, ***p≤0.001, ****p≤0.0001.

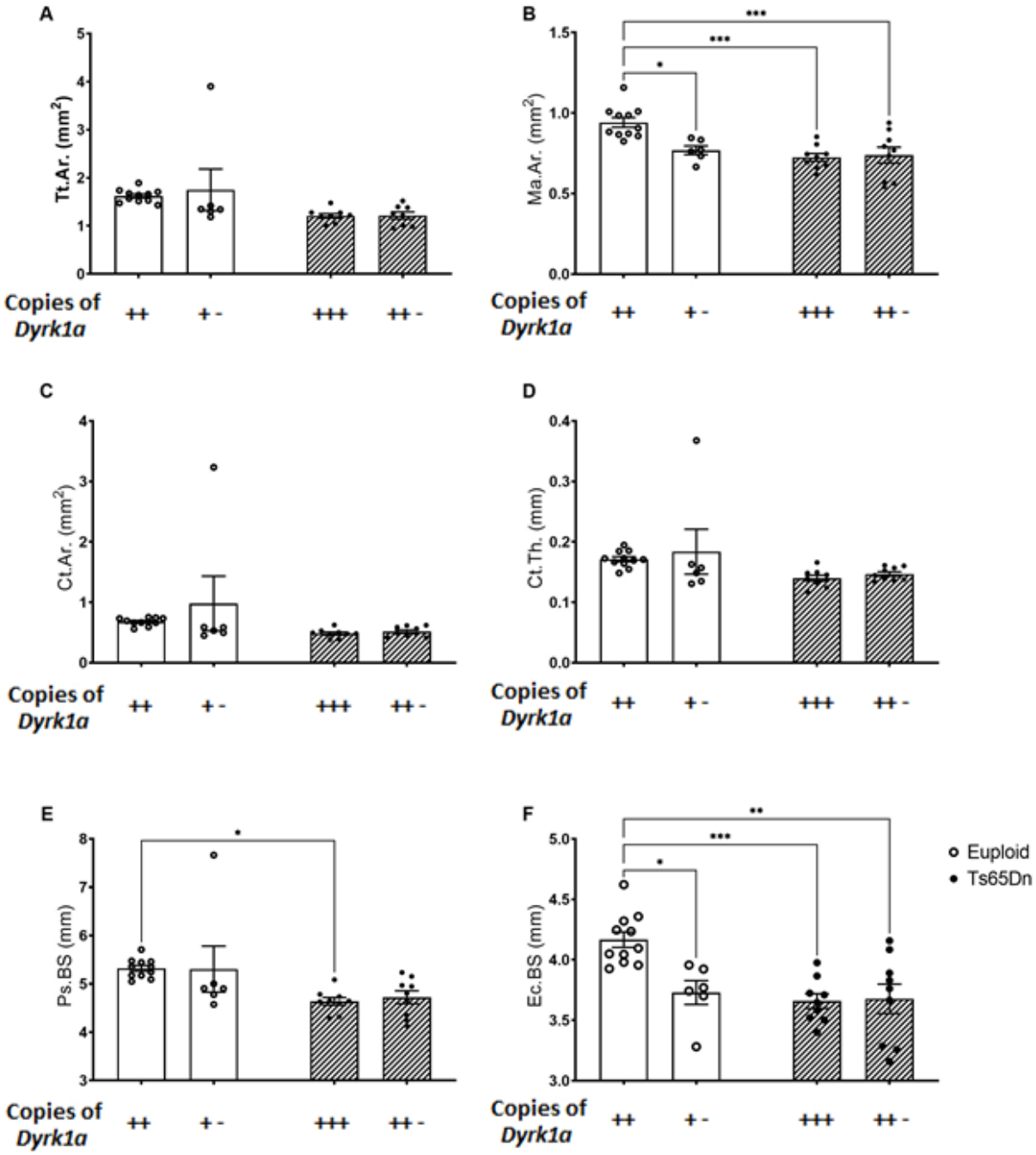

Figure 32. Cortical geometry measures of P30 male Ts65Dn, Dyrk1a+/- femurs. Dyrk1a +/+ have two intact Dyrk1a alleles; Dyrk1a +/- have one truncated Dyrk1a allele, verified by PCR. Bars represent means and error bars are SEM. Two-way ANOVA and Tukey's post hoc *p≤0.05, **p≤0.01, ***p≤0.001, ****p≤0.0001.

Figure 32. continued

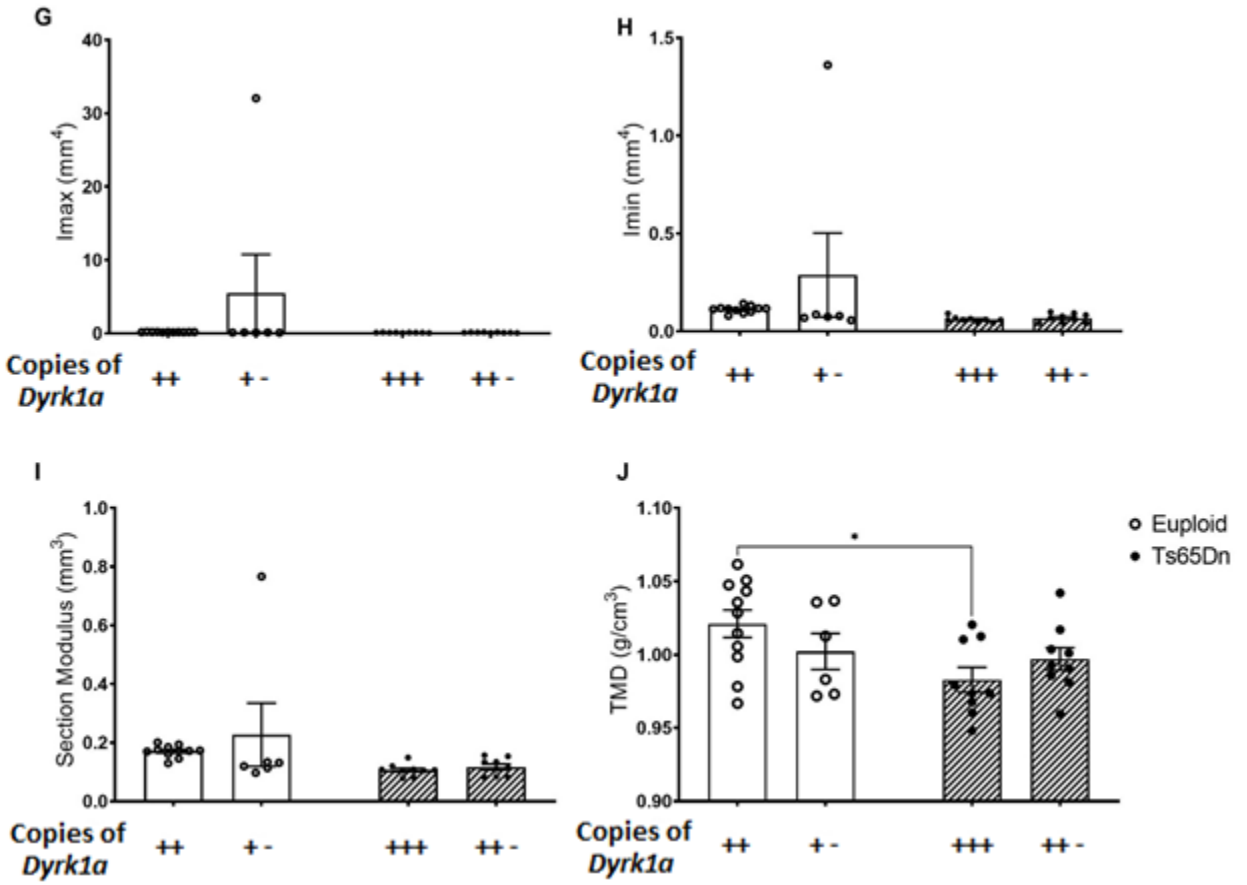

Trabecular defects between Euploid and Ts65Dn mice without gene dosage reduction were identical to those reported previously(Blazek, Abeysekera, et al., 2015), but gene dosage reduction had not corrected the defects at P30. A difference in Tb.Th was observed at P30 in the model used here but not in the model used to characterize skeletal development. The mice utilized for both all *in vivo* experiments herein were maintained on a 50% C57BL/6, 50% C3H background to minimize differences in genetic background; however, it seems that compromised Tb.Th is a unique phenotype at P30 in Ts65Dn, *Dyrk1a*$^{+/-}$ mice. Together, these results suggest that improvement in trabecular geometry in Ts65Dn, *Dyrk1a*$^{+/+}$ male mice must occur between P30 and P42 and that *Dyrk1a* does may not influence bone phenotypes up to P30.

3.5.2 Determine if Mechanical Properties are Affected by Gene Dosage Normalization of *Dyrk1a* at P30 in Ts65Dn, *Dyrk1a*$^{+/-}$ Mice

Femurs from Ts65Dn, *Dyrk1a*$^{+/-}$ model mice that were analyzed by μCT were also subjected to mechanical testing (**Table 11b.**). Three-point bending was utilized to assess mechanical strength (**Table 13.**). Two-way ANOVA of Euploid, *Dyrk1a*$^{+/+}$, Euploid, *Dyrk1a*$^{+/-}$, Ts65Dn, *Dyrk1a*$^{+/+}$, and Ts65Dn, *Dyrk1a*$^{+/-}$ mice was utilized to determine effects of genotype, gene dosage, and interactions affecting mechanical properties (**Table 14**). Two-way ANOVA showed a genotype effect in Ultimate Force (**Figure 33B.**), Stiffness (**Figure 33F.**), Modulus (**Figure 33N.**), and Ultimate Strain (**Figure 33T.**). An effect of gene dosage was observed in Ultimate Force and to a lesser extent Failure Force, but no other measures. An interaction between genotype and gene dosage was detected in Ultimate Force, Stiffness, and Failure Force (**Table 14**).

Tukey's multiple comparison post hoc test showed significant reductions in the mechanical properties of P30 male Ts65Dn, *Dyrk1a*$^{+/-}$ mice compared euploid littermates in the following measures: Yield Force (p=0.0249) (**Figure 33A.**), Ultimate Force (p=0.0005) (**Figure 33B.**), Stiffness (p=0.0020) (**Figure 33F.**), Work to Yield (p=0.0413) (**Figure 33G.**), Modulus (p=0.0460) (**Figure 33N.**), Failure Force (p=0.0126) (**Figure 33Q.**), and Ultimate Strain (p=0.0493) (**Figure 33T.**). The mechanical properties of euploid mice with reduced *Dyrk1a* gene dosage were mostly unaffected with the exception of reduced Ultimate Force (p=0.0533) and Failure Force (p=0.0574), although statistical significance was not reached.

Table 13. Means and SEM for mechanical analysis of male Ts65Dn, *Dyrk1a*$^{+/-}$ femurs at P30 following gene dosage reduction from conception. Disp. = Displacement. [a] Effect of genotype. [b] Effect of gene dosage. [c] Interactive effect

Measure	Euploid, *Dyrk1a*$^{+/=}$	Euploid, *Dyrk1a*$^{+/-}$	Ts65Dn, *Dyrk1a*$^{+/=}$	Ts65Dn, *Dyrk1a*$^{+/-}$
Functional *Dyrk1a*	++	+ -	+++	+ -
Sample Size	9	3	9	8
Yield Force (N)	6.00 ± 0.74	4.77 ± 0.82	3.60 ± 0.54	4.79 ± 0.30
Ultimate Force (N) [a,b,c]	13.95 ± 0.65	10.29 ± 1.25	9.53 ± 0.75	9.50 ± 0.62
Disp. to Yield (µm)	97.67 ± 11.61	101.67 ± 2.19	85.67 ± 10.90	102.25 ± 1.71
Postyield Disp. (mm)	1.08 ± 1.70	0.96 ± 0.26	1.06 ± 0.16	1.00 ± 0.14
Total Disp. (mm)	1.18 ± 0.17	1.06 ± 0.26	1.15 ± 0.16	1.11 ± 0.14
Stiffness (N/mm) [a,c]	63.91 ± 2.95	49.40 ± 9.32	44.45 ± 2.95	49.38 ± 3.62
Work to Yield (mJ)	0.35 ± 0.05	0.26 ± 0.04	0.19 ± 0.04	0.26 ± 0.01
Postyield Work (mJ)	11.09 ± 1.68	7.22 ± 1.97	7.36 ± 1.40	6.70 ± 0.78
Total Work (mJ)	11.44 ± 1.69	7.47 ± 2.01	7.55 ± 1.39	6.96 ± 0.79
Yield Stress (MPa)	31.17 ± 3.92	34.01 ± 4.54	31.81 ± 5.02	40.14 ± 2.77
Ultimate Stress (MPa)	72.57 ± 3.00	76.69 ± 5.60	80.94 ± 3.44	79.23 ± 5.18
Strain to Yield (me)	51.7 ± 6.07	49.79 ± 1.34	38.20 ± 4.75	46.41 ± 1.36
Total Strain (me)	622.65 ± 86.36	515.16 ± 116.66	519.62 ± 76.05	501.96 ± 63.99
Modulus (GPa) [a]	0.63 ± 0.03	0.72 ± 0.12	0.85 ± 0.05	0.92 ± 0.08
Resilience (MPa)	0.95 ± 0.15	0.90 ± 0.10	0.77 ± 0.15	1.00 ± 0.06
Toughness (MPa)	31.63 ± 4.65	25.86 ± 5.76	27.75 ± 3.92	26.17 ± 2.67
Failure Force (N) [c]	8.76 ± 0.87	5.11 ± 0.84	5.53 ± 0.56	5.76 ± 0.64
Ultimate Disp. (µm)	436.56 ± 23.71	423.00 ± 22.11	430.89 ± 16.57	411.88 ± 17.01
Failure Stress (MPa)	45.36 ± 4.21	36.76 ± 5.14	47.44 ± 4.31	46.90 ± 4.36
Ultimate Strain (me) [a]	232.08 ± 13.13	207.09 ± 10.52	193.32 ± 8.02	186.97 ± 9.00

Table 14. ANOVA results table for P30 male Ts65Dn, *Dyrk1a*$^{+/-}$ femur mechanical analysis following gene dosage reduction from conception. Disp. = Displacement. [a] Effect of genotype. [b] Effect of gene dosage. [c] Interactive effect

Measure	Source of Variation		
	Genotype	Gene Dosage	Interaction
Yield Force (N)	F (1, 25) = 3.024, p=0.0944	F (1, 25) = 0.0009004, p=0.9763	F (1, 25) = 3.109, p=0.0901
Ultimate Force (N) [a,b,c]	F (1, 25) = 9.798, p=0.0044	F (1, 25) = 4.904, p=0.0361	F (1, 25) = 4.765, p=0.0387
Disp. to Yield (µm)	F (1, 25) = 0.2595, p=0.6149	F (1, 25) = 0.8435, p=0.3672	F (1, 25) = 0.3153, p=0.5795
Postyield Disp. (mm)	F (1, 25) = 0.003540, p=0.9530	F (1, 25) = 0.2227, p=0.6411	F (1, 25) = 0.02980, p=0.8643
Total Disp. (mm)	F (1, 25) = 0.0008908, p=0.9764	F (1, 25) = 0.1766, p=0.6779	F (1, 25) = 0.04265, p=0.8381
Stiffness (N/mm) [a,c]	F (1, 25) = 5.543, p=0.0267	F (1, 25) = 1.345, p=0.2572	F (1, 25) = 5.526, p=0.0269
Work to Yield (mJ)	F (1, 25) = 2.422, p=0.1322	F (1, 25) = 0.02747, p=0.8697	F (1, 25) = 2.850, p=0.1038
Postyield Work (mJ)	F (1, 25) = 1.657, p=0.2098	F (1, 25) = 1.889, p=0.1815	F (1, 25) = 0.9448, p=0.3404
Total Work (mJ)	F (1, 25) = 1.760, p=0.3191	F (1, 25) = 1.887, p=0.1817	F (1, 25) = 1.034, p=0.1966
Yield Stress (MPa)	F (1, 25) = 0.4844, p=0.4928	F (1, 25) = 1.320, p=0.2616	F (1, 25) = 0.3195, p=0.5769
Ultimate Stress (MPa)	F (1, 25) = 2.231, p=0.1478	F (1, 25) = 0.004049, p=0.9498	F (1, 25) = 0.09216, p=0.7640
Strain to Yield (me)	F (1, 25) = 2.385, p=0.1351	F (1, 25) = 0.3326, p=0.5693	F (1, 25) = 0.8550, p=0.3640
Total Strain (me)	F (1, 25) = 0.3925, p=0.5367	F (1, 25) = 0.4551, p=0.5061	F (1, 25) = 0.2344, p=0.6325
Modulus (GPa) [a]	F (1, 25) = 9.163, p=0.0057	F (1, 25) = 1.311, p=0.2631	F (1, 25) = 0.02589, p=0.8735
Resilience (MPa)	F (1, 25) = 0.07171, p=0.7911	F (1, 25) = 0.3461, p=0.5616	F (1, 25) = 0.8399, p=0.3682
Toughness (MPa)	F (1, 25) = 0.1437, p=0.7079	F (1, 25) = 0.6070, p=0.4432	F (1, 25) = 0.1981, p=0.6601
Failure Force (N) [c]	F (1, 25) = 2.349, p=0.1379	F (1, 25) = 4.147, p=0.0524	F (1, 25) = 5.313, p=0.0298
Ultimate Disp. (µm)	F (1, 25) = 0.1305, p=0.7210	F (1, 25) = 0.4909, p=0.4900	F (1, 25) = 0.01379, p=0.9075
Failure Stress (MPa)	F (1, 25) = 1.430, p=0.2430	F (1, 25) = 0.7998, p=0.3797	F (1, 25) = 0.6212, p=0.4380
Ultimate Strain (me) [a]	F (1, 25) = 5.727, p=0.0245	F (1, 25) = 1.622, p=0.2145	F (1, 25) = 0.5739, p=0.4558

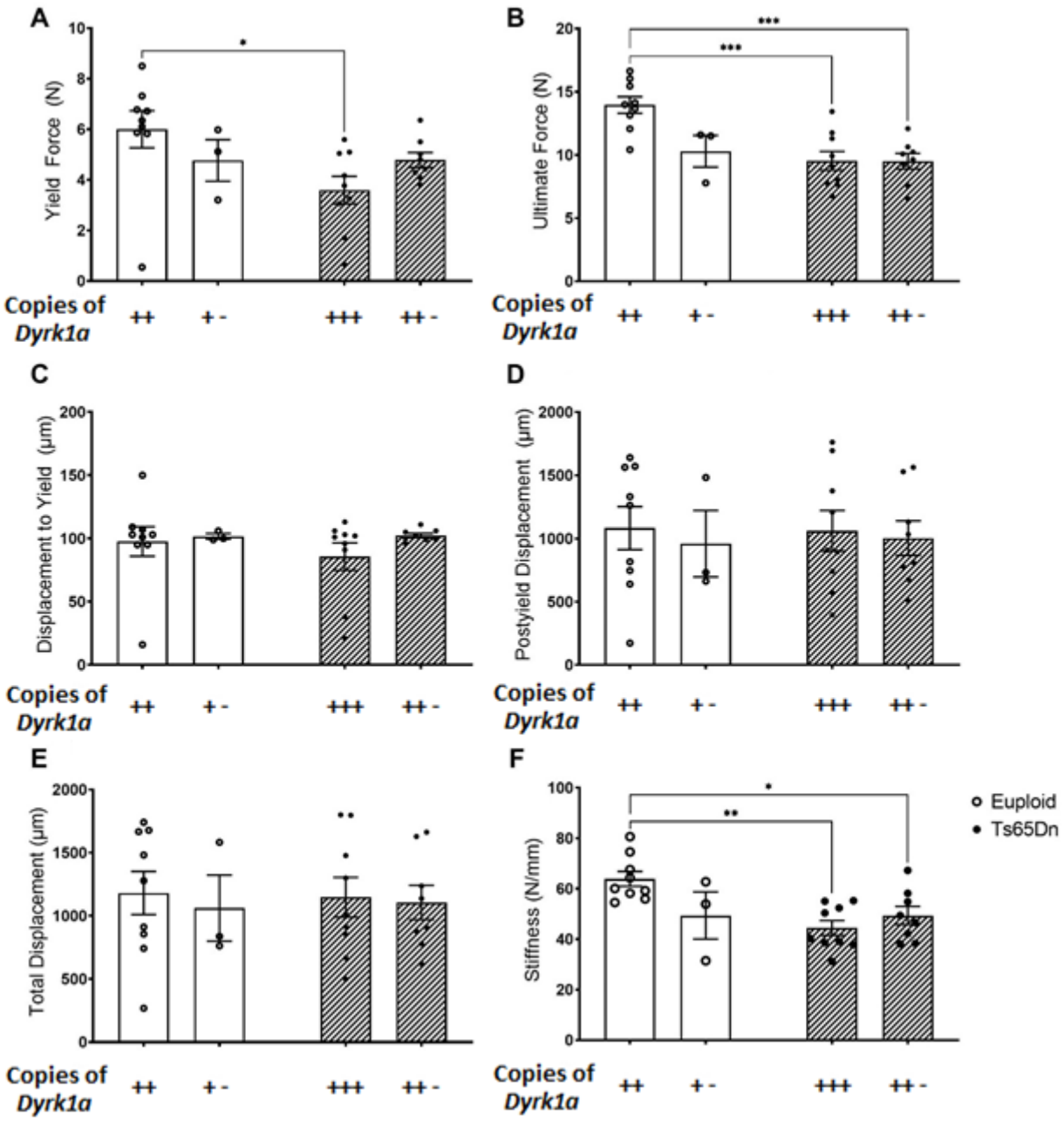

Figure 33. Three-point bending mechanical analysis of male P30 Ts65Dn, Dyrk1a+/- femurs. Dyrk1a +/+ have two intact Dyrk1a alleles; Dyrk1a +/- have one truncated Dyrk1a allele, verified by PCR. Bars represent means and error bars are SEM. Two-way ANOVA and Tukey's post hoc *p≤0.05, **p≤0.01, ***p≤0.001, ****p≤0.0001.

Figure 33. continued

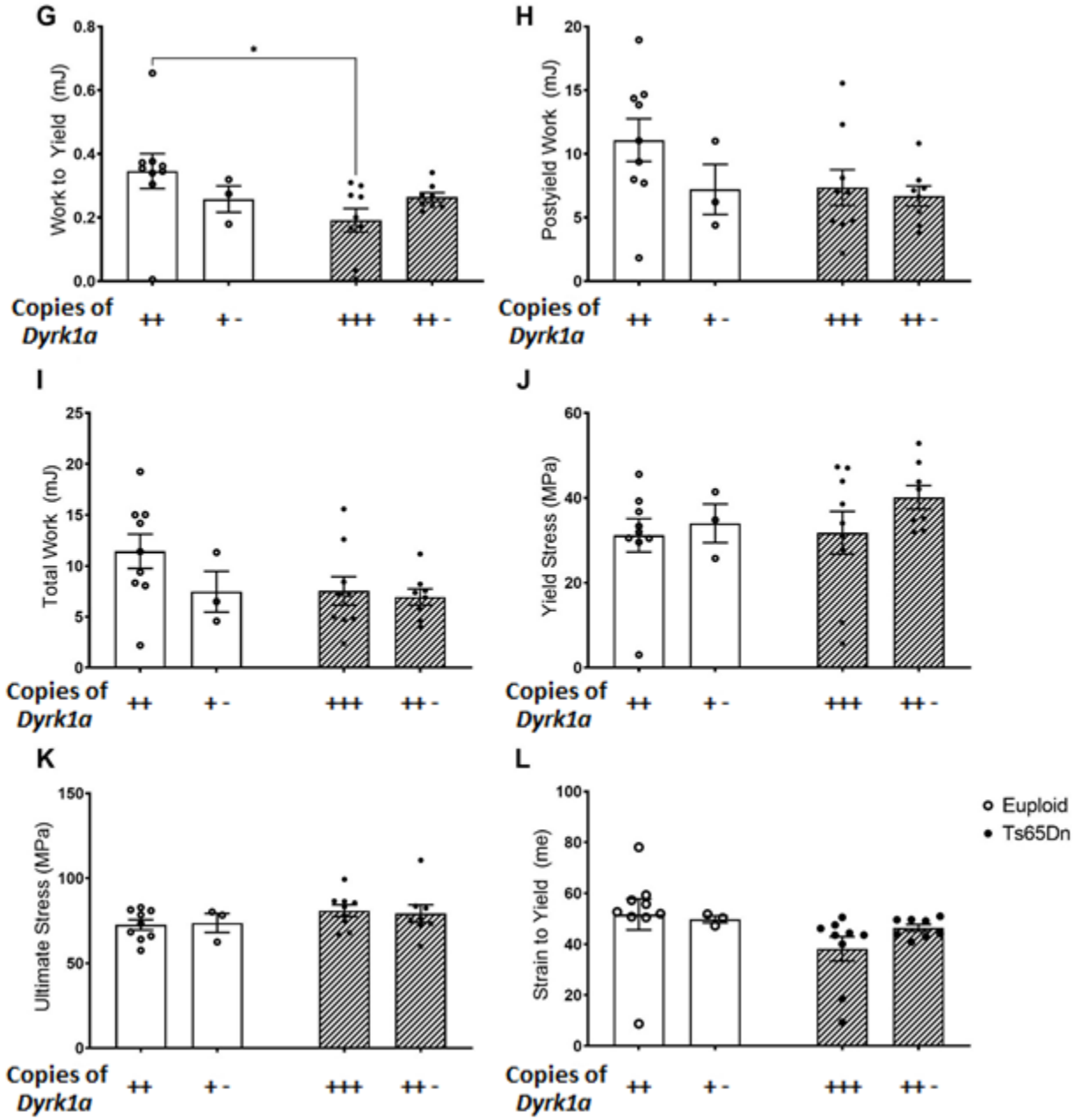

Figure 33. continued

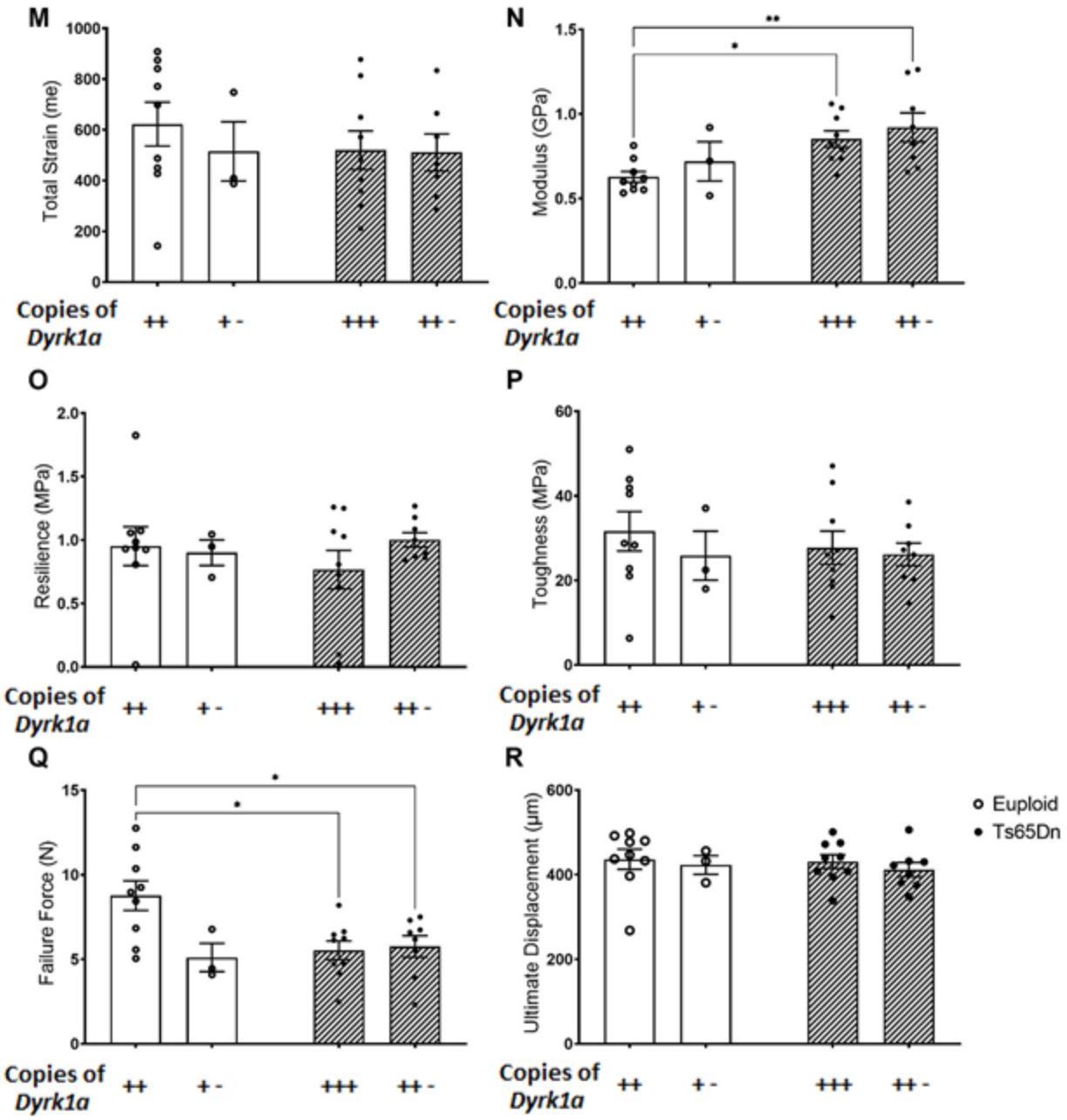

Figure 33. continued

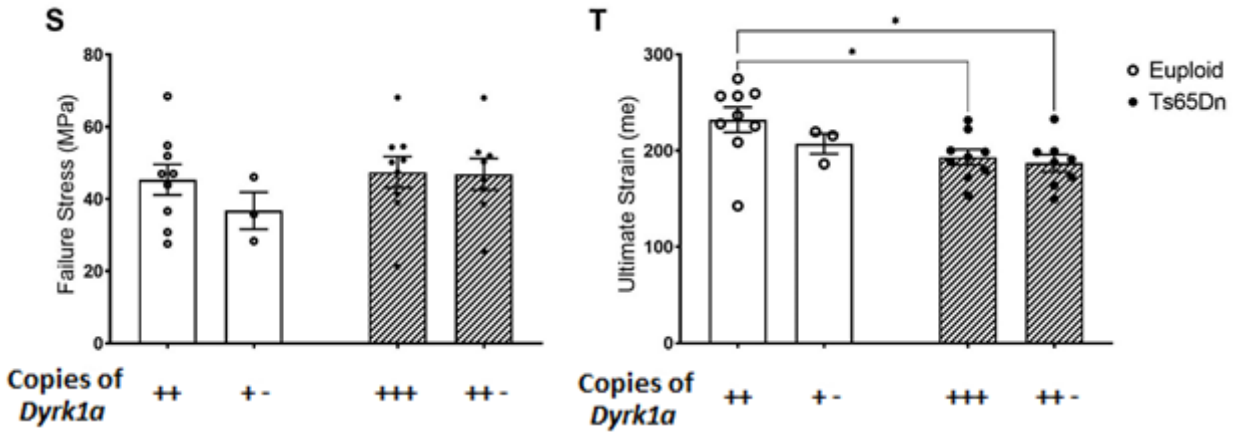

3.5.3 Verify Reduced *Dyrk1a* Gene Expression in P30 Male Ts65Dn, *Dyrk1a*$^{+/-}$ Mice

To verify that reduction of *Dyrk1a* copy number was successful in male Ts65Dn, *Dyrk1a*$^{+/-}$ mice, RNA was isolated from left femurs of experimental mice for qPCR gene expression analysis to provide a snapshot of femur structural geometry, mechanical strength, and *Dyrk1a* expression at P30 (**Table 15**). All RNA samples were derived from femurs opposite of those used for μCT skeletal analysis and mechanical testing. A probe designed to amplify *Dyrk1a* mRNA spanning the union of exon 5 and 6 was selected to specifically determine a difference in expression between control mice and experimental mice with a mutation in a functional region of *Dyrk1a*. Contrary to expectations, expression of *Dyrk1a* exon 5-6 was not significantly different between the Euploid, *Dyrk1a*$^{+/+}$ and Ts65Dn, *Dyrk1a*$^{+++}$ groups (p=0.3206) nor Ts65Dn, *Dyrk1a*$^{+++}$ and Ts65Dn, *Dyrk1a*$^{++-}$ (p=0.5955) (**Figure 34**). Lack of statistical significance may originate from lower statistical power compared to μCT and mechanical analysis (**Table 11a,b.**)

Table 15. Sample sizes for qPCR gene expression analysis of male Ts65Dn, *Dyrk1a*$^{+/-}$ femurs at P30 following gene dosage reduction from conception.

	P30 Ts65Dn, *Dyrk1a*$^{+/-}$ Gene Expression			
Genotype	**Euploid, *Dyrk1a*$^{+/+}$**	**Euploid, *Dyrk1a*$^{+/-}$**	**Ts65Dn, *Dyrk1a*$^{+/+}$**	**Ts65Dn, *Dyrk1a*$^{+/-}$**
Functional *Dyrk1a*	++	+ -	+++	+ -
Sample Size	5	3	5	5

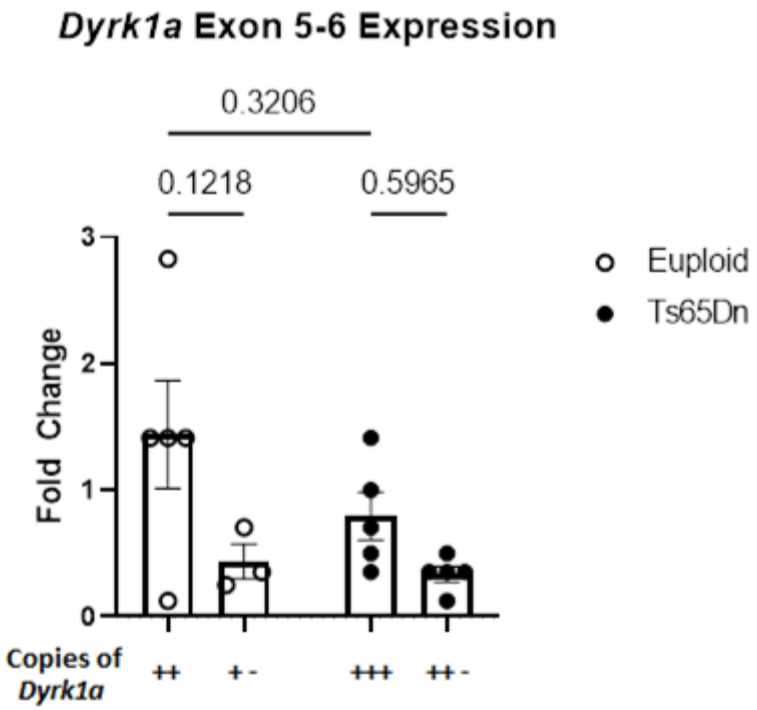

Figure 34. Expression of Dyrk1a exon 5-6 in P30 male Ts65Dn, Dyrk1a+/- femurs. Dyrk1a +/+ have two intact Dyrk1a alleles; Dyrk1a +/- have one truncated Dyrk1a allele, verified by PCR. Two-way ANOVA and Tukey's post hoc *p≤0.05, **p≤0.01, ***p≤0.001, ****p≤0.0001.

3.6 Aim 2.1 Characterize the effect of trisomy and DYRK1A inhibition on proliferation in bone marrow stem cells from 6-week-old male Ts65Dn mice

3.6.1 BMSC Proliferative Activity

To determine the effect of trisomy on bone marrow stem cell (BMSC) proliferation, BMSCs were collected from euploid and trisomic male Ts65Dn mice on a 50% C57BL/6 50% C3H background. Untreated cell wells were performed in quadruplicate and other treatment wells were performed in duplicate. BMSCs were derived from n=5 Euploid mice and n=3 Ts65Dn mice. Cells were stained with Hoechst to identify cell nuclei and EdU to identify proliferating cells. Percent Proliferation was calculated from the ratio of EdU/Hoechst (**Table 16.**). Two-way ANOVA of Hoechst+ cells suggested a main effect of genotype [$F(1,66)=4.078$, $p=0.0475$], but Tukey's multiple comparison post hoc test revealed no significant difference between any of the groups analyzed (**Figure 35A**). A main effect of treatment was observed in EdU+ cells [$F(2,66)=12.39$, $p<0.0001$]. Tukey's post hoc test revealed significant differences between Euploid:Untreated and Euploid:CX-4945 ($p=0.0409$), Euploid:CX-4945 and Ts65Dn: Untreated ($p=0.0006$), and Ts65Dn: Untreated and Ts65Dn:CX-4945 ($p=0.0025$). No differences were detected between no treatment and vehicle (**Figure 35B**). A main effect of treatment was also observed in the percentage of cells proliferating [$F(2,66)=17.93$, $p<0.0001$]. Tukey's post hoc analysis showed significant differences between the following groups: Euploid: Untreated vs Euploid:CX-4945 ($p=0.0042$) and vs Ts65Dn:CX-4945 ($p=0.0006$), Euploid:CX-4945 vs Ts65Dn: Untreated ($p=0.0016$), Euploid:Vehicle vs Ts65Dn:CX-4945 ($p=0.0419$), and Ts65Dn: Untreated vs Ts65Dn:CX-4945 ($p=0.0002$) (**Figure 35C**).

Counts revealed that 50.59% of the untreated euploid cells and 54.35% of the untreated trisomic cells were actively proliferating at the time of the assay. CX-4945 treatment severely and significantly impacted proliferation, dropping the rate to 9.01% in euploid cells and 11.85% in trisomic cells (**Figure 35C**). Furthermore, both CX-4945 and the vehicle DMSO impacted cell morphology, producing much larger cells than the untreated (α-MEM) group. Taken together, CX-4945 reduces proliferative activity in both euploid and trisomic male BMSCs.

Table 16. Sample sizes for assessment of proliferative activity in BMSCs from 6wk male Ts65Dn mice. Untreated cell wells were performed in quadruplicate and other treatment wells were performed in duplicate. BMSCs were derived from n=5 Euploid mice and n=3 Ts65Dn mice.

	Ts65Dn Proliferation Assay					
	Sample Sizes					
Cells Counted	**Euploid Untreated**	**Euploid + CX-4945**	**Euploid + Vehicle**	**Ts65Dn Untreated**	**Ts65Dn + CX-4945**	**Ts65Dn + Vehicle**
Hoechst +	20	10	10	16	8	8
EdU +	20	10	10	16	8	8
% Proliferating	20	10	10	16	8	8

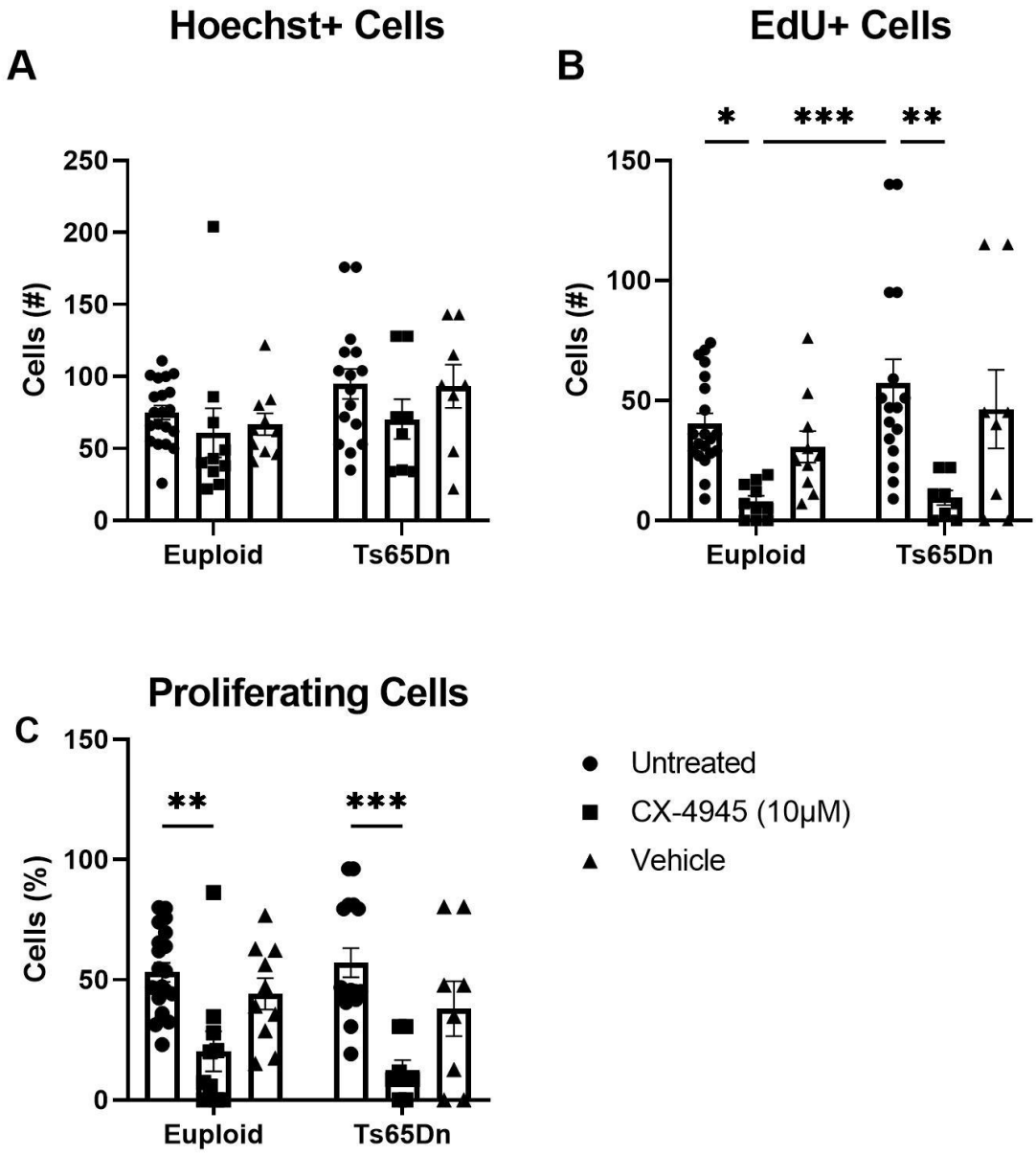

Figure 35. Proliferative activity of P42 Ts65Dn BMSCs with and without treatment of Dyrk1a inhibitor CX-4945 or vehicle (DMSO). Means and SEM shown. Two-way ANOVA and Tukey's post hoc *p≤0.05, **p≤0.01, ***p≤0.001, ****p≤0.0001.

3.7 Characterize the effect of trisomy and DYRK1A inhibition on the differentiation of bone marrow stem cells into osteoblasts

3.7.1 Osteoblast Alkaline Phosphatase Activity

Osteoblast alkaline phosphatase (ALP) activity was assessed in Ts65Dn BMSCs plated at $1x10^5$ cells/mL differentiated into osteoblasts and incubated 14 days (**Table 17a**). The effects of treatment with 10μM CX-4945 and the vehicle (DMSO) on ALP activity were assessed by a one-way ANOVA. A main effect of treatment was observed [F(2,15)=8.983, p=0.0027] and it was determined by Tukey's post hoc test that CX-4945 significantly reduces ALP activity in Ts65Dn osteoblasts (vs N/A p=0.0033, vs DMSO p=0.0137) (**Figure 36A**).

Table 17. Sample sizes for assessment of ALP and mineralization activity in osteoblasts from 6wk male Ts65Dn mice

Osteoblast Differentiation and Activity

a

	ALP Activity		
	Untreated	CX-4945 (10μM)	Vehicle (DMSO)
Ts65Dn	6	6	6

b

	Mineralization Activity		
	Untreated	CX-4945 (10μM)	Vehicle (DMSO)
Euploid	5	5	5
Ts65Dn	5	5	5

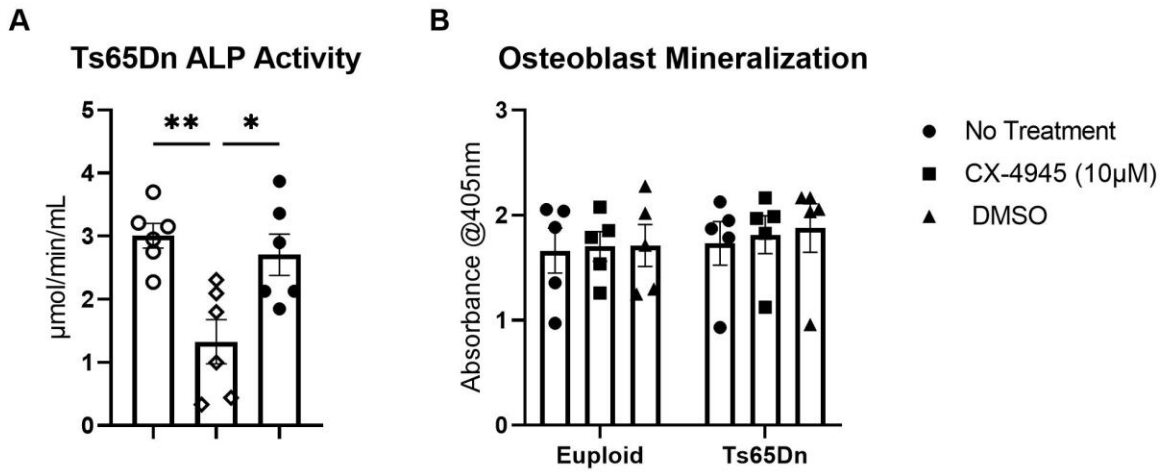

Figure 36. ALP and mineralization activity of P42 Ts65Dn osteoblasts with and without treatment of Dyrk1a inhibitor CX-4945 or vehicle (DMSO). Two-way ANOVA and Tukey's post hoc *p≤0.05, **p≤0.01, ***p≤0.001, ****p≤0.0001.

3.8 Determine the effect of trisomy and DYRK1A inhibition on osteoblast mineralization activity

3.8.1 Osteoblast Mineralization Activity

To assess the mineralization capacity of 6-week-old Ts65Dn osteoblasts, BMSCs differentiated into osteoblasts as previously described were incubated for 21 days. Mineralization was assessed with an Alizerin Red spectroscopy-based assay (**Table 17b**). Two-way ANOVA did not detect any main or interactive effects. Euploid and Ts65Dn osteoblasts mineralized the plate surface to a similar degree (1.661 and 1.732@405nm, respectively) (**Figure 36B**). Treatment of osteoblasts with 10μM CX-4945 yielded a similar mineralization of the plate surface both between Euploid and Ts65Dn and between untreated cells (1.703 and 1.814@405nm, respectively). Treatment of osteoblasts with the treatment vehicle DMSO did not affect mineralization and again there was not a difference between the mineralization capacity of Euploid and Ts65Dn osteoblasts. In conclusion, the mineralization capacity of P42 Ts65Dn osteoblasts is not different from Euploid osteoblasts.

3.9 Determine the effect of trisomic *Dyrk1a* on the expression of osteogenic genes at the age at which a phenotype emerges to establish a *Dyrk1a* signaling axis

Overexpression of *Dyrk1a* in male Ts65Dn mice at P18 was also associated with trabecular defects, but followed by a spike in growth that equalized most trabecular and some cortical measures by P24. Ts65Dn mice then experience a plateau in growth rate that results in an overall lower %BV/TV for the remainder of life (**Figure 17.**). Based on previous results, *Dyrk1a* expression in male Ts65Dn mice seems to equal Euploid littermates at P24 (**Figure 18D.**) and P27 (**Figure 18E.**) and is overexpressed at P30 (unpaired t-test: [t(16)=1.918, p=0.0366] (**Figure 18F.**), which aligns with the period when Ts65Dn mice experience a lack of growth resulting in lasting defects.

To test the hypothesis that there may be an interaction between *Dyrk1a* and osteogenic genes during the pause in growth that results in lasting defects, qPCR analysis was performed with probes for *Bglap*, *Runx2*, *Rbl2***,** and *Alpl* at P24 (**Table 18a.**), P27 (**Table 18b.**), and P30 (**Table 18c.**). *Rbl2*, also known as *P130*, is a gene transcribed via the transcription factor FOXO1. Nuclear FOXO1 competes with TCF/LEF1 for β-catenin to transcribe target genes, but is also exported from the nucleus after phosphorylation by DYRK1A. *P130* then is hypothesized to be a gene that indirectly reports DYRK1A activity; increased DYRK1A activity would result in reduced expression of *Rbl2*.

Table 18. Sample sizes for assessment of osteogenic gene expression in male Ts65Dn femurs at P24, P27, and P30.

***Dyrk1a* Osteogenic Gene Expression**

a

	P24	
	Euploid	**Ts65Dn**
Dyrk1a	5	5
Bglap	5	5
Runx2	5	5
Rbl2	5	3
Alpl	5	5

b

	P27	
	Euploid	**Ts65Dn**
Dyrk1a	5	5
Bglap	5	5
Runx2	5	5
Rbl2	5	5
Alpl	5	5

c

	P30	
	Euploid	**Ts65Dn**
Dyrk1a	6	7
Bglap	7	7
Runx2	7	7
Rbl2	6	7
Alpl	7	7

3.9.1 Osteogenic Gene Expression During Growth Arrest in Male Ts65Dn Femurs

No main effect of genotype, osteogenic gene expression, or interactions were observed at any age analyzed by two-way ANOVA and Bonferroni's post hoc analysis. In trisomic male Ts65Dn mice at P24, *Dyrk1a*, *Bglap*, *Runx2*, *Rbl2*, and *Alpl* were expressed at a level similar to euploid mice (**Figure 37A.**). Although trisomic mean fold change appeared to not equal Euploid, the measures failed to reach significance. At P27, *Dyrk1a*, *Bglap*, *Runx2*, *Rbl2*, and *Alpl* were similar to euploid mice, again failing to reach statistical significance (**Figure 37B.**). At P30, osteogenic genes and *Rbl2* were similar to euploid mice (**Figure 37C.**). Surprisingly, Bonferroni's multiple comparison post hoc test revealed that *Dyrk1a* was underexpressed in Ts65Dn mice ($p=0.0323$).

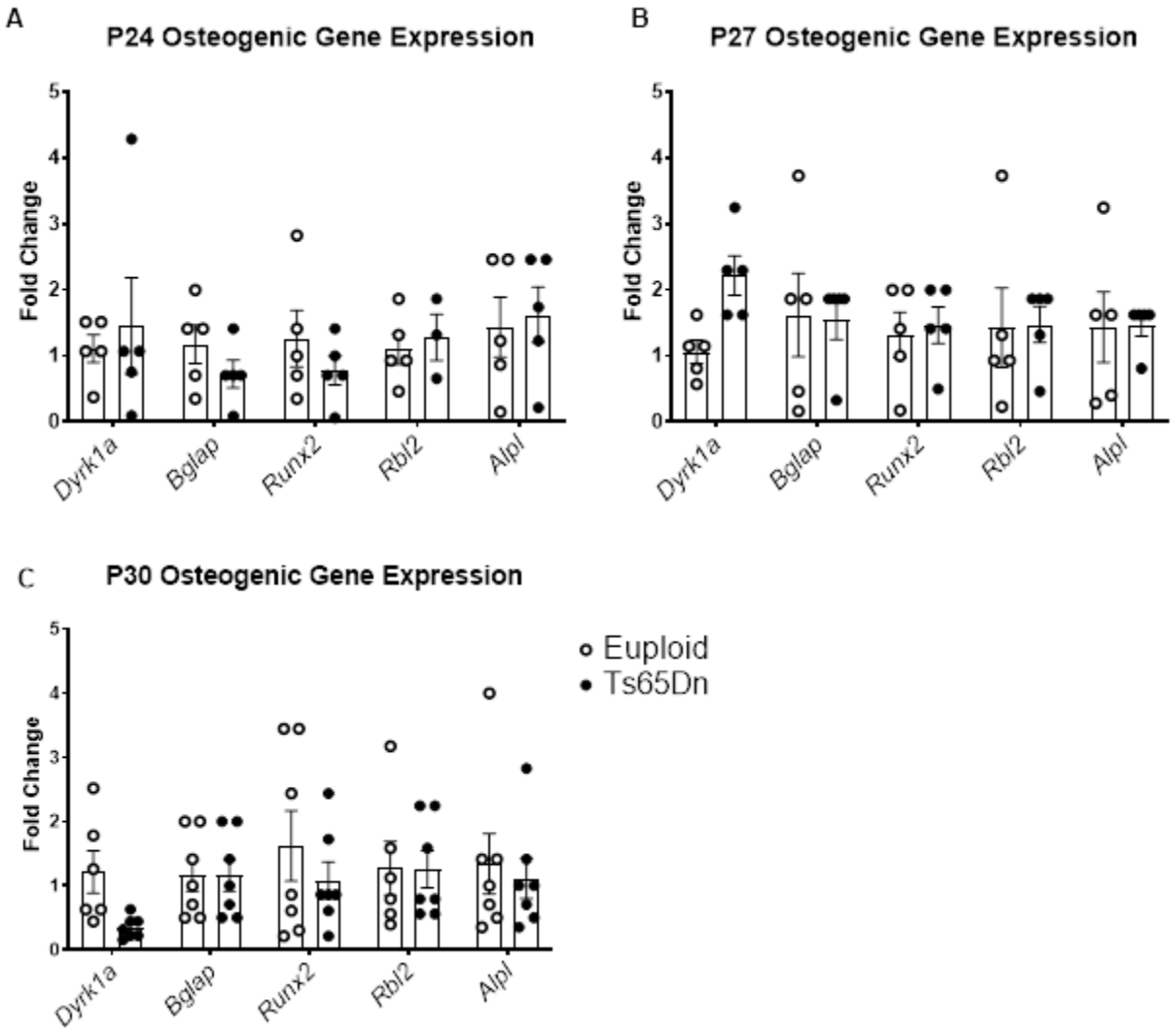

Figure 37. Osteogenic gene expression in male Ts65Dn mice at P24, P27, and P30. Means and SEM shown. Two-way ANOVA and Tukey's post hoc *p≤0.05, **p≤0.01, ***p≤0.001, ****p≤0.0001.

To determine the source of data discrepancy in *Dyrk1a* expression observed between studies, cycle thresholds (Ct) for the housekeeping gene *Rn18s* and the target gene *Dyrk1a* were analyzed. Ct of *Rn18s* and *Dyrk1a* were not significantly different in both previous analyses at P30 (**Figure 38A-D.**). The majority of samples analyzed in the first gene expression experiment which examined *Dyrk1a* gene expression across the developmental study were reanalyzed in the subsequent examination of osteogenic genes. To determine if differences exist between duplicate samples and samples added to the experiment later, Ct values were compared between the two groups. Unpaired one-tailed t tests revealed that *Rn18s* Ct was significantly higher in new Euploid samples compared to duplicated Euploid samples (**Figure 38E.**). Similarly, *Dyrk1a* Ct was significantly higher in new samples (**Figure 38F.**). Conversely, *Rn18s* and *Dyrk1a* Ct was significantly reduced in new Ts65Dn samples (**Figure 38G.,H.**). Analysis of duplicate samples revealed no discrepancy between repeated measures of *Rn18s* Ct (**Figure38I.,J**). Interestingly, repeated measures of *Dyrk1a* returned conflicting results between the initial analysis and secondary analysis. Euploid, and not Ts65Dn, had significantly reduced *Dyrk1a* Ct (**Figure38K.,L.**). This discrepancy translated to increased differences in ΔΔCt and Fold Change between genotypes and may account for the low levels of *Dyrk1a* expression observed in Ts65Dn mice at P30.

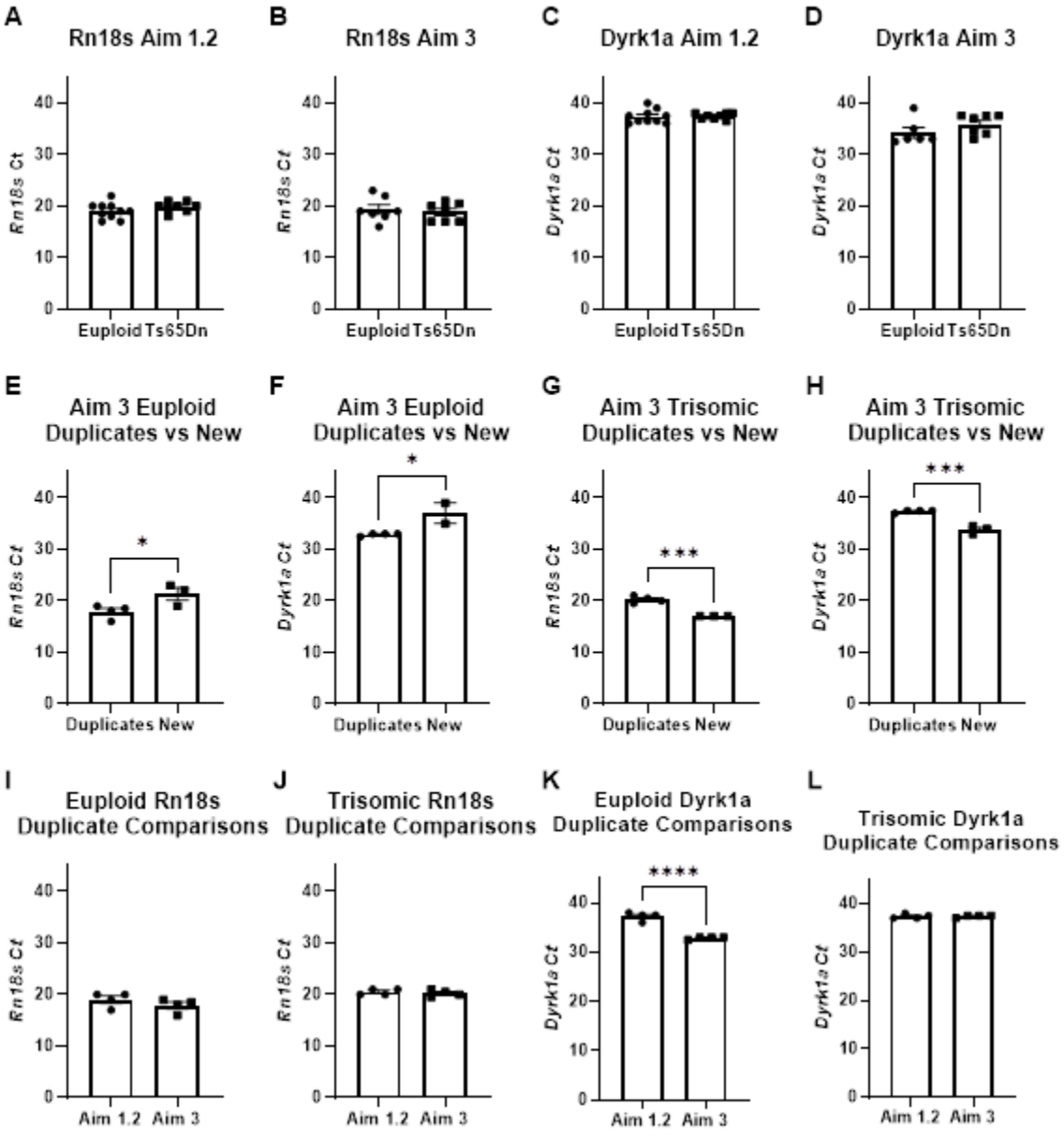

Figure 38. Cylcle thresholds forRn18s (A, B) and Dyrk1a (C, D) obtained in analysis of Aim 1.2 (A, C) and Aim 3 (B, D). Expression of Rn18s and Dyrk1a were analyzed in duplicate and compared to each sample added to increase sample size for each genotype (E-F). Duplicate samples were then compared to each other across experiments (I-L).

CHAPTER 4. DISCUSSION

4.1 Ts65Dn and *Dyrk1a*-related skeletal phenotypes

The genetic and molecular mechanisms surrounding the emergence of skeletal defects in male Ts65Dn mice have been largely unknown despite studies reporting defects in adult mice at P42, 3M, 4M, and 24M(Blazek, Abeysekera, et al., 2015; Fowler et al., 2012). While defects were reported at E17.5, a detailed analysis was not performed and it is difficult to determine the extent of defective microarchitecture(Blazek, Malik, et al., 2015). Blazek et al. went on to show that reduction of *Dyrk1a* gene dosage in otherwise trisomic mice improved Percent Bone Volume (%BV/TV), Trabecular Number (Tb.N), Trabecular Thickness (Tb.Th), and Total Cross-Sectional Cortical Area (Tt.Ar) in P42 male Ts65Dn mice. Mechanical properties Ultimate Force, Stiffness, Work to Yield, and Toughness were also improved, suggesting a relationship between gene dosage and skeletal development(Blazek, Abeysekera, et al., 2015). Gene dosage reduction in trisomic mice at E17.5 however, did not improve %BV/TV(Blazek, Malik, et al., 2015), suggesting that trisomic *Dyrk1a* does not cause prenatal skeletal defects, but defects arising in adolescence are attributable to increased *Dyrk1a* gene dosage. Together, these findings led to classification of *Dyrk1a*-related defects; specific skeletal and mechanical measures affected by *Dyrk1a* gene dosage in male Ts65Dn mice defined as increased Tb.Sp, decreased %BV/TV, Tb.N, Tb.Sp, Tb.Th, Tt.Ar, Ultimate Force, Stiffness, Work to Yield, and Toughness.

Armed with the knowledge that specific skeletal defects are attributable to increased *Dyrk1a* gene expression in male Ts65Dn mice and those defects are not always present, it was necessary to characterize femur structural geometry and quantify changes in *Dyrk1a* gene expression during skeletal development to test the hypothesis that *Dyrk1a*-related skeletal defects arise between birth and sexual maturity. Characterization of femur microarchitecture at ages P12, P15, P18, P24, P27, P30, and P42 revealed defects in cortical geometry of male Ts65Dn mice at every age. However, trabecular defects were present only at P18, P30, and P42. Analysis at different time points also revealed that defects in trabecular thickness seem to lag behind the emergence of other trabecular defects. Defects including %BV/TV, Tb.N, Tb.Sp, and Tb.Pf emerge at both P18 and P30, but Tb.Th isn't reduced in Ts65Dn mice until P24 and P42, respectively. *Dyrk1a* was overexpressed at P12, P18, and P30; overexpression was also observed

at P27, but statistical significance was not reached. *Dyrk1a*-related phenotypes also presented in male Ts65Dn mice at these ages: at P12, Tt.Ar was significantly reduced, %BV/TV, Tb.Th, Tb.Sp, and Tb.N appeared compromised, but did not reach statistical significance; at P18 all trabecular and cortical measures were significantly compromised; and at P30 all trabecular and cortical measures except Tb.Th were significantly compromised. Together, these data suggest a time- and expression-dependent relationship between *Dyrk1a* and bone phenotypes.

Due to the majority of *Dyrk1a*-related defects being located in the trabecular region of the femur in male Ts65Dn mice, trabecular measures are the focus of this discussion. Euploid males seem to have a mostly linear trabecular bone growth trajectory with a small depression in %BV/TV growth between P24 and P30, followed by a growth spurt and a return to a mostly linear growth rate. However, trisomic males experience a six-day period of no overall increase in %BV/TV from P24 to P30, followed by a growth rate similar to euploid males but at an overall reduced %BV/TV. The end result is compromised *Dyrk1a*-related trabecular geometry beginning at P30 that persists to P42 and according to a previous report, to three months and two years(Blazek, Abeysekera, et al., 2015; Fowler et al., 2012). A study in humans reports that skeletal growth velocity is impaired from six months to three years of age and during puberty(Myrelid et al., 2002). The study also reported that males with DS reach maximal height, which is lower overall, earlier than males in the general population(Angelopoulou et al., 1999). Here, we identified a period of static growth in the male Ts65Dn mouse model occurring during early puberty that causes lasting trabecular defects.

While cortical defects are not considered *Dyrk1a*-related, the cortical geometry and material properties of the bone directly affect mechanical strength. Mechanical testing was not performed due to size limitations prohibiting testing of small bones from young mice. Male Ts65Dn mice presented cortical defects at every age analyzed except P24. Total Cross-Sectional Area (Tt.Ar), Marrow Area (Ma.Ar), Periosteal Bone Surface (Ps.BS), and Endocortical Bone Surface (Ec.BS) were significantly impaired in male Ts65Dn mice at P15. Marrow Area (Ma.Ar) was significantly reduced at all ages except P12 and P24. Tissue Mineral Density (TMD) was significantly compromised in male Ts65Dn mice at P12, P18, and P30. All cortical measures were significantly affected in male trisomic mice at P18 and P30. The Tt.Ar., Maximum Polar Moment of Inertia (Imax), Minimum Polar Moment of Inertia (Imin), Ps.BS, Ec.BS, and Section Modulus were compromised in Ts65Dn mice at P42 (**Figure 2.**). Similar to the trabecular growth pattern

observed across development, cortical measures also have arrested growth during the P24 to P30 time point in male Ts65Dn mice. Together, the growth patterns in trabecular and cortical measures suggest a conserved mechanism that arrests growth during a time when euploid bone is growing.

4.2 Cellular mechanisms of BMSCs and osteoblasts reflect femur growth rates

The skeletal growth analysis that shows equal growth between Euploid and Ts65Dn mice from P30 to P42 suggests another controversial hypothesis: the cellular activity of Ts65Dn BMSCs and osteoblasts is equal to Euploid, allowing the growth rate of Ts65Dn mice to match Euploid mice during this period. This is in direct opposition to previous studies reporting defects in osteoblast mineralization activity in male Ts65Dn mice(Fowler et al., 2012). To test this hypothesis, cellular activity was assessed in BMSCs and osteoblasts isolated from male Ts65Dn mice at P42. Indeed, no difference in proliferation or mineralization activity was observed, suggesting three explanations: 1) these data represent a snapshot in cellular activity at P42, a time when there is no noticeable defect in Ts65Dn cells; 2) despite genetic defects, Ts65Dn cells are capable of acting in the same capacity as Euploid cells, but extracellular signaling dictates cellular activity; 3) differences in methodology between the present study and previous studies are the source of divergent results. If differences in methodology was the source of discrepancy between studies, that would provide evidence supporting the hypothesis that activity of Ts65Dn BMSCs and osteoblasts results from instructive signaling and any activity considered defective stems from the dysregulated signaling of other cells. Together, the available data suggest that the source of skeletal defects may not be attributable to a single cell type and may originate from the compound dysregulation of signaling from all cells in the microenvironment.

If methodology alone was the source of improved activity of Ts65Dn BMSCs and osteoblasts, it is imperative to identify exact differences in cell culture conditions that were responsible for producing the observed results. The Fowler study (mentioned previously) derives their cells for culture from femurs, but we do not know the age of the animals from which the BMSCs were derived. Age undoubtedly affects the overall quality of BMSCs(Chen, 2004; Zhang et al., 2008) so if the cells were derived from animals in that study (12 weeks and 24 months), BMSC and osteoblast activity would likely be different. BMSCs in the Fowler study were differentiated into osteoblasts with an α-MEM base supplemented with 15% fetal bovine serum (FBS), 10mM β-glycerophosphate (BGP), and ascorbic acid, but without dexamethasone (DXM).

While DXM has been shown to reduce ALP activity at concentrations from 10-100nM when added to culture before cell adherence(Chen, 2004), it promotes osteoblast proliferation and differentiation by upregulation of osteogenic genes(Ghali et al., 2015). This discrepancy could account for the lack of a difference in proliferative or mineralization activity between Euploid and Ts65Dn mice in the present study, but for it to both improve euploid activity and restore Ts65Dn activity to the point of improved euploid activity seems unlikely. A major pitfall of the cellular study is the lack of a wild type comparison for assessment of ALP activity. A baseline of activity for the euploid mice is necessary for assessing a difference in genotype and comparing to previous studies. Furthermore, there were only two Ts65Dn mice utilized, so the sample size should be increased at least to three to provide more accurate data to compare to Fowler et al. and others.

In the Fowler study, osteoblasts were allowed 28 days to mineralize 6-well plates then mineralized nodules were counted. In the present study, cells were allowed 21 days to mineralize the bottom of a 24-well plate. Following the incubation period, mineralization was assessed by spectrophotometer. Using the spectrophotometer to measure mineralization promised many advantages over counting nodules. Eliminated was the need to determine what qualified as a nodule. Also, it assessed the activity of all osteoblasts plated in the well as opposed to the activity of colonies on the plate. Considering the differences in methodology, the studies should be evaluated independently. The value from Fowler's mineralization study should then be considered an evaluation of osteoblast colony formation instead of an assessment of mineralization activity.

4.3 DYRK1A inhibition in BMSCs and osteoblasts

Previous experiments with DYRK1A inhibitors showed promise in improving trabecular but not cortical skeletal phenotypes in P42 male Ts65Dn mice(Blazek, Abeysekera, et al., 2015). Unfortunately, the treatment was insufficient to improve behavioral phenotypes, so increased concentrations were explored(Stringer et al., 2015). Subsequent reports demonstrated that at higher doses of the DYRK1A inhibitor epigallo-3-catechin-gallate (EGCG) were detrimental to skeletal geometry and mechanical strength(Goodlett et al., 2020; Stringer et al., 2017). Because behavior was unaffected by treatment at all concentrations, the bioavailability and specificity of EGCG was questioned. Indeed, EGCG has been reported to degrade quickly and have poor bioavailability compared to commercial drugs(Abeysekera et al., 2016; Goodlett et al., 2020; Ramachandran et al., 2016; Sang, Lee, Hou, Ho, & Yang, 2005). CX-4945 (Silmitasertib), an anticancer drug valued

for its CK2-inhibitory activity, was also shown to have inhibitory activity against DYRK1A(H. Kim et al., 2016). Other reports describing improved osteoblast activity suggested the potential for improving skeletal defects(Son et al., 2013). Together, these reports served as the foundation for the hypothesis that Ts65Dn osteoblast cellular activity would be improved with CX-4945 treatment. Treatment of BMSCs with 10μM CX-4945 reduced proliferation in Euploid and Ts65Dn alike, an expected result considering the involvement of CK2 in cell proliferation(Chon et al., 2015; Lebrin, Chambaz, & Bianchini, 2001; Son et al., 2013). These results are in disagreement with another report that described no difference in human mesenchymal cell line proliferation at 3μM(Takahashi et al., 2017). The report was misleading in this assessment; the effect of higher concentrations of CX-4545 on cell proliferation was not assessed, but higher concentrations of the drug were used in subsequent experiments. It is likely that if the group assessed proliferation at higher concentrations, their results would reflect ours. Contrary to expectations, ALP activity was significantly compromised in Ts65Dn osteoblasts. Also surprising, mineralization activity was not affected in both genotypes. The effect on ALP activity was a surprise since the drug was touted to increase expression of ALP by 40-fold and the osteogenic Wnt gene BMP-4(Son et al., 2013) by 15-fold with 10μM CX-4945 while maintaining >80% viability, suggesting improved mineralization activity of osteoblasts. The glaring difference is again the media formula. Son et al. (referenced above) used DMEM supplemented with 5% FBS and 25ng/mL BMP-2. BMP-2 and CX-4945 may have a synergistic effect that improved ALP expression. The group also did not use DXM, which has been shown to reduce ALP activity despite increasing expression of other osteogenic genes(Chen, 2004; Ghali et al., 2015). Another explanation for the negative impact of CX-4945 is that the drug also inhibits casein kinase 2 (CK2). Knockout of *Csnk2b*, the gene coding CK2, caused a catastrophic reduction in ALP activity in addition to a significant drop in *Osterix* (*Osx, Sp7*), *Collagen1a1* (*Col1a1*), and *Runx2* expression(J. M. Kim et al., 2020). Together, these factors suggest that inhibition of CK2 could negatively affect osteogenic gene expression and activity, thus providing an explanation for the poor performance of osteoblasts treated with 10μM CX-4945 in the present study. Considering that no defect has been detected in cellular activity between genotypes suggests that improvements in skeletal phenotypes by inhibiting DYRK1A *in vivo* would depend on effects on cells in the microenvironment instructing osteoblasts through extracellular signaling, not through direct effects on osteogenic cells.

4.4 Inhibition of DYRK1A in male Ts65Dn mice

Determining an effective delivery method for CX-4945 treatment in male Ts65Dn mice proved challenging. CX-4945 was not soluble in water or PBS, limiting initial dissolution to DMSO. Due to health concerns over multiple treatments with DMSO, the total percentage of each treatment was limited to 10% total DMSO. Unfortunately, CX-4945 did not remain dissolved at 90%PBS:10%DMSO however, it formed a suspension that was relatively stable at 37°C.Treatment with 75mg/kg/day CX-4945 in a 90%PBS:10%DMSO suspension via oral gavage proved ineffective in improving *Dyrk1a*-related phenotypes in male Ts65Dn mice. More unexpected was the effect of vehicle treatment on Ts65Dn mice; the mean %BV/TV in vehicle treated mice was approximately 25%, compared to untreated P30 Ts65Dn mice that were characterized earlier which had a mean approximate %BV/TV of 15%. Vehicle treatment of male Ts65Dn mice from P21 to P29 essentially improved trabecular measures to Euploid levels. However, not all *Dyrk1a*-related phenotypes were affected; Tt.Ar was significantly reduced in Vehicle-treated Ts65Dn mice compared to Euploid, suggesting an effect on trabecular bone. Also, previous reports administering DYRK1A inhibitors via oral gavage showed significant differences in *Dyrk1a*-related measures in Ts65Dn mice receiving the vehicle(Goodlett et al., 2020; Stringer et al., 2017), suggesting that DMSO, 10% of the vehicle used in the present study, improved trabecular defects in vehicle-treated mice. While unlikely, it is possible that because the CX-4945-treated cohorts were treated before Vehicle-treated cohorts, genetic drift or seasonal growth effects may have impacted analysis between the two groups. Genetic drift is likely not a factor because the mice used in DYRK1A inhibition experiments were obtained within two months, but seasonal effects on bone phenotypes have been reported in B6 mice(Delahunty et al., 2009). If this is the case, a potential benefit is reduced variability within the CX-4945 and Vehicle groups. Another possible explanation for the lack of a difference between Euploid and Trisomic *Dyrk1a*-related measures after Vehicle treatment is an effect of DMSO on cellular signaling and activity. Cell-based studies using CX-4945 and DMSO as a vehicle suggest a negative effect on BMSC proliferation. Changes in morphology were also noted, but these changes may be random as described in a comprehensive study on BMSC age and plating density(Neuhuber, Swanger, Howard, Mackay, & Fischer, 2008). The present study also showed no difference between the mineralization activity of osteoblasts treated with CX-4945 and osteoblasts treated with the vehicle. Together, the data seem to suggest

that the vehicle DMSO may improve trabecular phenotypes *in vivo* when administered between P21 and P29 in male Ts65Dn mice.

DMSO has been reported to decrease osteoclast maturation in a dose-dependent manner(Lemieux, Wu, Morgan, & Kacena, 2011; Yang et al., 2015). Others have reported increased osteoblast differentiation and activity in mouse and human osteoblasts treated with DMSO, along with increased osteogenic gene expression(Cheung, Ng, & Kung, 2006; Stephens et al., 2011). Stephens et al. did not report what type of mice their osteoblasts were derived from(Stephens et al., 2011). Also different in the both the Stephens and Cheung studies exploring the effect of DMSO on osteoblast activity was the osteoblast differentiation-inducing media, which had a lower percentage of FBS and lacked dexamethasone (DXM) when compared with the media utilized in the current study(Cheung et al., 2006; Stephens et al., 2011). While there are striking differences in the methodologies between previous reports and the present study, an explanation that fits the data is that DMSO is responsible for improving trabecular defects in male Ts65Dn mice to the point that no statistical difference was observed when compared to Euploid littermates also receiving the vehicle. In Euploid mice receiving CX-4945, it seemed that trabecular measures were improved but measures did not reach statistical significance. In conclusion, CX-4945 failed to improve *Dyrk1a*-related skeletal defects more than administration of the vehicle.

4.5 Genetic modulation of *Dyrk1a* in male Ts65Dn mice

To determine the effect of time-dependent *Dyrk1a* expression, male Ts65Dn mice generated from a cross permitting a conditional excision of one allele of *Dyrk1a* upon doxycycline administration in otherwise trisomic mice were utilized. Doxycycline was administered beginning on the day of weaning, P21. Excision of one allele of *Dyrk1a* was confirmed at P30 by PCR, but qPCR results did not validate a reduction in expression. These results seem to align with the results of skeletal geometry analysis due to no statistical effect of gene dosage, but multiple mechanical measures including Displacement to Yield, Work to Yield, Strain to Yield, Resilience, and Failure Stress demonstrate an effect of gene dosage that flirts with statistical significance due to the profound effects on Euploid, $Dyrk1a^{+/fl}$, Cre + group. Surprisingly, differences are not observed in cortical bone geometry, suggesting a change in material properties that makes the shaft of the femur more rigid.

Compared to Euploid and Ts65Dn skeletal phenotypes characterized earlier at P30, trabecular measures were similar in mice receiving doxycycline regardless of genotype. Measures such as %BV/TV and Tb.N were increased and Tb.Sp was decreased in Euploid and Ts65Dn mice receiving doxycycline, but statistical significance between the studies was not achieved (**Figure 39.**). Doxycycline has been reported to inhibit osteoblast activity in culture at concentrations over 100μg/mL(Rathbone, Cross, Brown, Murray, & Wenke, 2011), but has no effect at 20μg/mL(Kinugawa et al., 2012). Osteoclast differentiation was shown to be reduced at concentrations as low as 3μg/mL and completely inhibited at 10μg/mL doxycycline(Kinugawa et al., 2012). These cellular data suggest a potential improvement in bone geometry with an appropriate dosage of doxycycline due to reduced resorptive activity by osteoclasts. Experiments with ovariectomy-induced osteopenia receiving 10 and 30mg/kg/day doxycycline for sixty days demonstrated improvements in cancellous bone, but negative effects were observed in control mice receiving doxycycline(de Figueiredo et al., 2019). Another group demonstrated improvements in recovery of alveolar bone as a result of increased osteoblast activity and decreased osteoclast activity following extraction of a molar and treatment with 10 and 25mg/kg/day doxycycline in a dose-dependent manner(Gomes, Alves, Dutra, & Viana, 2017). Together, these data and previous reports suggest that doxycycline treatment may have a therapeutic application for defects observed in male Ts65Dn mice. Contrary to the hypothesis, *Dyrk1a* gene dosage between P21 to P30 does not affect the emergence of related defects.

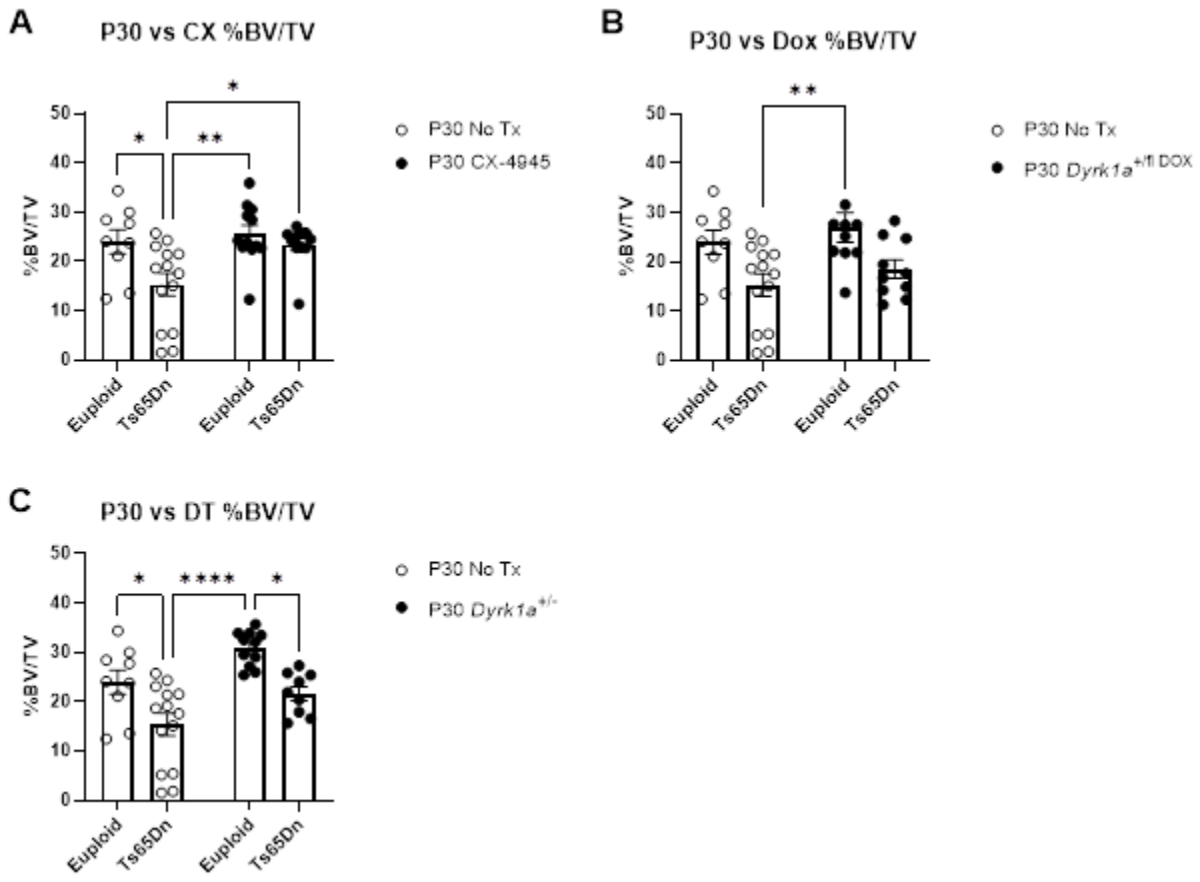

Figure 39. Cross-sectional analyses of %BV/TV between Untreated P30 and Vehicle-Treated (A), Untreated P30 and P30, Dyrk1a+/fl DOX (B), and Untreated P30 and P30 Dyrk1a+/- (C).

To verify that increased *Dyrk1a* gene dosage and overexpression of *Dyrk1a* does not influence the emergence of defects in femur structural geometry and mechanical strength, *Dyrk1a* gene dosage was reduced in otherwise trisomic mice from conception and analyzed at P30. The mice used in this analysis are on a relatively simple background (Ts65Dn x B6C3F1) by comparison to the conditional model, which has an extra generation involved in the breeding scheme. The extra generation and addition of the rtTA and TetOCre driver may introduce variations to Ts65Dn phenotypes and differences between studies. These analyses revealed that gene dosage reduction in male Ts65Dn, *Dyrk1a*$^{+/fl}$ Cre + mice did not significantly affect bone geometry or mechanical strength, but reduction in Euploid, *Dyrk1a*$^{+/fl}$ Cre + male mice caused several significant structural defects. Mechanical defects were observed in similar measures reported by Blazek at al. in P30 Ts65Dn mice compared to Euploid mice. Contrary to mechanical analysis in previous studies at P42, gene dosage does not have an effect on bone strength with the

exception of marginal increases in Stiffness. High variation was observed in the Euploid, *Dyrk1a*$^{+/fl}$ Cre – group and the Euploid and the *Dyrk1a*$^{+/fl}$ Cre + group only had a sample size of three, both likely contributing to the lack of statistical significance between groups in mechanical measures. Effects of gene dosage reduction on mechanical properties in Euploid mice resembles previously reported data(Blazek, Abeysekera, et al., 2015). Together, studies exploring *Dyrk1a* expression in the femurs of male Euploid and Ts65Dn mice have demonstrated the necessity of intact gene dosage in Euploid mice and no noticeable detrimental effect of *Dyrk1a* gene dosage on skeletal development in Ts65Dn mice up to P30. Humans with mutated *DYRK1A* (diagnosed as MRD7) have contrasting bone phenotypes; one female proband had no noticeable skeletal deficiencies besides microcephaly, while the other female proband had slightly delayed bone age in addition to microcephaly. Differences between results in this study and the conditional gene dosage reduction study could be due to differences in genetic background or doxycycline administration. In a previous study, significant changes in weight were observed between trisomic Ts65Dn x B6C3F1 and trisomic Ts65Dn, *Dyrk1a*$^{+/fl}$ mice, suggesting an effect of genetic background on phenotypes (unpublished). These data suggest that improvement of *Dyrk1a*-related bone phenotypes in Ts65Dn mice by gene dosage reduction must occur between P30 and P42.

4.6 Osteogenic gene expression and *Dyrk1a*

To explore the genetic mechanisms at work during the period of static growth in male Ts65Dn mice between P24 and P30, osteogenic gene expression was assessed by qPCR at P24, P27, and P30. Most eventful was P24 when it seemed that *Osteocalcin* (*Bglap*) and *Runx2* expression was reduced in Ts65Dn mice compared to Euploid, but statistical significance was not achieved. The expression of *Dyrk1a* was not increased in Ts65Dn at P24, suggesting that *Bglap*, *Runx2*, and *Dyrk1a* interact. This notion was further supported by results at P27 when *Dyrk1a* expression increased while *Bglap* and *Runx2* returned to levels similar to Euploid. Expression of these osteogenic genes and others were not noticeably different at P30. These results came as a surprise considering that Ts65Dn male mice experience a period of zero net skeletal growth during this period that causes defects that, by all current accounts(Blazek, Abeysekera, et al., 2015; Fowler et al., 2012), remain throughout adolescence and adulthood. Additionally, osteogenic genes typically interact with each other, so dysregulated expression of one gene often affects expression of another. That explanation however, does not necessarily rule out the possibility that other

osteogenic genes are dysregulated. Osterix (*Sp7*) is considered a master regulator of osteoblast differentiation. While other studies are ongoing exploring the effect of *Dyrk1a* in *Sp7*-expressing cells (osteoblasts), there have been no reports on *Sp7* expression at P24, P27, and P30. Future studies may explore osteogenic gene expression defects at these ages to explain the pause in skeletal growth.

A striking difference between *Dyrk1a* expression between Euploid and Ts65Dn mice assessed in the initial study and the osteogenic gene expression study prompted further investigation. Expression of *Dyrk1a* was reassessed using a mixture of samples analyzed in an earlier study and new samples obtained from mice born several months later. Results from qPCR analysis at P24 and P27 were in accordance with what was observed in the first assessment of *Dyrk1a* expression; no differences were observed between Euploid and Ts65Dn mice at P24 and *Dyrk1a* seemed to be overexpressed at P27, but failed to reach statistical significance. Expression of *Dyrk1a* at P30 in Ts65Dn mice was surprising and as previously mentioned, a deeper investigation determined that discrepancies between analyses were likely driven by lower *Dyrk1a* Ct values in Euploids. The analysis method applies the average Euploid ΔCt value to calculate both Euploid and Ts65Dn ΔΔCt and Fold Change. Lower Euploid *Dyrk1a* Ct values would reduce the average Euploid ΔCt and ΔΔCt, then increased Fold Change. Ts65Dn ΔΔCt was calculated for each sample by the difference of Ts65Dn *Dyrk1a* ΔCt and the average Euploid ΔCt, which being reduced compared to previous experiments, resulted in an increased average Trisomic ΔΔCt and a reduced Fold Change compared to Euploid. Because these discrepancies were limited to the P30 Euploid *Dyrk1a* Ct, the validity of the results of the other genes analyzed stands.

4.7 Conclusion and Future Directions

This study is the first to systematically quantify trabecular and cortical microarchitecture in the femur of male Ts65Dn mice at several time points during early and adolescent development from P12 to P42. Also for the first time, femur *Dyrk1a* expression (presumably from osteocytes) was characterized across development from P12 to P30. Activity of BMSC and osteoblasts was shown to be similar *in vitro*, suggesting either that Ts65Dn BMSC and osteoblast activity at P42 *in vivo* is similar to Euploid and contributes to a relatively equal growth rate between genotypes or that the cell culture methodology employed in these studies improved Ts65Dn BMSC and

osteoblast activity in and of itself. To test this hypothesis, cells should be cultured from P30 BMSCs and subjected to the same analyses. At the surface level, treatment with CX-4945 failed to support the hypothesis that DYRK1A inhibition from P21 to P30, encompassing both the static growth phase from P24 to P30 and *Dyrk1a* overexpression at P30. Improvements in some *Dyrk1a*-related trabecular measurements during the course of treatment suggest that pharmacological intervention during this period can improve *Dyrk1a*-related defects in Ts65Dn mice. Genetic reduction experiments both prior to the static growth period and from conception yielded two important findings: 1) Trisomic *Dyrk1a* does not have pathological effects on skeletal defects in Ts65Dn mice up to age P30 and 2) while doxycycline has osteogenic effects, the dosage and duration of treatment was insufficient in producing improvements in skeletal geometry that are statistically different from untreated P30 male Ts65Dn mice. Expression of *Dyrk1a* was not statistically different between Euploid and Ts65Dn mice with gene dosage reduction, suggesting that an unknown feedback mechanism may be compensating for the missing allele.

The current study challenges the central dogma that gene expression is correlated with gene dosage in a static relationship(Blazek, Malik, et al., 2015; Thompson et al., 2015). Data reported here challenge that hypothesis and suggest that increased gene dosage does not directly correlate with the expression of triplicated genes nor does it remain at the same level over time. The plasticity of *Dyrk1a* expression is demonstrated by data provided by the present study. These results echo a study reporting changes in trisomic *App* expression in Ts65Dn mice at various ages(Choi et al., 2009). At every age *Dyrk1a* is overexpressed during development in the present study, it is overexpressed in male Ts65Dn mice on average of at least twice that of Euploid. The equal expression of *Dyrk1a* in Ts65Dn mice at P24 and P27 compared to Euploid littermates happens to correlate with a static growth period in the femur and may be related in some way.

The current study has laid a foundation for future skeletal studies utilizing the Ts65Dn mouse model. It has filled a critical gap in knowledge by characterizing skeletal development from P12 to P30, exemplifying the developmental nature of skeletal phenotypes in DS. Cortical defects seem to be present during embryonic development(Blazek, Malik, et al., 2015) and persist through P42. Unlike trabecular defects, cortical defects are not improved by gene dosage reduction from conception. While trabecular defects that emerge at P30 are not *Dyrk1a*-dependent, previous studies have demonstrated that rescue of the phenotype is possible by gene dosage reduction from conception to P42(Blazek, Abeysekera, et al., 2015). Current studies have provided more evidence

supporting the hypothesis that femur geometry can be improved with pharmacological intervention. Future studies must explore the gap between P30 and P42 to determine the growth trajectory between those ages and when *Dyrk1a*-dependent skeletal phenotypes are improved in male Ts65Dn mice. To do so, *Dyrk1a* knockout mice should be aged to P33, P36, and P39 and analyzed by μCT. When an age is determined to be undergoing improvements, osteogenic gene expression should be assessed as well. If the knowledge gained here translates to humans with DS, there may be a therapeutic window to improve bone development. Studies like these will open the path for therapeutics that improve DS phenotypes and our understanding of gene dosage.

APPENDIX A. OTHER METHODOLOGY DESCRIBED IN PUBLICATIONS

A1. Protein Quantification

Protein concentrations of samples isolated from the cerebral cortex, hippocampus, and cerebellum were quantified using the Bradford assay. Protein was isolated from samples by homogenizing tissues in RIPA buffer supplemented with a protease inhibitor using a hand-held tissue homogenizer with a disposable pestle inside a 1.5mL microcentrifuge tube. Samples were centrifuged and the supernatant was transferred to a new microcentrifuge tube. Quantification of the protein concentrations of the samples was obtained through the Bradford assay with only 10µL of the protein suspension and 1mL of Bradford reagent. 200µL of each sample was then transferred to a 96-well plate. This colorimetric assay relies on the color change of the Bradford reagent from a brown color to a blue color, depending on the amount of protein in the sample. The absorbance value, determined by a plate spectrophotometer, is compared to a standard curve made with bovine serum albumin at known concentrations to determine the concentration of the sample.

A2. Analysis of Protein Activity with High- Performance Liquid Chromatography

DYRK1A activity was measured using a high-performance liquid chromatography (HPLC)-based assay as described in Stringer et al. 2017. Briefly, snap-frozen protein samples were allowed to thaw over ice. In separate tubes, 100µg of each sample was incubated with a 5-carboxyfluorescein tagged Woodtide peptide (2mg/mL) and kinase buffer for 1 minute at 37°C. ATP (1mM) was then added to each reaction tube before a subsequent incubation at 37°C for 30 minutes. After incubation, the reaction was stopped with the addition of $HClO_4$ (15%). Tubes were centrifuged at 4°C for 10 minutes at 14,655g. Supernatant was transferred to a conical glass insert and placed into a 2mL sampler vial for analysis using the Agilent 1260 HPLC module. Separation was achieved with a liquid phase consisting initially of 85% solvent A (H_2O + 0.1% formic acid) and 15% solvent B (ACN + 0.1% formic acid) held for 1 minute followed by a step-wise gradient ending with 5% solvent A and 95% solvent B over 11 minutes. FAM-Woodtide fluorescence was measured with a fluorescence detector with an excitation wavelength of 485nm and an emission of 530nm. The peak height and retention times were used to calculate the area under the curve

(AUC) for p-FAM-Woodtide and FAM-Woodtide. Results were analyzed using OpenLab CDS Chemstation software(Stringer et al., 2017).

A3. Analysis of EGCG Serum Concentration Following a Two-Day Pulse Treatment

In vivo administration of EGCG and analysis of blood serum EGCG concentrations were conducted as described in Goodlett et al. 2020. A homogenous solution of pure EGCG in PBS at a concentration of 15mg/mL was prepared daily and 200mg/kg/day was administered via oral gavage to 6-week-old euploid and trisomic male Ts65Dn, *Dyrk1a*$^{+/fl}$ mice for two days. Control animals received the PBS vehicle. Serum concentrations were measured in serum collected by cardiac draw from mice euthanized by isoflurane 30, 60, and 90 minutes after the final treatment on day 2. Samples were analyzed with an Agilent 1200SL high performance liquid chromatography (HPLC) module coupled to an Agilent quadrupole time-of-flight mass spectrometer (MS). Samples were separated using reverse phase chromatography with a Zorbax Eclipse Plus C18 column (2.1 x 50mm, 1.8µm particle size) at 55°C with a solvent ratio of 30% A (H_2O + 0.1% formic acid) and 70% B (ACN + 0.1% formic acid). Standards were made with serum from PBS treated animals spiked with 0, 0.001, 0.003, 0.005, 0.01, and 0.06µg/mL pure EGCG. Data was analyzed using ChemStation software (version/build). The area under the curve (AUC) from the abundance of fragments 124.7m/z and 168.8m/z were used for quantification of EGCG(Goodlett et al., 2020).

REFERENCES

Abeysekera, I., Thomas, J., Georgiadis, T. M., Berman, A. G., Hammond, M. A., Dria, K. J., . . . Roper, R. J. (2016). Differential effects of Epigallocatechin-3-gallate containing supplements on correcting skeletal defects in a Down syndrome mouse model. *Mol Nutr Food Res, 60*(4), 717-726. doi:10.1002/mnfr.201500781

Adayev, T., Chen-Hwang, M. C., Murakami, N., Wegiel, J., & Hwang, Y. W. (2006). Kinetic properties of a MNB/DYRK1A mutant suitable for the elucidation of biochemical pathways. *Biochemistry, 45*(39), 12011-12019. doi:10.1021/bi060632j

Agarwal Gupta, N., & Kabra, M. (2014). Diagnosis and management of Down syndrome. *Indian J Pediatr, 81*(6), 560-567. doi:10.1007/s12098-013-1249-7

Allen, E. G., Freeman, S. B., Druschel, C., Hobbs, C. A., O'Leary, L. A., Romitti, P. A., . . . Sherman, S. L. (2009). Maternal age and risk for trisomy 21 assessed by the origin of chromosome nondisjunction: a report from the Atlanta and National Down Syndrome Projects. *Hum Genet, 125*(1), 41-52. doi:10.1007/s00439-008-0603-8

Altafaj, X., Dierssen, M., Baamonde, C., Marti, E., Visa, J., Guimera, J., . . . Estivill, X. (2001). Neurodevelopmental delay, motor abnormalities and cognitive deficits in transgenic mice overexpressing Dyrk1A (minibrain), a murine model of Down's syndrome. *Hum Mol Genet, 10*(18), 1915-1923. doi:10.1093/hmg/10.18.1915

Amend, S. R., Valkenburg, K. C., & Pienta, K. J. (2016). Murine Hind Limb Long Bone Dissection and Bone Marrow Isolation. *J Vis Exp*(110). doi:10.3791/53936

Angelopoulou, N., Souftas, V., Sakadamis, A., & Mandroukas, K. (1999). Bone mineral density in adults with Down's syndrome. *Eur Radiol, 9*(4), 648-651. doi:10.1007/s003300050726

Arron, J. R., Winslow, M. M., Polleri, A., Chang, C. P., Wu, H., Gao, X., . . . Crabtree, G. R. (2006). NFAT dysregulation by increased dosage of DSCR1 and DYRK1A on chromosome 21. *Nature, 441*(7093), 595-600. doi:10.1038/nature04678

Bain, J., McLauchlan, H., Elliott, M., & Cohen, P. (2003). The specificities of protein kinase inhibitors: an update. *Biochem J, 371*(Pt 1), 199-204. doi:10.1042/BJ20021535

Bain, J., Plater, L., Elliott, M., Shpiro, N., Hastie, C. J., McLauchlan, H., . . . Cohen, P. (2007). The selectivity of protein kinase inhibitors: a further update. *Biochem J, 408*(3), 297-315. doi:10.1042/BJ20070797

Baptista, F., Varela, A., & Sardinha, L. B. (2005). Bone mineral mass in males and females with and without Down syndrome. *Osteoporos Int, 16*(4), 380-388. doi:10.1007/s00198-004-1687-1

Barden, H. S. (1983). Growth and development of selected hard tissues in Down syndrome: a review. *Hum Biol, 55*(3), 539-576. Retrieved from https://www.ncbi.nlm.nih.gov/pubmed/6227546

Bean, L. J., Allen, E. G., Tinker, S. W., Hollis, N. D., Locke, A. E., Druschel, C., . . . Sherman, S. L. (2011). Lack of maternal folic acid supplementation is associated with heart defects in Down syndrome: a report from the National Down Syndrome Project. *Birth Defects Res A Clin Mol Teratol, 91*(10), 885-893. doi:10.1002/bdra.22848

Becker, W., & Joost, H. G. (1999). Structural and functional characteristics of Dyrk, a novel subfamily of protein kinases with dual specificity. *Prog Nucleic Acid Res Mol Biol, 62*, 1-17. doi:10.1016/s0079-6603(08)60503-6

Benavides-Piccione, R., Dierssen, M., Ballesteros-Yanez, I., Martinez de Lagran, M., Arbones, M. L., Fotaki, V., . . . Elston, G. N. (2005). Alterations in the phenotype of neocortical pyramidal cells in the Dyrk1A+/- mouse. *Neurobiol Dis, 20*(1), 115-122. doi:10.1016/j.nbd.2005.02.004

Bittles, A. H., & Glasson, E. J. (2004). Clinical, social, and ethical implications of changing life expectancy in Down syndrome. *Dev Med Child Neurol, 46*(4), 282-286. doi:10.1017/s0012162204000441

Blazek, J. D., Abeysekera, I., Li, J., & Roper, R. J. (2015). Rescue of the abnormal skeletal phenotype in Ts65Dn Down syndrome mice using genetic and therapeutic modulation of trisomic Dyrk1a. *Hum Mol Genet, 24*(20), 5687-5696. doi:10.1093/hmg/ddv284

Blazek, J. D., Gaddy, A., Meyer, R., Roper, R. J., & Li, J. (2011). Disruption of bone development and homeostasis by trisomy in Ts65Dn Down syndrome mice. *Bone, 48*(2), 275-280. doi:10.1016/j.bone.2010.09.028

Blazek, J. D., Malik, A. M., Tischbein, M., Arbones, M. L., Moore, C. S., & Roper, R. J. (2015). Abnormal mineralization of the Ts65Dn Down syndrome mouse appendicular skeleton begins during embryonic development in a Dyrk1a-independent manner. *Mech Dev, 136*, 133-142. doi:10.1016/j.mod.2014.12.004

Bromley, B., Lieberman, E., Shipp, T. D., & Benacerraf, B. R. (2002a). Fetal nose bone length: a marker for Down syndrome in the second trimester. *J Ultrasound Med, 21*(12), 1387-1394. doi:10.7863/jum.2002.21.12.1387

Bromley, B., Lieberman, E., Shipp, T. D., & Benacerraf, B. R. (2002b). The genetic sonogram: a method of risk assessment for Down syndrome in the second trimester. *J Ultrasound Med, 21*(10), 1087-1096; quiz 1097-1088. doi:10.7863/jum.2002.21.10.1087

Burr, D. B., & Allen, M. R. (2013). *Basic and applied bone biology*. Amsterdam: Elsevier/Academic Press.

Carfi, A., Liperoti, R., Fusco, D., Giovannini, S., Brandi, V., Vetrano, D. L., . . . Onder, G. (2017). Bone mineral density in adults with Down syndrome. *Osteoporos Int, 28*(10), 2929-2934. doi:10.1007/s00198-017-4133-x

Chakrabarti, L., Best, T. K., Cramer, N. P., Carney, R. S., Isaac, J. T., Galdzicki, Z., & Haydar, T. F. (2010). Olig1 and Olig2 triplication causes developmental brain defects in Down syndrome. *Nat Neurosci, 13*(8), 927-934. doi:10.1038/nn.2600

Chen, T. L. (2004). Inhibition of growth and differentiation of osteoprogenitors in mouse bone marrow stromal cell cultures by increased donor age and glucocorticoid treatment. *Bone, 35*(1), 83-95. doi:10.1016/j.bone.2004.03.019

Cheung, W. M., Ng, W. W., & Kung, A. W. (2006). Dimethyl sulfoxide as an inducer of differentiation in preosteoblast MC3T3-E1 cells. *FEBS Lett, 580*(1), 121-126. doi:10.1016/j.febslet.2005.11.062

Chiang, J. C., Jiang, J., Newburger, P. E., & Lawrence, J. B. (2018). Trisomy silencing by XIST normalizes Down syndrome cell pathogenesis demonstrated for hematopoietic defects in vitro. *Nat Commun, 9*(1), 5180. doi:10.1038/s41467-018-07630-y

Choi, J. H., Berger, J. D., Mazzella, M. J., Morales-Corraliza, J., Cataldo, A. M., Nixon, R. A., . . . Mathews, P. M. (2009). Age-dependent dysregulation of brain amyloid precursor protein in the Ts65Dn Down syndrome mouse model. *J Neurochem, 110*(6), 1818-1827. doi:10.1111/j.1471-4159.2009.06277.x

Chon, H. J., Bae, K. J., Lee, Y., & Kim, J. (2015). The casein kinase 2 inhibitor, CX-4945, as an anti-cancer drug in treatment of human hematological malignancies. *Front Pharmacol, 6*, 70. doi:10.3389/fphar.2015.00070

Costa, R., De Miguel, R., Garcia, C., de Asua, D. R., Castaneda, S., Moldenhauer, F., & Suarez, C. (2017). Bone Mass Assessment in a Cohort of Adults With Down Syndrome: A Cross-Sectional Study. *Intellect Dev Disabil, 55*(5), 315-324. doi:10.1352/1934-9556-55.5.315

Costa, R., Gullon, A., De Miguel, R., de Asua, D. R., Bautista, A., Garcia, C., . . . Moldenhauer, F. (2018). Bone Mineral Density Distribution Curves in Spanish Adults With Down Syndrome. *J Clin Densitom, 21*(4), 493-500. doi:10.1016/j.jocd.2018.03.001

Czerminski, J. T., & Lawrence, J. B. (2020). Silencing Trisomy 21 with XIST in Neural Stem Cells Promotes Neuronal Differentiation. *Dev Cell, 52*(3), 294-308 e293. doi:10.1016/j.devcel.2019.12.015

Davisson, M. T., Schmidt, C., Reeves, R. H., Irving, N. G., Akeson, E. C., Harris, B. S., & Bronson, R. T. (1993). Segmental trisomy as a mouse model for Down syndrome. *Prog Clin Biol Res, 384*, 117-133. Retrieved from https://www.ncbi.nlm.nih.gov/pubmed/8115398

de Figueiredo, F. A. T., Shimano, R. C., Ervolino, E., Pitol, D. L., Gerlach, R. F., & Issa, J. P. M. (2019). Doxycycline reduces osteopenia in female rats. *Sci Rep, 9*(1), 15316. doi:10.1038/s41598-019-51702-y

de Graaf, G., Buckley, F., & Skotko, B. G. (2015). Estimates of the live births, natural losses, and elective terminations with Down syndrome in the United States. *Am J Med Genet A, 167A*(4), 756-767. doi:10.1002/ajmg.a.37001

De la Torre, R., De Sola, S., Pons, M., Duchon, A., de Lagran, M. M., Farre, M., . . . Dierssen, M. (2014). Epigallocatechin-3-gallate, a DYRK1A inhibitor, rescues cognitive deficits in Down syndrome mouse models and in humans. *Mol Nutr Food Res, 58*(2), 278-288. doi:10.1002/mnfr.201300325

de Moraes, M. E., Tanaka, J. L., de Moraes, L. C., Filho, E. M., & de Melo Castilho, J. C. (2008). Skeletal age of individuals with Down syndrome. *Spec Care Dentist, 28*(3), 101-106. doi:10.1111/j.1754-4505.2008.00020.x

Delahunty, K. M., Horton, L. G., Coombs, H. F., 3rd, Shultz, K. L., Svenson, K. L., Marion, M. A., . . . Rosen, C. J. (2009). Gender- and compartment-specific bone loss in C57BL/6J mice: correlation to season? *J Clin Densitom, 12*(1), 89-94. doi:10.1016/j.jocd.2008.10.008

Dempster, D. W., Compston, J. E., Drezner, M. K., Glorieux, F. H., Kanis, J. A., Malluche, H., . . . Parfitt, A. M. (2013). Standardized nomenclature, symbols, and units for bone histomorphometry: a 2012 update of the report of the ASBMR Histomorphometry Nomenclature Committee. *J Bone Miner Res, 28*(1), 2-17. doi:10.1002/jbmr.1805

Dobson, K. R., Reading, L., Haberey, M., Marine, X., & Scutt, A. (1999). Centrifugal isolation of bone marrow from bone: an improved method for the recovery and quantitation of bone marrow osteoprogenitor cells from rat tibiae and femurae. *Calcif Tissue Int, 65*(5), 411-413. doi:10.1007/s002239900723

Duchon, A., Raveau, M., Chevalier, C., Nalesso, V., Sharp, A. J., & Herault, Y. (2011). Identification of the translocation breakpoints in the Ts65Dn and Ts1Cje mouse lines: relevance for modeling Down syndrome. *Mamm Genome, 22*(11-12), 674-684. doi:10.1007/s00335-011-9356-0

Esbensen, A. J., Johnson, E. B., Amaral, J. L., Tan, C. M., & Macks, R. (2016). Differentiating Aging Among Adults With Down Syndrome and Comorbid Dementia or Psychopathology. *Am J Intellect Dev Disabil, 121*(1), 13-24. doi:10.1352/1944-7558-121.1.13

Feng, X., & Teitelbaum, S. L. (2013). Osteoclasts: New Insights. *Bone Res, 1*(1), 11-26. doi:10.4248/BR201301003

Fotaki, V., Dierssen, M., Alcantara, S., Martinez, S., Marti, E., Casas, C., . . . Arbones, M. L. (2002). Dyrk1A haploinsufficiency affects viability and causes developmental delay and abnormal brain morphology in mice. *Mol Cell Biol, 22*(18), 6636-6647. doi:10.1128/mcb.22.18.6636-6647.2002

Fotaki, V., Martinez De Lagran, M., Estivill, X., Arbones, M., & Dierssen, M. (2004). Haploinsufficiency of Dyrk1A in mice leads to specific alterations in the development and regulation of motor activity. *Behav Neurosci, 118*(4), 815-821. doi:10.1037/0735-7044.118.4.815

Fowler, T. W., McKelvey, K. D., Akel, N. S., Vander Schilden, J., Bacon, A. W., Bracey, J. W., . . . Suva, L. J. (2012). Low bone turnover and low BMD in Down syndrome: effect of intermittent PTH treatment. *PLoS One, 7*(8), e42967. doi:10.1371/journal.pone.0042967

Garcia-Cerro, S., Rueda, N., Vidal, V., Lantigua, S., & Martinez-Cue, C. (2017). Normalizing the gene dosage of Dyrk1A in a mouse model of Down syndrome rescues several Alzheimer's disease phenotypes. *Neurobiol Dis, 106*, 76-88. doi:10.1016/j.nbd.2017.06.010

Gardiner, K., Fortna, A., Bechtel, L., & Davisson, M. T. (2003). Mouse models of Down syndrome: how useful can they be? Comparison of the gene content of human chromosome 21 with orthologous mouse genomic regions. *Gene, 318*, 137-147. doi:10.1016/s0378-1119(03)00769-8

Ghali, O., Broux, O., Falgayrac, G., Haren, N., van Leeuwen, J. P., Penel, G., . . . Chauveau, C. (2015). Dexamethasone in osteogenic medium strongly induces adipocyte differentiation of mouse bone marrow stromal cells and increases osteoblast differentiation. *BMC Cell Biol, 16*, 9. doi:10.1186/s12860-015-0056-6

Ghosh, S., Feingold, E., & Dey, S. K. (2009). Etiology of Down syndrome: Evidence for consistent association among altered meiotic recombination, nondisjunction, and maternal age across populations. *Am J Med Genet A, 149A*(7), 1415-1420. doi:10.1002/ajmg.a.32932

Gomes, K. D. N., Alves, A., Dutra, P. G. P., & Viana, G. S. B. (2017). Doxycycline induces bone repair and changes in Wnt signalling. *Int J Oral Sci, 9*(3), 158-166. doi:10.1038/ijos.2017.28

Goodlett, C. R., Stringer, M., LaCombe, J., Patel, R., Wallace, J. M., & Roper, R. J. (2020). Evaluation of the therapeutic potential of Epigallocatechin-3-gallate (EGCG) via oral gavage in young adult Down syndrome mice. *Sci Rep, 10*(1), 10426. doi:10.1038/s41598-020-67133-z

Gregory, C. A., Gunn, W. G., Peister, A., & Prockop, D. J. (2004). An Alizarin red-based assay of mineralization by adherent cells in culture: comparison with cetylpyridinium chloride extraction. *Anal Biochem, 329*(1), 77-84. doi:10.1016/j.ab.2004.02.002

Grimwood, J. S., Kumar, A., Bickerstaff, D. R., & Suvarna, S. K. (2000). Histological assessment of vertebral bone in a Down's syndrome adult with osteoporosis. *Histopathology, 36*(3), 279-280. Retrieved from https://www.ncbi.nlm.nih.gov/pubmed/10809596

Gu, Y., Moroy, G., Paul, J. L., Rebillat, A. S., Dierssen, M., de la Torre, R., . . . Janel, N. (2020). Molecular Rescue of Dyrk1A Overexpression Alterations in Mice with Fontup((R)) Dietary Supplement: Role of Green Tea Catechins. *Int J Mol Sci, 21*(4). doi:10.3390/ijms21041404

Guimera, J., Casas, C., Estivill, X., & Pritchard, M. (1999). Human minibrain homologue (MNBH/DYRK1): characterization, alternative splicing, differential tissue expression, and overexpression in Down syndrome. *Genomics, 57*(3), 407-418. doi:10.1006/geno.1999.5775

Gupta, M., Dhanasekaran, A. R., & Gardiner, K. J. (2016). Mouse models of Down syndrome: gene content and consequences. *Mamm Genome, 27*(11-12), 538-555. doi:10.1007/s00335-016-9661-8

Hasen, J., Boyar, R. M., & Shapiro, L. R. (1980). Gonadal function in trisomy 21. *Horm Res, 12*(6), 345-350. doi:10.1159/000179141

Hestnes, A., Stovner, L. J., Husoy, O., Folling, I., Fougner, K. J., & Sjaastad, O. (1991). Hormonal and biochemical disturbances in Down's syndrome. *J Ment Defic Res, 35 (Pt 3)*, 179-193. doi:10.1111/j.1365-2788.1991.tb01051.x

Hollis, N. D., Allen, E. G., Oliver, T. R., Tinker, S. W., Druschel, C., Hobbs, C. A., . . . Bean, L. J. (2013). Preconception folic acid supplementation and risk for chromosome 21 nondisjunction: a report from the National Down Syndrome Project. *Am J Med Genet A, 161A*(3), 438-444. doi:10.1002/ajmg.a.35796

Hsiang, Y. H., Berkovitz, G. D., Bland, G. L., Migeon, C. J., & Warren, A. C. (1987). Gonadal function in patients with Down syndrome. *Am J Med Genet, 27*(2), 449-458. doi:10.1002/ajmg.1320270223

Hunter, J. E., Allen, E. G., Shin, M., Bean, L. J., Correa, A., Druschel, C., . . . Sherman, S. L. (2013). The association of low socioeconomic status and the risk of having a child with Down syndrome: a report from the National Down Syndrome Project. *Genet Med, 15*(9), 698-705. doi:10.1038/gim.2013.34

Jilka, R. L. (2013). The relevance of mouse models for investigating age-related bone loss in humans. *J Gerontol A Biol Sci Med Sci, 68*(10), 1209-1217. doi:10.1093/gerona/glt046

Kazuki, Y., Gao, F. J., Li, Y., Moyer, A. J., Devenney, B., Hiramatsu, K., . . . Reeves, R. H. (2020). A non-mosaic transchromosomic mouse model of down syndrome carrying the long arm of human chromosome 21. *Elife, 9*. doi:10.7554/eLife.56223

Kii, I., Sumida, Y., Goto, T., Sonamoto, R., Okuno, Y., Yoshida, S., . . . Hagiwara, M. (2016). Selective inhibition of the kinase DYRK1A by targeting its folding process. *Nat Commun, 7*, 11391. doi:10.1038/ncomms11391

Kim, H., Lee, K. S., Kim, A. K., Choi, M., Choi, K., Kang, M., . . . Cho, S. (2016). A chemical with proven clinical safety rescues Down-syndrome-related phenotypes in through DYRK1A inhibition. *Dis Model Mech, 9*(8), 839-848. doi:10.1242/dmm.025668

Kim, J. M., Yang, Y. S., Park, K. H., Ge, X., Xu, R., Li, N., . . . Shim, J. H. (2020). A RUNX2 stabilization pathway mediates physiologic and pathologic bone formation. *Nat Commun, 11*(1), 2289. doi:10.1038/s41467-020-16038-6

Kinugawa, S., Koide, M., Kobayashi, Y., Mizoguchi, T., Ninomiya, T., Muto, A., . . . Udagawa, N. (2012). Tetracyclines convert the osteoclastic-differentiation pathway of progenitor cells to produce dendritic cell-like cells. *J Immunol, 188*(4), 1772-1781. doi:10.4049/jimmunol.1101174

Kleschevnikov, A. M., Yu, J., Kim, J., Lysenko, L. V., Zeng, Z., Yu, Y. E., & Mobley, W. C. (2017). Evidence that increased Kcnj6 gene dose is necessary for deficits in behavior and dentate gyrus synaptic plasticity in the Ts65Dn mouse model of Down syndrome. *Neurobiol Dis, 103*, 1-10. doi:10.1016/j.nbd.2017.03.009

LaCombe, J. M., & Roper, R. J. (2020). Skeletal dynamics of Down syndrome: A developing perspective. *Bone, 133*, 115215. doi:10.1016/j.bone.2019.115215

Lamb, N. E., Feingold, E., Savage, A., Avramopoulos, D., Freeman, S., Gu, Y., . . . Sherman, S. L. (1997). Characterization of susceptible chiasma configurations that increase the risk for maternal nondisjunction of chromosome 21. *Hum Mol Genet, 6*(9), 1391-1399. doi:10.1093/hmg/6.9.1391

Lana-Elola, E., Watson-Scales, S., Slender, A., Gibbins, D., Martineau, A., Douglas, C., . . . Tybulewicz, V. (2016). Genetic dissection of Down syndrome-associated congenital heart defects using a new mouse mapping panel. *Elife, 5*. doi:10.7554/eLife.11614

Lana-Elola, E., Watson-Scales, S. D., Fisher, E. M., & Tybulewicz, V. L. (2011). Down syndrome: searching for the genetic culprits. *Dis Model Mech, 4*(5), 586-595. doi:10.1242/dmm.008078

Lebrin, F., Chambaz, E. M., & Bianchini, L. (2001). A role for protein kinase CK2 in cell proliferation: evidence using a kinase-inactive mutant of CK2 catalytic subunit alpha. *Oncogene, 20*(16), 2010-2022. doi:10.1038/sj.onc.1204307

Lee, Y., Ha, J., Kim, H. J., Kim, Y. S., Chang, E. J., Song, W. J., & Kim, H. H. (2009). Negative feedback Inhibition of NFATc1 by DYRK1A regulates bone homeostasis. *J Biol Chem, 284*(48), 33343-33351. doi:10.1074/jbc.M109.042234

Lemieux, J. M., Wu, G., Morgan, J. A., & Kacena, M. A. (2011). DMSO regulates osteoclast development in vitro. *In Vitro Cell Dev Biol Anim, 47*(3), 260-267. doi:10.1007/s11626-011-9385-8

Longo, D., DeFigueiredo, D., Cicero, S., Sacchini, C., & Nicolaides, K. H. (2004). Femur and humerus length in trisomy 21 fetuses at 11-14 weeks of gestation. *Ultrasound Obstet Gynecol, 23*(2), 143-147. doi:10.1002/uog.970

Marti, E., Altafaj, X., Dierssen, M., de la Luna, S., Fotaki, V., Alvarez, M., . . . Estivill, X. (2003). Dyrk1A expression pattern supports specific roles of this kinase in the adult central nervous system. *Brain Res, 964*(2), 250-263. doi:10.1016/s0006-8993(02)04069-6

Masaki, S., Kii, I., Sumida, Y., Kato-Sumida, T., Ogawa, Y., Ito, N., . . . Hagiwara, M. (2015). Design and synthesis of a potent inhibitor of class 1 DYRK kinases as a suppressor of adipogenesis. *Bioorg Med Chem, 23*(15), 4434-4441. doi:10.1016/j.bmc.2015.06.018

Masukawa, Y., Matsui, Y., Shimizu, N., Kondou, N., Endou, H., Kuzukawa, M., & Hase, T. (2006). Determination of green tea catechins in human plasma using liquid chromatography-electrospray ionization mass spectrometry. *J Chromatogr B Analyt Technol Biomed Life Sci, 834*(1-2), 26-34. doi:10.1016/j.jchromb.2006.02.008

McKelvey, K. D., Fowler, T. W., Akel, N. S., Kelsay, J. A., Gaddy, D., Wenger, G. R., & Suva, L. J. (2013). Low bone turnover and low bone density in a cohort of adults with Down syndrome. *Osteoporos Int, 24*(4), 1333-1338. doi:10.1007/s00198-012-2109-4

Meissner, L. E., Macnamara, E. F., D'Souza, P., Yang, J., Vezina, G., Undiagnosed Diseases, N., . . . Adams, D. R. (2020). DYRK1A pathogenic variants in two patients with syndromic intellectual disability and a review of the literature. *Mol Genet Genomic Med, 8*(12), e1544. doi:10.1002/mgg3.1544

Middlebrooks, C. D., Mukhopadhyay, N., Tinker, S. W., Allen, E. G., Bean, L. J., Begum, F., . . . Sherman, S. L. (2014). Evidence for dysregulation of genome-wide recombination in oocytes with nondisjoined chromosomes 21. *Hum Mol Genet, 23*(2), 408-417. doi:10.1093/hmg/ddt433

Moller, R. S., Kubart, S., Hoeltzenbein, M., Heye, B., Vogel, I., Hansen, C. P., . . . Kalscheuer, V. M. (2008). Truncation of the Down syndrome candidate gene DYRK1A in two unrelated patients with microcephaly. *Am J Hum Genet, 82*(5), 1165-1170. doi:10.1016/j.ajhg.2008.03.001

Moore, C. S., Hawkins, C., Franca, A., Lawler, A., Devenney, B., Das, I., & Reeves, R. H. (2010). Increased male reproductive success in Ts65Dn "Down syndrome" mice. *Mamm Genome, 21*(11-12), 543-549. doi:10.1007/s00335-010-9300-8

Musial, C., Kuban-Jankowska, A., & Gorska-Ponikowska, M. (2020). Beneficial Properties of Green Tea Catechins. *Int J Mol Sci, 21*(5). doi:10.3390/ijms21051744

Myrelid, A., Gustafsson, J., Ollars, B., & Anneren, G. (2002). Growth charts for Down's syndrome from birth to 18 years of age. *Arch Dis Child, 87*(2), 97-103. doi:10.1136/adc.87.2.97

Neuhuber, B., Swanger, S. A., Howard, L., Mackay, A., & Fischer, I. (2008). Effects of plating density and culture time on bone marrow stromal cell characteristics. *Exp Hematol, 36*(9), 1176-1185. doi:10.1016/j.exphem.2008.03.019

O'Doherty, A., Ruf, S., Mulligan, C., Hildreth, V., Errington, M. L., Cooke, S., . . . Fisher, E. M. (2005). An aneuploid mouse strain carrying human chromosome 21 with Down syndrome phenotypes. *Science, 309*(5743), 2033-2037. doi:10.1126/science.1114535

Ogawa, Y., Nonaka, Y., Goto, T., Ohnishi, E., Hiramatsu, T., Kii, I., . . . Hagiwara, M. (2010). Development of a novel selective inhibitor of the Down syndrome-related kinase Dyrk1A. *Nat Commun, 1*, 86. doi:10.1038/ncomms1090

Ohlsson, C., & Vandenput, L. (2009). The role of estrogens for male bone health. *Eur J Endocrinol, 160*(6), 883-889. doi:10.1530/EJE-09-0118

Oliver, T. R., Feingold, E., Yu, K., Cheung, V., Tinker, S., Yadav-Shah, M., . . . Sherman, S. L. (2008). New insights into human nondisjunction of chromosome 21 in oocytes. *PLoS Genet, 4*(3), e1000033. doi:10.1371/journal.pgen.1000033

Olson, L. E., Richtsmeier, J. T., Leszl, J., & Reeves, R. H. (2004). A chromosome 21 critical region does not cause specific Down syndrome phenotypes. *Science, 306*(5696), 687-690. doi:10.1126/science.1098992

Olson, L. E., Roper, R. J., Sengstaken, C. L., Peterson, E. A., Aquino, V., Galdzicki, Z., . . . Reeves, R. H. (2007). Trisomy for the Down syndrome 'critical region' is necessary but not sufficient for brain phenotypes of trisomic mice. *Hum Mol Genet, 16*(7), 774-782. doi:10.1093/hmg/ddm022

Papavassiliou, P., Charalsawadi, C., Rafferty, K., & Jackson-Cook, C. (2015). Mosaicism for trisomy 21: a review. *Am J Med Genet A, 167A*(1), 26-39. doi:10.1002/ajmg.a.36861

Papavassiliou, P., York, T. P., Gursoy, N., Hill, G., Nicely, L. V., Sundaram, U., . . . Jackson-Cook, C. (2009). The phenotype of persons having mosaicism for trisomy 21/Down syndrome reflects the percentage of trisomic cells present in different tissues. *Am J Med Genet A, 149A*(4), 573-583. doi:10.1002/ajmg.a.32729

Patel, S. S., Beer, S., Kearney, D. L., Phillips, G., & Carter, B. A. (2013). Green tea extract: a potential cause of acute liver failure. *World J Gastroenterol, 19*(31), 5174-5177. doi:10.3748/wjg.v19.i31.5174

Penders, M. H. G. M., Jones, D. P., Needham, D., & Pelan, E. G. (1998). Mechanistic study of equilibrium and kinetic behaviour of tea cream formation. *Food Hydrocolloids, 12*(1), 9-15. doi:https://doi.org/10.1016/S0268-005X(98)00040-X

Pueschel, S. M., Orson, J. M., Boylan, J. M., & Pezzullo, J. C. (1985). Adolescent development in males with Down syndrome. *Am J Dis Child, 139*(3), 236-238. doi:10.1001/archpedi.1985.02140050030014

Ramachandran, B., Jayavelu, S., Murhekar, K., & Rajkumar, T. (2016). Repeated dose studies with pure Epigallocatechin-3-gallate demonstrated dose and route dependant hepatotoxicity with associated dyslipidemia. *Toxicol Rep, 3*, 336-345. doi:10.1016/j.toxrep.2016.03.001

Rathbone, C. R., Cross, J. D., Brown, K. V., Murray, C. K., & Wenke, J. C. (2011). Effect of various concentrations of antibiotics on osteogenic cell viability and activity. *J Orthop Res, 29*(7), 1070-1074. doi:10.1002/jor.21343

Reeves, R. H., Irving, N. G., Moran, T. H., Wohn, A., Kitt, C., Sisodia, S. S., . . . Davisson, M. T. (1995). A mouse model for Down syndrome exhibits learning and behaviour deficits. *Nat Genet, 11*(2), 177-184. doi:10.1038/ng1095-177

Reinholdt, L. G., Ding, Y., Gilbert, G. J., Czechanski, A., Solzak, J. P., Roper, R. J., . . . Davisson, M. T. (2011). Molecular characterization of the translocation breakpoints in the Down syndrome mouse model Ts65Dn. *Mamm Genome, 22*(11-12), 685-691. doi:10.1007/s00335-011-9357-z

Rice, A. M., & McLysaght, A. (2017). Dosage-sensitive genes in evolution and disease. *BMC Biol, 15*(1), 78. doi:10.1186/s12915-017-0418-y

Richtsmeier, J. T., Baxter, L. L., & Reeves, R. H. (2000). Parallels of craniofacial maldevelopment in Down syndrome and Ts65Dn mice. *Dev Dyn, 217*(2), 137-145. doi:10.1002/(SICI)1097-0177(200002)217:2<137::AID-DVDY1>3.0.CO;2-N

Roper, R. J., Goodlett, C. R., Martinez de Lagran, M., & Dierssen, M. (2020). Behavioral Phenotyping for Down Syndrome in Mice. *Curr Protoc Mouse Biol, 10*(3), e79. doi:10.1002/cpmo.79

Roper, R. J., & Reeves, R. H. (2006). Understanding the basis for Down syndrome phenotypes. *PLoS Genet, 2*(3), e50. doi:10.1371/journal.pgen.0020050

Roper, R. J., St John, H. K., Philip, J., Lawler, A., & Reeves, R. H. (2006). Perinatal loss of Ts65Dn Down syndrome mice. *Genetics, 172*(1), 437-443. doi:10.1534/genetics.105.050898

Roper, R. J., VanHorn, J. F., Cain, C. C., & Reeves, R. H. (2009). A neural crest deficit in Down syndrome mice is associated with deficient mitotic response to Sonic hedgehog. *Mech Dev, 126*(3-4), 212-219. doi:10.1016/j.mod.2008.11.002

Sang, S., Lee, M. J., Hou, Z., Ho, C. T., & Yang, C. S. (2005). Stability of tea polyphenol (-)-epigallocatechin-3-gallate and formation of dimers and epimers under common experimental conditions. *J Agric Food Chem, 53*(24), 9478-9484. doi:10.1021/jf0519055

Schnabel, F., Smogavec, M., Funke, R., Pauli, S., Burfeind, P., & Bartels, I. (2018). Down syndrome phenotype in a boy with a mosaic microduplication of chromosome 21q22. *Mol Cytogenet, 11*, 62. doi:10.1186/s13039-018-0410-4

Seto, R., Nakamura, H., Nanjo, F., & Hara, Y. (1997). Preparation of Epimers of Tea Catechins by Heat Treatment. *Bioscience, Biotechnology, and Biochemistry, 61*(9), 1434-1439. doi:10.1271/bbb.61.1434

Shin, M., Siffel, C., & Correa, A. (2010). Survival of children with mosaic Down syndrome. *Am J Med Genet A, 152A*(3), 800-801. doi:10.1002/ajmg.a.33295

Siebert, K. J., Troukhanova, N. V., & Lynn, P. Y. (1996). Nature of Polyphenol−Protein Interactions. *Journal of Agricultural and Food Chemistry, 44*(1), 80-85. doi:10.1021/jf9502459

Smith, D. J., Stevens, M. E., Sudanagunta, S. P., Bronson, R. T., Makhinson, M., Watabe, A. M., . . . Rubin, E. M. (1997). Functional screening of 2 Mb of human chromosome 21q22.2 in transgenic mice implicates minibrain in learning defects associated with Down syndrome. *Nat Genet, 16*(1), 28-36. doi:10.1038/ng0597-28

Son, Y. H., Moon, S. H., & Kim, J. (2013). The protein kinase 2 inhibitor CX-4945 regulates osteoclast and osteoblast differentiation in vitro. *Mol Cells, 36*(5), 417-423. doi:10.1007/s10059-013-0184-9

Song, W. J., Sternberg, L. R., Kasten-Sportes, C., Keuren, M. L., Chung, S. H., Slack, A. C., . . . Kurnit, D. M. (1996). Isolation of human and murine homologues of the Drosophila minibrain gene: human homologue maps to 21q22.2 in the Down syndrome "critical region". *Genomics, 38*(3), 331-339. doi:10.1006/geno.1996.0636

Stephens, A. S., Stephens, S. R., Hobbs, C., Hutmacher, D. W., Bacic-Welsh, D., Woodruff, M. A., & Morrison, N. A. (2011). Myocyte enhancer factor 2c, an osteoblast transcription factor identified by dimethyl sulfoxide (DMSO)-enhanced mineralization. *J Biol Chem, 286*(34), 30071-30086. doi:10.1074/jbc.M111.253518

Stewart, G. D., Hassold, T. J., Berg, A., Watkins, P., Tanzi, R., & Kurnit, D. M. (1988). Trisomy 21 (Down syndrome): studying nondisjunction and meiotic recombination by using cytogenetic and molecular polymorphisms that span chromosome 21. *Am J Hum Genet, 42*(2), 227-236. Retrieved from https://www.ncbi.nlm.nih.gov/pubmed/2893544

Stringer, M., Abeysekera, I., Dria, K. J., Roper, R. J., & Goodlett, C. R. (2015). Low dose EGCG treatment beginning in adolescence does not improve cognitive impairment in a Down syndrome mouse model. *Pharmacol Biochem Behav, 138*, 70-79. doi:10.1016/j.pbb.2015.09.002

Stringer, M., Abeysekera, I., Thomas, J., LaCombe, J., Stancombe, K., Stewart, R. J., . . . Roper, R. J. (2017). Epigallocatechin-3-gallate (EGCG) consumption in the Ts65Dn model of Down syndrome fails to improve behavioral deficits and is detrimental to skeletal phenotypes. *Physiol Behav, 177*, 230-241. doi:10.1016/j.physbeh.2017.05.003

Takahashi, K., Setoguchi, T., Tsuru, A., Saitoh, Y., Nagano, S., Ishidou, Y., . . . Komiya, S. (2017). Inhibition of casein kinase 2 prevents growth of human osteosarcoma. *Oncol Rep, 37*(2), 1141-1147. doi:10.3892/or.2016.5310

Tang, J. Y. M., Luo, H., Wong, G. H. Y., Lau, M. M. Y., Joe, G. M., Tse, M. A., . . . Lum, T. Y. S. (2019). Bone mineral density from early to middle adulthood in persons with Down syndrome. *J Intellect Disabil Res, 63*(8), 936-946. doi:10.1111/jir.12608

Tejedor, F., Zhu, X. R., Kaltenbach, E., Ackermann, A., Baumann, A., Canal, I., . . . Pongs, O. (1995). minibrain: a new protein kinase family involved in postembryonic neurogenesis in Drosophila. *Neuron, 14*(2), 287-301. doi:10.1016/0896-6273(95)90286-4

Thomas, J. R., LaCombe, J., Long, R., Lana-Elola, E., Watson-Scales, S., Wallace, J. M., . . . Roper, R. J. (2020). Interaction of sexual dimorphism and gene dosage imbalance in skeletal deficits associated with Down syndrome. *Bone, 136*, 115367. doi:10.1016/j.bone.2020.115367

Thompson, B. J., Bhansali, R., Diebold, L., Cook, D. E., Stolzenburg, L., Casagrande, A. S., . . . Crispino, J. D. (2015). DYRK1A controls the transition from proliferation to quiescence during lymphoid development by destabilizing Cyclin D3. *J Exp Med, 212*(6), 953-970. doi:10.1084/jem.20150002

van Bon, B. W., Coe, B. P., Bernier, R., Green, C., Gerdts, J., Witherspoon, K., . . . Eichler, E. E. (2016). Disruptive de novo mutations of DYRK1A lead to a syndromic form of autism and ID. *Mol Psychiatry, 21*(1), 126-132. doi:10.1038/mp.2015.5

van Bon, B. W., Hoischen, A., Hehir-Kwa, J., de Brouwer, A. P., Ruivenkamp, C., Gijsbers, A. C., . . . de Vries, B. B. (2011). Intragenic deletion in DYRK1A leads to mental retardation and primary microcephaly. *Clin Genet, 79*(3), 296-299. doi:10.1111/j.1399-0004.2010.01544.x

van Bon, B. W. M., Coe, B. P., de Vries, B. B. A., & Eichler, E. E. (1993). DYRK1A-Related Intellectual Disability Syndrome. In M. P. Adam, H. H. Ardinger, R. A. Pagon, S. E. Wallace, L. J. H. Bean, G. Mirzaa, & A. Amemiya (Eds.), *GeneReviews((R))*. Seattle (WA).

Vandenput, L., & Ohlsson, C. (2009). Estrogens as regulators of bone health in men. *Nat Rev Endocrinol, 5*(8), 437-443. doi:10.1038/nrendo.2009.112

Wang, X., Yang, L., Wang, J., Zhang, Y., Dong, R., Wu, X., . . . Zhang, J. (2019). A mouse model of subacute liver failure with ascites induced by step-wise increased doses of (-)-epigallocatechin-3-gallate. *Sci Rep, 9*(1), 18102. doi:10.1038/s41598-019-54691-0

Yang, C., Madhu, V., Thomas, C., Yang, X., Du, X., Dighe, A. S., & Cui, Q. (2015). Inhibition of differentiation and function of osteoclasts by dimethyl sulfoxide (DMSO). *Cell Tissue Res, 362*(3), 577-585. doi:10.1007/s00441-015-2245-1

Yashima, M., Sato, Y., & Kazama, I. (2021). Catechin synergistically potentiates mast cell-stabilizing property of caffeine. *Allergy Asthma Clin Immunol, 17*(1), 1. doi:10.1186/s13223-020-00502-5

Zhang, W., Ou, G., Hamrick, M., Hill, W., Borke, J., Wenger, K., . . . Shi, X. M. (2008). Age-related changes in the osteogenic differentiation potential of mouse bone marrow stromal cells. *J Bone Miner Res, 23*(7), 1118-1128. doi:10.1359/jbmr.080304

Zhao, W. W., Wu, M., Chen, F., Jiang, S., Su, H., Liang, J., . . . Yu, S. (2015). Robertsonian translocations: an overview of 872 Robertsonian translocations identified in a diagnostic laboratory in China. *PLoS One, 10*(5), e0122647. doi:10.1371/journal.pone.0122647